



2017

Photochemical Generation of Carbenes and Ketenes from Phenanthrene-based Precursors Part I: Dimethylalkylidene Part II: Diphenylketene

Tarini S. Hardikar
Student

Tarini Hardikar
Colby College

Follow this and additional works at: <https://digitalcommons.colby.edu/honorstheses>

 Part of the [Organic Chemistry Commons](#)

Colby College theses are protected by copyright. They may be viewed or downloaded from this site for the purposes of research and scholarship. Reproduction or distribution for commercial purposes is prohibited without written permission of the author.

Recommended Citation

Hardikar, Tarini S. and Hardikar, Tarini, "Photochemical Generation of Carbenes and Ketenes from Phenanthrene-based Precursors Part I: Dimethylalkylidene Part II: Diphenylketene" (2017). *Honors Theses*. Paper 948.
<https://digitalcommons.colby.edu/honorstheses/948>

This Honors Thesis (Open Access) is brought to you for free and open access by the Student Research at Digital Commons @ Colby. It has been accepted for inclusion in Honors Theses by an authorized administrator of Digital Commons @ Colby.

**Photochemical Generation of Carbenes and Ketenes
from Phenanthrene-based Precursors**

Part I: Dimethylalkylidene

Part II: Diphenylketene

TARINI HARDIKAR

A Thesis Presented to the Department of Chemistry,
Colby College, Waterville, ME

In Partial Fulfillment of the Requirements for Graduation
With Honors in Chemistry

SUBMITTED MAY 2017

Photochemical Generation of Carbenes and Ketenes from
Phenanthrene-based Precursors

Part I: Dimethylalkylidene

Part II: Diphenylketene

TARINI HARDIKAR

Approved:

(Mentor: Dasan M. Thamattoor, Professor of Chemistry)

(Reader: Rebecca R. Conry, Associate Professor of Chemistry)

“NOW WE KNOW”

- Dasan M. Thamattoor

Vitae

Tarini Shekhar Hardikar was born in Vadodara, Gujarat, India in 1996. She graduated from the S.N. Kansagra School, Rajkot, Gujarat, India in 2013. She joined Colby in the fall of 2013, with a vague notion of majoring in some natural science field. With an interest in physical and organic chemistry, she joined Professor Dasan Thamattoor's research group in January 2015. She will be graduating from Colby on May 21st, 2017 with a Chemistry and Mathematics major, and a minor in Physics. She is completing an Honors thesis in both Chemistry and Mathematics.

At Colby, Tarini has worked to build a community for women in STEM fields. She hopes to continue this work on a broader scale post-Colby. Additionally, in the future, she wishes to magically improve the scientific research environment in India, with a desire to develop a culture that celebrates good science and curiosity.

In the coming years, Tarini intends to pursue a PhD in chemistry and continue in the world of scientific research.

Acknowledgments

I'm extremely grateful for the existence of a lot of people in my life.

Firstly, Professor Dasan M. Thamattoor. I decided to talk to Das to ask if I could join his research group quite randomly at the end of my first year at Colby. Thankfully, he did not ask me my chemistry grades (they were unideal at the time), and saw my interest as a sufficient starting point. That was probably the best decision I have made in college; working in Das Lab has been a remarkable experience. I'm incredibly grateful for Das's advice, mentorship, guidance, and encouragement. I have learned so much from him, be it organic chemistry, lab skills, or a vague understanding of baseball. It is thanks to his passion and enthusiasm that I have developed a deep fascination with physical organic chemistry. He has extraordinary patience for all my questions (including some about solving crosswords). It is telling that my phone auto-suggests his name all the time! His optimism and curiosity are infectious, and I'm very glad to have such a fantastic storyteller as a chemistry teacher and role model. Thank you Das, for being wonderful.

Next, all the Das Lab members I have worked with. Working in lab has been so much more enjoyable because of your company. I have learned a lot from you, and I cherish memories of our work together: sharing the excitement of butyllithium reactions, arguing over music preferences, and (avoiding) doing the dishes. I would specially like to thank Tracy Fan and Dan Maurer. Tracy, since it's been great to have a friend to share the highs and lows of writing a chemistry thesis. Dan, for all his help in sharing his experiences of typesetting in \LaTeX and writing a monumental thesis.

Next, all the Colby Chemistry professors, you have been amazing role models. I have learned a lot from you, and I'm very grateful for your patience, passion, and enthusiasm. Your high standards have challenged me to do better. A special thanks to Professor Conry for her guidance as second reader for the thesis.

To all my friends, thank you for your support, confidence and for tolerating my perpetual lab-stemmed tardiness.

Next, I would like to thank my family for their constant motivation and help. I would especially like to thank my parents, Anjali and Shekhar Hardikar for their steadfast faith in my ability to do things and their endless love and help.

This work would, quite literally, not be possible without the National Science Foundation (CHE-1300937).

Thank you!

Contents

Vitae	i
Acknowledgements	ii
List of Figures	vi
Part I: Dimethylalkylidene	1
1 Introduction	3
1.1 A Brief History and Overview of Carbenes	3
1.2 An Introduction to Carbene Behavior and Stability	4
1.3 Generation of Carbenes	6
1.3.1 Generation of Saturated Carbenes	6
1.3.2 Generation of Unsaturated Carbenes	7
1.3.3 Photochemical Generation of Carbenes from Phenanthrene-based Precursors	7
1.4 Carbene Reactivity	10
1.5 Benzyldiene and α -methyl Benzyldiene Carbene	11
1.6 Motivation and Goals	13
2 Results and Discussion	14
2.1 The Synthesis of Phenanthrene-based Precursors	14
2.2 Photolysis of the Dimethylalkylidene Precursor	18
2.2.1 Neat Photolysis	19
2.3 Computational Work	20
2.4 Time-Resolved Laser Flash Photolysis	23
3 Conclusion	25
3.1 Future Work	26
4 Experimental Procedures	27
4.1 General Remarks	27
4.1.1 Reactions	27
4.1.2 Spectra	27
4.1.3 Photolysis	27

4.1.4	Computational Studies	27
4.1.5	X-ray Structures	27
4.2	1,1-dibromo-1a,9b-dihydro-1H-cyclopropa[l]phenanthrene (9) ¹⁴	28
4.3	1-Monobromo-1a,9b-dihydrocyclopropa[l]phenanthrene (10) ¹⁵	29
4.4	1-(propan-2-ylidene)-1a,9b-dihydrocyclopropa[l]phenanthrene (11)	29
4.4.1	Method 1: Petasis ¹⁶	29
4.4.2	Method 2: Takeda ¹⁷	30
4.5	1,1-dichloro-1a,9b-dihydro-1H-cyclopropa[l]phenanthrene (14) ³⁰	31
4.6	2-(1-bromo-1a,9b-dihydro-1H-cyclopropa[l]phenanthren -1-yl)propan-2-ol (18) ¹⁹	31
4.7	Photolysis	32
Part II: Diphenyl Ketene		32
5	Introduction	35
5.1	A Brief History and Overview of Ketenes	35
5.2	Methods of Generation of Ketenes	36
5.3	Reactivity of Ketenes	38
5.3.1	Some Characteristic Ketene Reactions	38
5.3.2	Geometry and Orientation of Ketene Reactions	39
5.4	Where Are We Going? Where Have We Come From?	41
6	Results and Discussion	43
6.1	Synthesis of Phenanthrene-based Precursor	43
6.2	Photolysis	45
6.2.1	Photolysis with Methanol	47
6.2.2	Photolysis with Diethylamine	48
6.2.3	Photolysis 2,3-dimethyl 2-butene	48
6.2.4	Neat Photolysis	50
6.3	Computational Studies	50

7 Conclusion	51
7.1 Future Work	51
8 Experimental Procedures	53
8.1 General Remarks	53
8.1.1 Reactions	53
8.1.2 Spectra	53
8.1.3 Photolysis	53
8.1.4 Computational Studies	53
8.1.5 X-ray Structures	53
8.2 2,2-diphenyl-2a,10b-dihydrocyclobuta[1]phenanthren -1(2H)-one (22) ^{19,41,43}	54
8.3 Photolysis	54
8.3.1 With Methanol	54
8.3.2 With Diethylamine	55
8.3.3 With 2,3-dimethyl 2-butene	55
8.3.4 Neat Photolysis	55
Bibliography	55
9 Appendix A: Spectra	58
10 Appendix B: Computational Studies	85
Coordinates and Energies for Optimized Dimethylalkylidene Carbene Singlet, (3S) Report . .	85
Coordinates and Energies for Optimized Dimethylalkylidene carbene Triplet (3T) Report . . .	87
Coordinates and Energies for Optimized Dimethylalkylidene carbene Transition State Report	88
Coordinates and Energies for Optimized 2-Butyne Report	89
Summary of Calculations Report	90
Coordinates and Energies for Optimized Diphenyl Ketene (24) Report	91
Coordinates and Energies for Optimized Diphenyl Ketene Precursor (22) Report	92
Coordinates and Energies for Optimized Phenanthrene Report	93
11 Appendix C: Crystal Structure Determination	94

List of Figures

1.1	Saturated carbene (left); Unsaturated carbene (right).	4
1.2	Orbital occupation and spin states for saturated carbenes (top). (from L to R): singlet, excited singlet, triplet. Orbital occupation and spin states for unsaturated carbenes (bottom). (from L to R): singlet, excited singlet, triplet.	5
1.3	Dimethylalkylidene is an unsaturated carbene where both substituents on the double bond are methyl groups. This carbene, 3 , is the principle focus of this work.	5
1.4	Generation of carbenes via the decomposition of diazo compounds.	6
1.5	Generation of carbenes via the photolysis of ketenes.	6
1.6	Generation of carbenes via the hydrolysis of haloforms.	7
1.7	(top) Generation of alkylidenes using diazo compounds. (bottom) Photochemical generation of alkylidenes using ketenes.	7
1.8	Richardson and coworkers generated methylene by photolyszing a cyclopropanated phenanthrene derivative.	8
1.9	The method used by the Thamattoor group to generate alkylidenes via the photolysis of phenanthrene based derivatives.	8
1.10	The synthesis of the di-bromo substituted cyclopropyl phenanthrene system. ¹⁴	9
1.11	A proposed method of synthesizing the precursor for dimethylalkylidene. ^{15,16}	9
1.12	A second proposed synthesis for the precursor for dimethylalkylidene. ¹⁷	9
1.13	A summary of unsaturated carbene reactions.	11
1.14	Moore and Viduarri-Martinez's work in 2012 showed that the photolysis of the phenanthrene based precursor resulted in the synthesis of phenylacetylene.	11
1.15	With this precursor, photolysis resulted in 73% alkyne rearrangement and 1.5% carbene trapping.	12
1.16	The phenanthrene derivative precursor for dimethylalkylidene.	13
2.1	A synthesis of dibrominated cyclopropanated phenanthrene. ¹⁴	14
2.2	A synthetic pathway to convert 9 to the monobrominated species 10 ¹⁵ , followed by a Wittig-type process to convert it to the precursor 11 . ¹⁶	15
2.3	The mechanism for the Petasis reaction. Note that the cyclopropyl species is connected to phenanthrene, but is not shown here for clarity.	15

2.4	The mechanism for the Takeda reaction. Note that the cyclopropyl species is connected to phenanthrene, but is not shown here for clarity.	16
2.5	An alternative method of synthesizing the carbene precursor 11 . ¹⁹	17
2.6	Photolysis of the dimethylalkylidene precursor 11	18
2.7	Rearrangement of the dimethylalkylidene precursor 11 to form a 7-member ring in 18	19
2.8	Energetics of the rearrangement of 3S to 2-butyne. Calculations were performed at the CCSD(T)/cc-pVTZ//B3LYP/6-311++G** level. Note that the 3T is 50.4 kcal/mol higher in energy than the “ground state” singlet.	20
2.9	Energetics of the rearrangement of benzylidene carbene to phenylacetylene (CCSD(T)/cc-pVTZ//B3LYP/6-31+G**) (left). Energetics of the rearrangement of α -methylbenzylidene carbene to the alkyne (CCSD(T)/cc-pVTZ//B3LYP/6-311+G**) (right). ^{12,13}	21
2.10	An overview of the generation of small cycloalkynes from phenanthrene based precursors. Maurer et al. explored systems with $n = 1, 2$. ²¹	21
2.11	Energetics of the rearrangement of cyclic alkylidene carbenes to form cycloalkynes. Calculations were performed at the CCSD(T)/cc-pVTZ//B3LYP/6-31+G* level. Image from Maurer et al. ²¹	22
2.12	A schematic for the bond lengths and angles in the transition state for the methyl shift. Image from Modarelli et al. ⁸	22
2.13	The change in absorbance of 12 over time. The shoulder at 325 nm indicates the generation of the benzylidene carbene. ²²	23
2.14	(top) Theoretical predicted spectrum for the benzylidene carbene using TD-DFT at the B3LYP/6-311G** level of theory. (bottom) Experimentally observed spectrum for the carbene. ²²	23
2.15	Absorbance spectrum for precursor 11 . ²²	24
3.1	A summary of the work done on generating and trapping dimethylalkylidene.	25
5.1	The structure of a ketene and its bonding.	35
5.2	The synthesis of ketenes by reacting acid chlorides with a tertiary amine.	36
5.3	The synthesis of ketenes by reacting acid chlorides with a strong base. ³⁷	36
5.4	Wolff rearrangement is a photochemical route to generating ketenes. The first mechanism shows the possibility of the carbene intermediate while the second one doesn't.	37

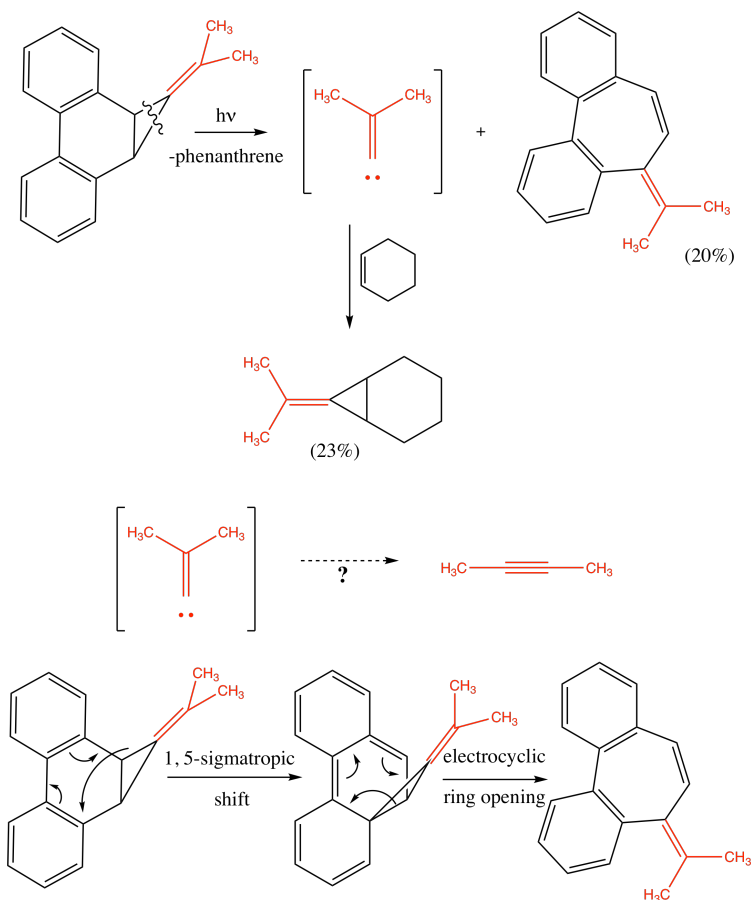
5.5	The synthesis of ketenes by photolysis of diazoketones. (a) The study by Hacker showing the rearrangement via ring contraction. Scaiano studied a similar reaction with a fluorenone base (b). ^{38,39}	37
5.6	A summary of the synthesis of sulfur and selenium based precursors for ketene generation. ⁴⁰	38
5.7	The electron density map for diphenylketene. The red portion shows electron rich regions. The two phenyl planes are orthogonal to each other. Image from Lectka et al. ³¹ . .	38
5.8	Mechanism of attack of nucleophiles on ketenes.	39
5.9	Examples of cycloadditions with ketenes. (top) [2+2], (middle) [3+2], (bottom) [4+2]. ³⁴ . .	39
5.10	Examples of reactions of different functional groups with ketenes. Image from Lectka et al. ³¹	40
5.11	The orthogonal approach of attack for cycloaddition reactions. R _s refers to a small R group, while R _l is a large R group. ³⁴	40
5.12	The diphenylalkylidene carbene 20 , generated by the photolysis of a phenanthrene-based precursor.	41
5.13	The alternate product obtained while trying to synthesize 21	41
5.14	The photolysis of cyclobutanone 22 results in phenanthrene and diphenyl ketene 24 being formed.	42
6.1	The proposed method of synthesizing 21	43
6.2	This compound was the product of the Takeda reaction with benzophenone.	44
6.3	An overview of the proposed synthesis of 21 via the bromohydrin 21	44
6.4	The molecule that was synthesized from 9	45
6.5	The mechanism for the formation of 22 . Note that phenanthrene system is not shown for clarity, but is connected to the cyclopropyl ring.	46
6.6	When dibromo substituent 9 is reacted with fluorenone, the epoxide is formed instead of the cyclobutanone product. ⁴¹	47
6.7	The above intermediate is anti-aromatic and prevents the fluorenone system from proceeding to the cyclobutanone. ⁴¹	47
6.8	The photolysis of 22 with methanol produces an ester 25	48
6.9	The photolysis of 22 with an amine produces an amide 26	49
6.10	The photolysis of 22 with an alkene, should have produced cyclobutane 28	49
7.1	A summary of the photolysis experiments of compound 22	51

9.1	^1H NMR spectrum for 9	59
9.2	^{13}C NMR spectrum for 9	60
9.3	^1H NMR spectrum for 10	61
9.4	^{13}C NMR spectrum for 10	62
9.5	GC/MS data for 10	63
9.6	^1H NMR spectrum for 11	64
9.7	^{13}C NMR spectrum for 11	65
9.8	GC/MS data for 11	66
9.9	IR spectrum for 11	67
9.10	^1H NMR spectrum for 14	68
9.11	GC/MS data for 14	69
9.12	GC/MS data for 15	70
9.13	^1H NMR spectrum for 17	71
9.14	^{13}C NMR spectrum for 17	72
9.15	GC/MS data for 17	73
9.16	^1H NMR spectrum for 18	74
9.17	GC/MS data for 18	75
9.18	Change in peak for 11 over time as the photolysis progresses. (left) is 2 hours of photolysis, while the (right) is 18 hours of photolysis.	76
9.19	^1H NMR spectrum for 22	77
9.20	^{13}C NMR spectrum for 22	78
9.21	GC/MS data for 22	79
9.22	IR spectrum for 22	80
9.23	Change in peak for 25 over time as the photolysis progresses. (left) is 7 hours of photolysis, while the (right) is 16 hours of photolysis.	81
9.24	Change in peak for 26 over time as the photolysis progresses. (left) is 7 hours of photolysis, while the (right) is 12 hours of photolysis.	82
9.25	Change in peak for 24 over time as the photolysis progresses. (left) is 19 hours of photolysis, while the (right) is 38 hours of photolysis.	83
9.26	GC/MS for neat photolysis of 22 at time 16 hours.	84
11.1	Crystal structure for the dimethylalkylidene precursor 11	94
11.2	Crystal structure for the diphenyl ketene precursor 22	102

PART I: DIMETHYLALKYLIDENE

Abstract

Previous studies have shown that the photolysis of phenanthrene-based cyclopropyl precursors can generate carbenes. In this work, a novel phenanthrene precursor was synthesized and photolyzed to generate the dimethylalkylidene carbene, which was subsequently trapped by cyclohexene. The carbene was not prone to an internal rearrangement as some other carbenes are, and instead favored the intermolecular addition reaction. The precursor also underwent a rearrangement via pericyclic processes (figure below). A theoretical analysis of the potential energy surface of the system is presented using coupled cluster and density functional methods. Preliminary analysis for the precursor via time-resolved laser flash photolysis (LFP) was performed. Future experiments include more comprehensive LFP studies on this system in addition to experiments to isolate the elusive rearrangement to 2-butyne. This work provides a safe and synthetically viable route to generate and trap alkylidene carbenes. These alkylidene carbenes provide interesting opportunities to study the migratory aptitudes of various substituents, and provide a fascinating plethora of opportunities to study such intermediates both experimentally and theoretically.



Introduction

1.1 A Brief History and Overview of Carbenes

Carbenes are molecules that contain a neutral divalent carbon atom. Since carbon is typically tetravalent, carbenes tend to be highly reactive. First attempts to generate methylene carbene pre-date knowledge of the tetravalency of carbon. Dumas and Regnault separately tried to dehydrate methanol using phosphorus pentoxide and concentrated sulfuric acid respectively (1830s). Similarly, Perrot studied chloromethane pyrolysis hoping to study the elimination of hydrogen chloride (1857). Butlerov tried treating di-iodomethane with copper to generate methylene, but only observed ethylene (1861). In the 1890s, Nef still believed that methylene ($:\text{CH}_2$) was stable, and that it would be “available in the future.” Clearly, he believed that the issue was the synthesis of methylene, not its stability.¹

It was only with Staudinger’s work in the 1910s that the instability of carbenes was recognized. He studied the decomposition of diazo compounds and ketenes. For a while then, carbenes were classified as diradicals and treated similarly.¹ In 1956, Doering and coworkers reported that methylene was “the most indiscriminate reagent known in organic chemistry,” because of its ability to insert into many C-H bonds, and also add across double bonds.² That was the time when carbenes began to be treated separately from radicals.¹ Just a few years earlier (in 1950), Hine had published remarkable work examining the kinetics of the base-catalyzed hydrolysis of haloforms and the nature of the intermediate.³ This intermediate was identified as “carbon dichloride”, and with Doering’s work a few years later, the dichloride species was connected to methylene carbene.¹

Since the 1950s, much progress has been made in the world of carbene chemistry. Advances in experimental techniques, especially with matrix isolation, laser flash photolysis (LFP), and crystallography, have made carbenes increasingly well-studied intermediates. In 1964, Fischer and Maasböl attached a transition metal, tungsten, to a carbene, creating the first “metal-carbene complex.”⁴ In 1988, Guy Bertrand and coworkers reported the synthesis of a stable phosphinocarbene,⁵ while in 1991, Arduengo reported a crystalline carbene stabilized by (-N-Ad) groups.⁶

In recent years, carbenes have found synthetic uses in catalysis. N-Heterocyclic carbenes (NHCs) have been central components of organometallic synthesis and catalysis.⁴ Carbenes have also been used to synthesize highly-strained cyclopropyl systems, and have found applications in astrochem-

istry.⁴ High oxidation state alkylidene complexes, carbene-based magnets, and metal complexes for organic synthesis are other research areas where carbenes have proven to be useful.⁴ Additionally, carbenes present a unique, exciting, and novel opportunity to study the fundamental chemistry of carbon bond formation and reactivity.

1.2 An Introduction to Carbene Behavior and Stability

Broadly speaking, carbenes can be classified as saturated or unsaturated as shown in Figure 1.1. The carbene carbon atom (**1**) in a saturated carbene forms two σ bonds, and is approximately sp^2 hybridized. However, for an unsaturated carbene (**2**) the carbene carbon forms a double bond with another atom and this π bond makes it approximately sp hybridized instead.

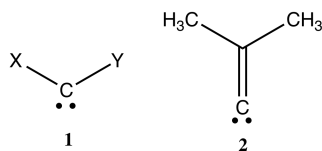


Figure 1.1: Saturated carbene (left); Unsaturated carbene (right).

The orbitals that the two nonbonded electrons occupy play a crucial role in determining carbene reactivity. If the electrons are spin-paired and in the same orbital, then the carbene is said to be a singlet. If electrons are spin-paired, but placed in different orbitals, the carbene is said to be an excited singlet or an open-shell singlet. Finally, if the electrons are not spin-paired, but have parallel spins, and are in different orbitals, then the carbene is a triplet (Figure 1.2). Note that the Pauli exclusion principle precludes a triplet carbene having an empty p orbital, since two electrons with the same spin cannot be in the same orbital.

The terms “singlet” and “triplet” come from the spin multiplicity ($2S + 1$) of the system, where S is the total spin. Electrons are given a quantum number m_s of magnitude $1/2$ where opposite spins are given opposite signs. In the case of the paired electrons, the m_s values add to a total spin of 0, and a multiplicity of 1, from which the name “singlet” is derived. Similarly, in the case of the unpaired electrons, the total spin is 1, leading to a multiplicity of 3, hence, a “triplet.”

Note in the case of the saturated singlet that the electrons are placed in the sp^2 hybrid orbital as opposed to the empty p -orbital. This is because the hybridized orbital has some s character, and therefore has a lower energy than the empty p orbital. Similarly, for unsaturated singlets, the electrons are located in the sp hybrid orbital.

The relative stabilities of the singlet and triplet states for a given carbene depend on the sub-

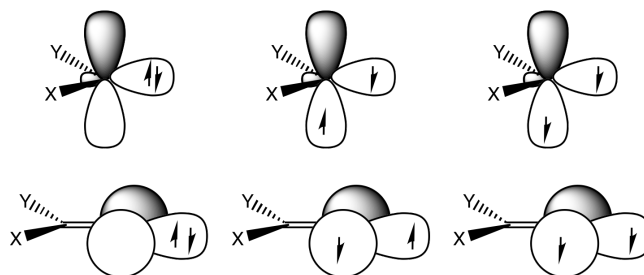


Figure 1.2: Orbital occupation and spin states for saturated carbenes (top). (from L to R): singlet, excited singlet, triplet. Orbital occupation and spin states for unsaturated carbenes (bottom). (from L to R): singlet, excited singlet, triplet.

stituents on the carbene. Triplet states minimize electron-electron repulsion by distributing the electrons over two orbitals. For example, the simplest carbene, methylene, is known to be a triplet while halogenated carbenes tend to be singlets. But, saturated carbenes are typically more reactive in their singlet state, leading to interesting questions regarding thermodynamic versus kinetic reactivity.⁷ However, in unsaturated carbenes, the sp hybridization provides much higher s -character to the electrons (compared to the sp^2 hybridization). This leads to greater stabilization for the electron lone pair, and consequently, the closely held singlet state is much more favorable.

This work focuses on unsaturated carbenes, which are also called alkylidenes. Specifically, this project examines dimethylalkylidene (Figure 1.3). Previous calculations on **3** have shown that it is a ground state singlet with singlet-triplet energy gap of 44-50 kcal/mol.^{8,9}

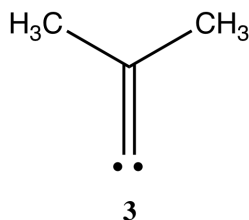


Figure 1.3: Dimethylalkylidene is an unsaturated carbene where both substituents on the double bond are methyl groups. This carbene, **3**, is the principle focus of this work.

1.3 Generation of Carbenes

Some of the oldest methods of generating carbenes were mentioned in the previous section. Several newer methods of carbene generation have been developed and are discussed here.

1.3.1 Generation of Saturated Carbenes

1. Decomposition of Diazo Compounds

In this method of carbene generation, diazo compounds of type **4** or **5** (diazirines) are either photolyzed or pyrolyzed to produce nitrogen gas and a carbene. Figure 1.4 shows the mechanism.¹ While this method of generation is fairly common, these diazo compounds are unsafe to handle, typically being shock sensitive, potentially explosive, and/or carcinogenic.

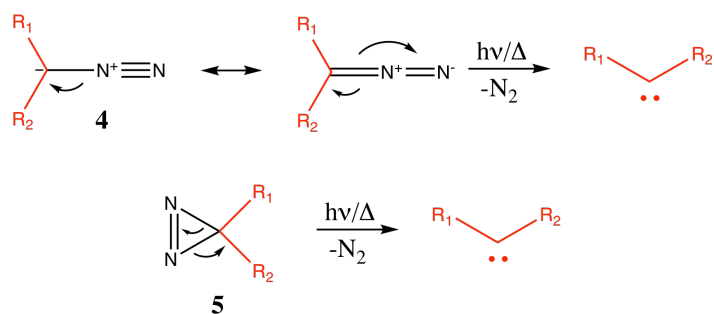


Figure 1.4: Generation of carbenes via the decomposition of diazo compounds.

2. Decomposition of Ketenes

Upon photolysis, ketenes break down to give a carbene and carbon monoxide. When photolyzed at higher frequencies, the breakdown of **6** is immediate, while an excited ketene mechanism is predicted at lower frequencies.¹

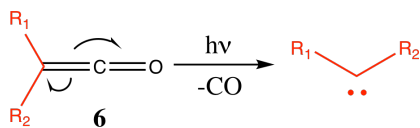


Figure 1.5: Generation of carbenes via the photolysis of ketenes.

3. Base-induced hydrolysis of Haloforms

In a basic environment, haloforms lose a proton and a halogen to form the corresponding dihalo-carbene (Figure 1.6). This method is severely limited by the acidity of the hydrogen, because less

acidic hydrogens cannot be abstracted by the base. After the formation of the anion, a halide is lost to generate the carbene. This method doesn't allow much synthetic flexibility.⁷

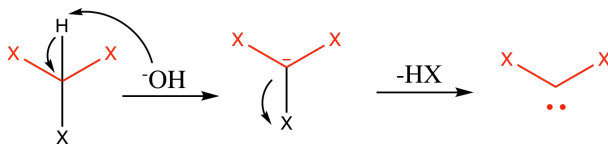


Figure 1.6: Generation of carbenes via the hydrolysis of haloforms.

1.3.2 Generation of Unsaturated Carbenes

Unsaturated carbenes have not been as extensively studied as saturated carbenes. A few common methods of generating saturated carbenes can be used for generating alkylidenes. Thus, appropriate diazo compounds and ketenes can form unsaturated carbenes, as shown in Figure 1.7.

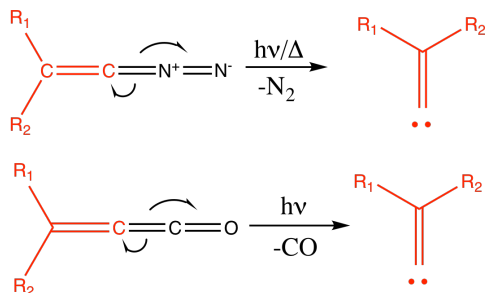


Figure 1.7: (top) Generation of alkylidenes using diazo compounds. (bottom) Photochemical generation of alkylidenes using ketenes.

1.3.3 Photochemical Generation of Carbenes from Phenanthrene-based Precursors

In 1965, Richardson and coworkers reported the generation of methylene from the photolysis of a phenanthrene derivative with a cyclopropyl substituent (Figure 1.8, compound **7** with R₁ = R₂ = H).¹⁰ Using di-iodomethane and zinc dust, they cyclopropanated the phenanthrene system across the 9,10 bond to synthesize **7**. The photolysis causes the cyclopropyl bonds to break and generate the carbene **1** (R₁ = R₂ = H) as shown in Figure 1.8. This method of carbene generation went unnoticed until 1990 when Chateauneuf and coworkers used the same precursor to generate dichlorocarbene.¹¹ Since then, many groups have used similar precursors to generate saturated carbenes.

This reaction is thermodynamically driven since the photolysis relieves the system of ring strain, and there is an overall gain in resonance stabilization energy. This is because phenanthrene's res-

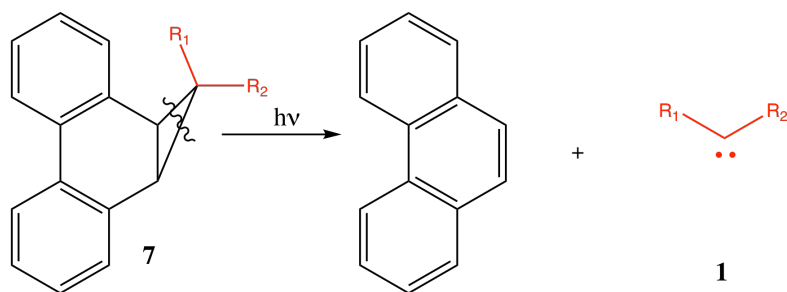


Figure 1.8: Richardson and coworkers generated methylene by photolysing a cyclopropanated phenanthrene derivative.

onance stabilization energy is 92 kcal/mol compared to the energy of the two benzene rings in the precursor (resonance stabilization energy of $2 \times 36 = 72$ kcal/mol).

In recent years, the absence of photochemical methods for alkylidene generation have prompted the Thamattoor lab to explore similar phenanthrene-based precursors for alkylidene generation, with great success.^{12,13} Figure 1.9 presents an overview of such methods. This project specifically examines a phenanthrene-based system that is used to photochemically generate the dimethylalkylidene carbene (**2**, R₁ = R₂ = CH₃).

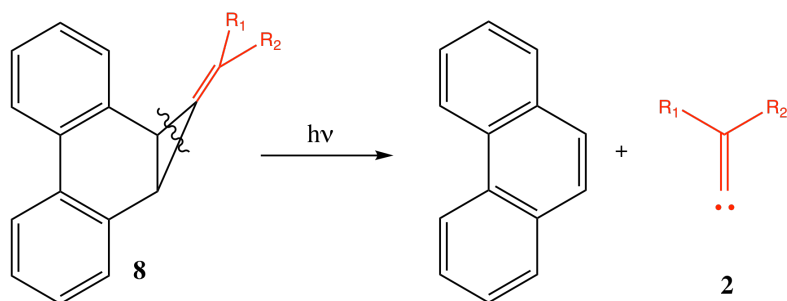


Figure 1.9: The method used by the Thamattoor group to generate alkylidenes via the photolysis of phenanthrene based derivatives.

Synthesis of Phenanthrene-based Precursors

There are various routes to synthesizing phenanthrene systems (**8**) of the type shown in Figure 1.9. In 2007, Nguyen and Thamattoor reported a relatively easy route to synthesizing brominated cyclopropanated-phenanthrene **9** (Figure 1.10).¹⁴ From this dibromo compound, **9**, the goal is to replace the halogenated groups with a substituted double bond. While multiple synthetic routes for this transformation were considered and tried, two of the most promising ones are presented below.

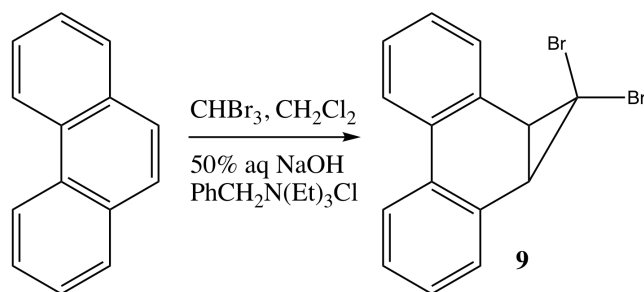


Figure 1.10: The synthesis of the di-bromo substituted cyclopropyl phenanthrene system.¹⁴

1. Synthesis via the mono-brominated substituent

In this method of synthesis, the di-bromo substituent would be reduced to a mono-bromo substituent (**10**) using *n*-BuLi. Then, **10** would be subjected to a titanium promoted Wittig-type reaction with acetone.^{15,16} This reaction is shown in Figure 1.11 and is an adaption of a method presented by Petasis et al.

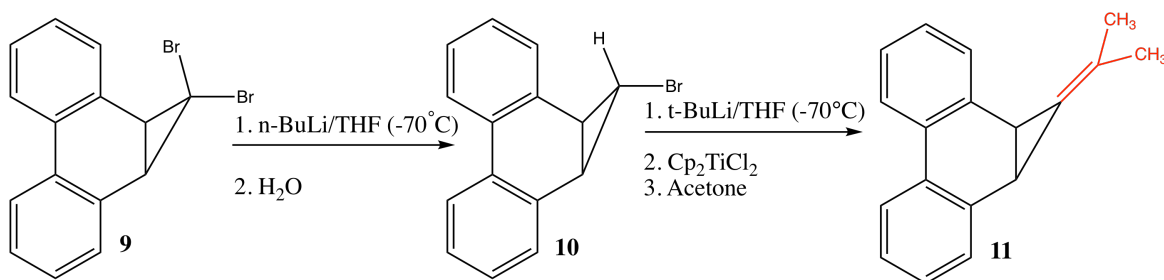


Figure 1.11: A proposed method of synthesizing the precursor for dimethylalkylidene.^{15,16}

2. Synthesis from the di-bromo substituent

In this method of synthesis, the di-bromo substituent is directly reacted with a titanium promoter along with triethylphosphite and magnesium followed by the addition of acetone.¹⁷ This reaction is shown in Figure 1.12 and is an adaptation of the method presented by Takeda et al.

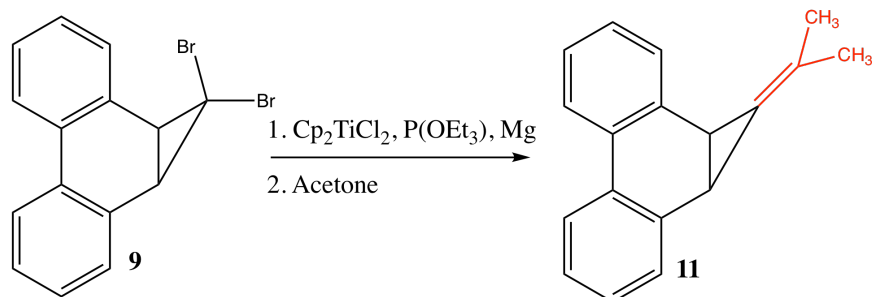


Figure 1.12: A second proposed synthesis for the precursor for dimethylalkylidene.¹⁷

1.4 Carbene Reactivity

Carbenes undergo a few characteristic reactions that distinguish them from other intermediates and unstable species. As discussed earlier, carbenes can insert themselves into σ bonds, such as C-H and O-H. As early as 1956, Doering had reported that methylene is indiscriminate in its insertion into various types of C-H in a wide variety of alkanes. Similarly, carbenes can also insert themselves into O-H bonds to convert hydroxy groups to alkoxy groups. However, neither reaction is the focus of this work, and is therefore not presented in much detail here.

Then, the most important and relevant carbene reaction to this work is its addition across a double bond. When a carbene interacts with a double bond, the nonbonded electrons and the π electrons from the double bond are used to make two σ bonds to form a cyclopropyl ring. This addition plays an important role in this work for both synthesis and analysis.

The spin multiplicity of the carbene in this addition reaction is crucial in determining the adduct's stereochemistry. In 1956, Woodworth and Skell proposed a mechanism that uses the law of spin conservation to explain the stereochemistry of this addition.¹⁸ A singlet carbene reacts in a single-step mechanism, since both electrons are spin-paired and can directly form a bond with the π system in the double bond of the alkene. Since this is a concerted mechanism, the stereochemistry about the double bond is maintained. However, in the case of triplets, both electrons have the same spin. Therefore, to actually construct a bonding orbital, one electron needs to undergo a spin flip. Without this spin flip, the bonding cannot occur, because two electrons with the same spin cannot be in the same orbital. Such a spin flip is typically occurs on a slower timescale than that for carbon-carbon bond rotation, and this leads in a loss of stereoselectivity for the alkene.

A reaction that is specific to an alkyldiene is its rearrangement to an alkyne by a 1,2-shift. In this reaction, the lone pair on the carbene carbon moves to the C=C bond to form a triple bond while one of the groups on the sp^2 carbon migrates to the carbene carbon to give a substituted alkyne. For non-identical substituents, either substituent has the potential to migrate. The substituent that has a pathway with a lower transition state energy is expected to migrate, which is ultimately determined by the steric and electronic stabilities of the corresponding transition state.

The addition and rearrangement reactions are crucial mechanisms for "taming" the carbene (Figure 1.13). In the case of the first, an alkene addition results in a cyclopropyl ring that can be used to distinguish and identify the carbene. In case of rearrangement, the alkyne provides important information regarding the carbene. A ^{13}C labeled carbene also allows the identification of the mobile

substituent group. However, the rearrangement to the alkyne offers no evidence of carbene formation since there is no “trapping” of the carbene—the alkyne formation may well be a concerted mechanism from the precursor. This difference will be of crucial importance and will be discussed further later.

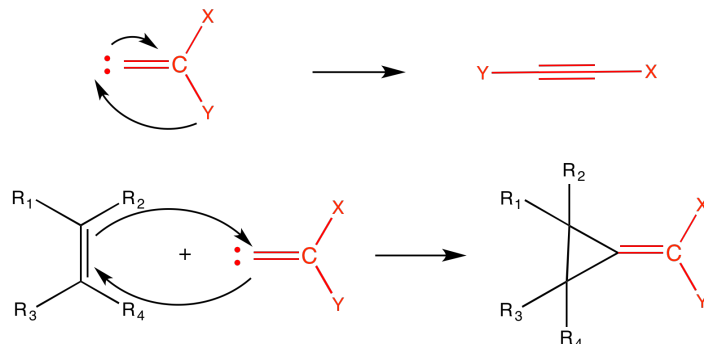


Figure 1.13: A summary of unsaturated carbene reactions.

1.5 Benzylidene and α -methyl Benzylidene Carbenes

In 2012, Moore and Vidaurri-Martinez¹² presented a novel study wherein they synthesized a cyclopropanated phenanthrene system, **12**. It was observed that upon photolysis, phenylacetylene was formed. When the same experiment was repeated with a labeled precursor, the ¹³C carbon was found bonded to the phenyl ring, suggesting a hydrogen shift (Figure 1.14).

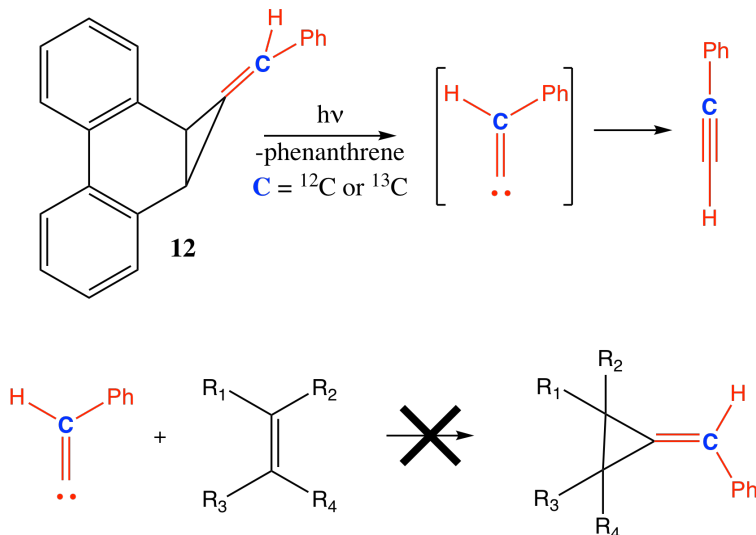


Figure 1.14: Moore and Vidaurri-Martinez’s work in 2012 showed that the photolysis of the phenanthrene based precursor resulted in the synthesis of phenylacetylene.

Experimental work was supported by computational studies. Hydrogen's migration was thermodynamically more favorable than the phenyl migration by roughly an order of magnitude. However, the proposed carbene intermediate could not be trapped in the presence of a variety of alkenes, and therefore, the carbene mechanism could not be fully supported. This work led to a few important questions about alkyne formation and migratory aptitudes: what group chooses to move? What drives this movement? Does an alkyne rearrangement have to occur?

In 2016 Yang and Languet¹³ explored these questions further by considering a similar phenanthrene system with phenyl and methyl substituents. Upon photolysis, prop-1-yn-1-ylbenzene was formed as the main product (Figure 1.15). When a similar labeling experiment was performed, the phenyl group was found to migrate to form the alkyne. The carbene intermediate was trapped by cyclohexene, albeit in a very low quantity (1.5% yield). In this case, computational work supported the movement of the phenyl group. The phenyl group, despite being more sterically hindered, stabilizes the transition state with its π electron ring.

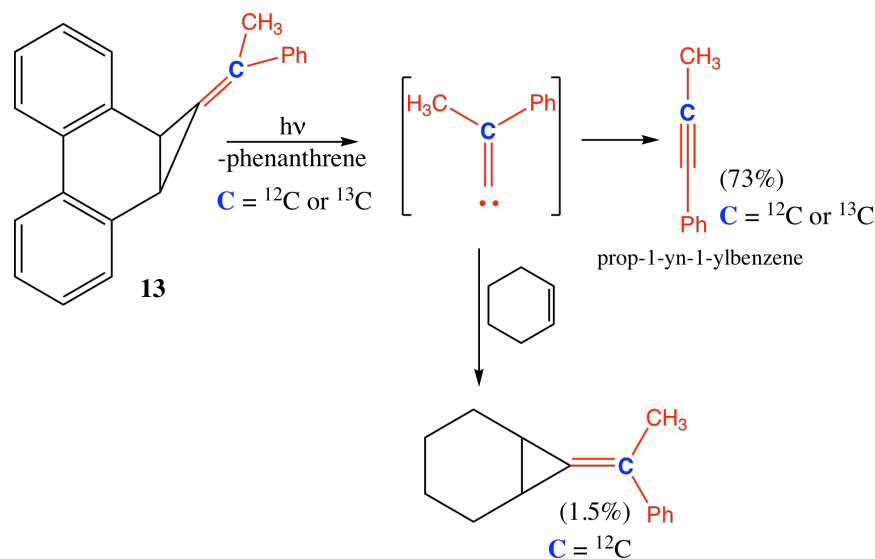


Figure 1.15: With this precursor, photolysis resulted in 73% alkyne rearrangement and 1.5% carbene trapping.

This work provided further evidence that the photolysis reaction resulted in the formation of a carbene intermediate that subsequently rearranged to form a thermodynamically stable product. Furthermore, it demonstrated a need for more studies to better understand the substituent migration properties of alkylidenes.

1.6 Motivation and Goals

Modarelli et al., in 2001, generated dimethylalkylidene in an argon matrix at 14 K. They trapped the carbene in the matrix with CO. Analyzing their products via IR spectroscopy and comparing spectra to computed spectral patterns, they did not find the presence of 2-butyne.⁸ They calculated the barrier to a 1,2-methyl shift to be around 10-12 kcal/mol, which is considerably higher than the energies required for a hydrogen and phenyl shift as calculated by Moore and Yang respectively.^{12,13} This high barrier provides an exciting opportunity to trap the carbene and truly “tame” it, providing concrete evidence for a carbene mechanism for the post-photolysis chemistry. Therefore, this project’s goal was to synthesize **11** (Figure 1.16), probe its photochemical reactivity, and attempt to trap carbene **3**. If the rate of rearrangement is slower than the rate of alkene addition, then this alkylidene would indeed provide support for a carbene generation during the photolysis. The photolysis of this phenanthrene precursor is strongly thermodynamically driven, since it gains resonance stabilization energy from the regeneration of phenanthrene. However, the final stable product, be it the trapped carbene or the rearranged carbene, is determined by the transition state barriers, and their relative rates. If the methyl groups provide a sufficiently high enough barrier to migration, the trapping would indeed be the favorable outcome. This project also examines various methods of synthesizing the precursor **11**.

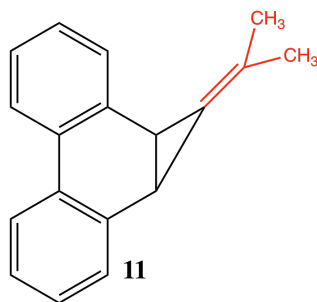


Figure 1.16: The phenanthrene derivative precursor for dimethylalkylidene.

Furthermore, calculations at the CCSD(T)/cc-pVTZ//B3LYP/6-311++G** level were undertaken. Previous calculations are outdated, and new calculations at enhanced levels of theory would allow comparison to those for other carbenes. Additionally, laser flash photolysis at a femto- and pico- second level was used to study the carbene on timescales comparable to its lifetimes.

The successful trapping of the carbene leads to many other interesting questions and fields of study. Can methyl groups migrate? Can substituent migration be predicted? And indeed, can this system of photochemically generating alkylidenes provide a safe and flexible method to explore alkylidenecarbene reactivity, stability, and bonding?

Results and Discussion

2.1 The Synthesis of Phenanthrene-based Precursors

The phenanthrene-based precursor **11** was synthesized via a three step pathway beginning with phenanthrene. In the first step, **9** was synthesized via a carbene reaction as shown in Figure 2.1.¹⁴ A strong base, sodium hydroxide was used to deprotonate bromoform, making the tribromomethyl anion. The subsequent loss of a bromine ion generated the dibromocarbene which added across the 9,10 double bond in phenanthrene to form **9**. Triethylbenzylammonium chloride was used as a phase transfer catalyst to facilitate the interaction of reactants between the aqueous and organic phases. While there are multiple double bonds in phenanthrene, addition only occurs across the 9,10 bond. This is because this addition maintains the aromaticity of the two benzene rings to provide a resonance stabilization energy of $2 \times 36 \text{ kcal/mol} = 72 \text{ kcal/mol}$, which is greater compared to the resonance stabilization energy of naphthalene (if the addition was across any other non-fused bond) which is only 60 kcal/mol. The product was identified by NMR spectroscopy and spectra were compared with literature.¹⁴

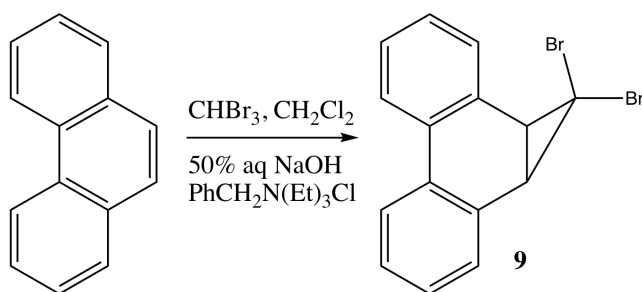


Figure 2.1: A synthesis of dibrominated cyclopropanated phenanthrene.¹⁴

This dibromo-cyclopropyl substituent **9** was then reacted with *n*-butyllithium to form **10** (Figure 2.2). This reaction causes a bromine-lithium exchange, driven by the fact that the corresponding cyclopropyl anion is more stable than a butyl anion. Upon quenching with water, the anion was protonated to form **10**. This monobromo substituent is the *exo*-isomer as opposed to the *endo*-isomer. This was confirmed via proton NMR using coupling constants. The monobromo product was identified by NMR spectroscopy and spectra were compared with literature.¹⁵

The monobromo substituent **10** was then reacted with *t*-butyllithium, titanocene dichloride and acetone to form the desired precursor **11**. This method, adapted from the Petasis reaction, follows a

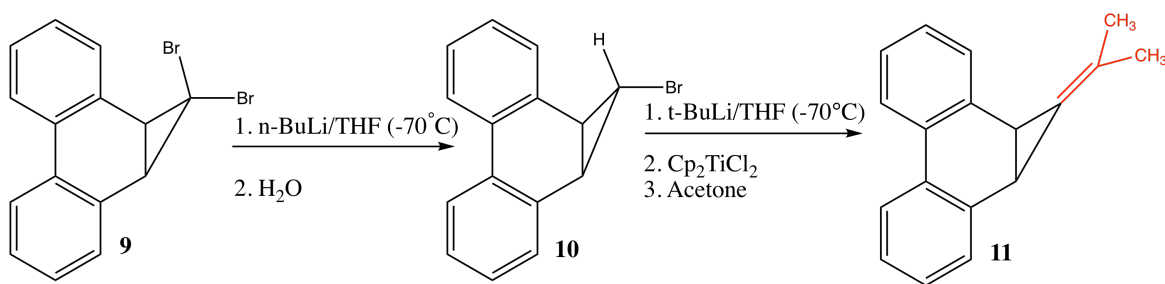


Figure 2.2: A synthetic pathway to convert **9** to the monobrominated species **10**¹⁵, followed by a Wittig-type process to convert it to the precursor **11**.¹⁶

Wittig-type mechanism. The *t*-butyllithium first dehalogenates **10** to create a cyclopropyl anion. Note that just as in second step, the driving force for the halogen-lithium exchange is the relative stability of the cyclopropyl anion. However, in this case a stronger organolithium is needed compared to the earlier step since the anion derived from **10** is less stable than that from **9**. Upon generation of the anion, titanocene dichloride loses its chloride ligands via attack of the anion. Steric proximity allows one cyclopropyl substituent to deprotonate the other, leading to a doubly bonded titanium species. However, the other cyclopropyl species forms **7** ($R_1 = R_2 = H$). This is a major drawback of the method, since the yield is necessarily at most 50%. After the loss of the dihydrogen phenanthrene species, the ketone adds across the titanium species, to create a 4-member intermediate, which then gives the final precursor (Figure 2.3).

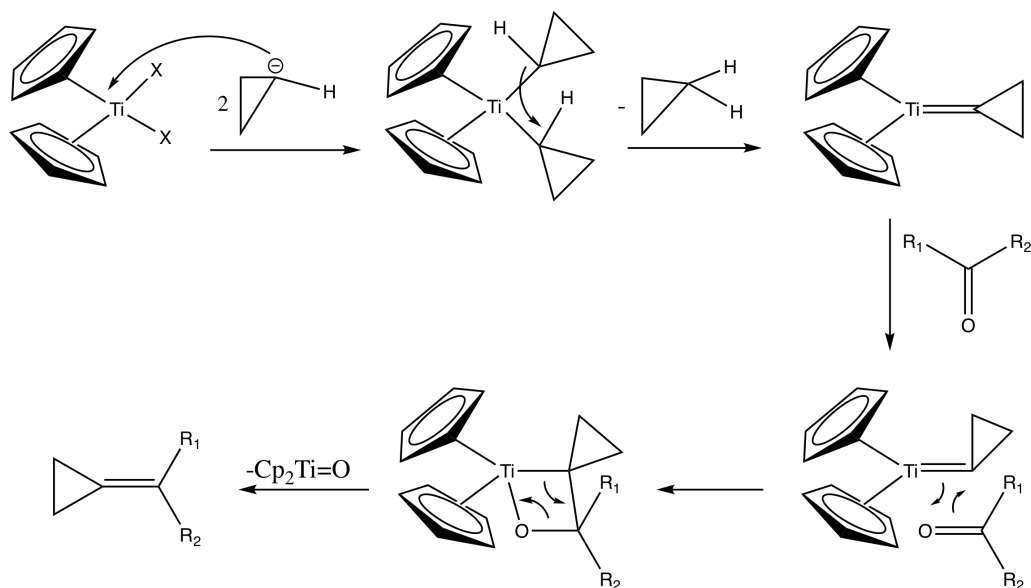


Figure 2.3: The mechanism for the Petasis reaction. Note that the cyclopropyl species is connected to phenanthrene, but is not shown here for clarity.

In addition to losing half the starting material as a byproduct, this reaction is resource-intensive. The synthesis consists of two reactions involving organolithium reagents, with the Petasis method needing molar quantities of titanocene dichloride and an overnight reflux. Therefore, another method of synthesizing **11** was sought.

This procedure is an adaptation of a method from Takeda group, which again follows a Wittig type mechanism (Figure 2.4). In this mechanism, the dibrominated phenanthrene compound, **9**, directly reacts with titanocene dichloride and acetone to give the precursor **11**. First, the triethyl phosphite reduces Ti(IV) to Ti(II). The magnesium recovers the lost chloride ions. Then, the halogenated phenanthrene compound **9** forms a double bond with titanium. The addition of the ketone leads to a four-member intermediate, which breaks to give the desired compound, **11**.

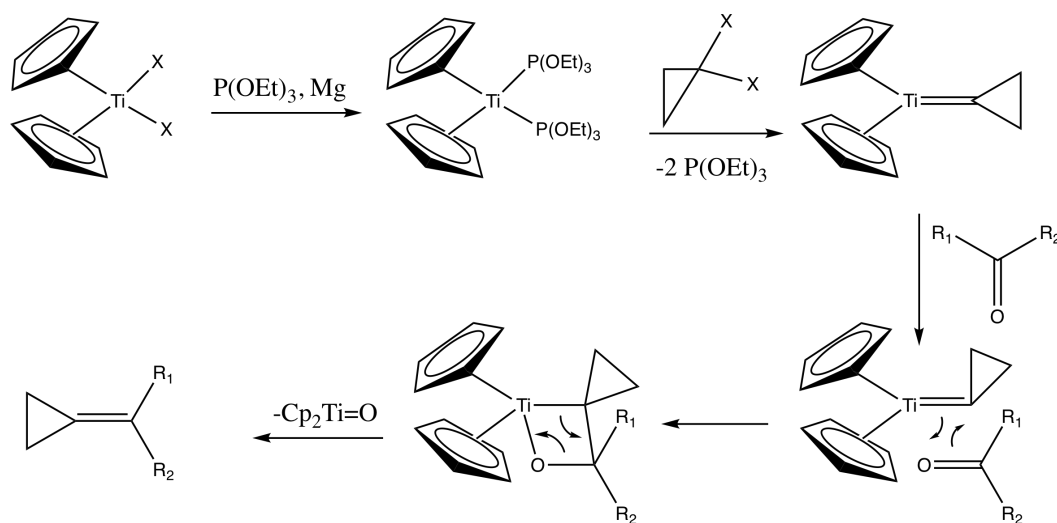


Figure 2.4: The mechanism for the Takeda reaction. Note that the cyclopropyl species is connected to phenanthrene, but is not shown here for clarity.

There are many advantages to this route of synthesis. First, 50% product is not necessarily lost as a byproduct. Additionally, this reduces the synthesis to two steps using commercially available products. Finally, the reaction procedure doesn't necessitate the use of highly reactive organolithium species and can be performed at room temperature. Irrespective of method of synthesis employed, the precursor **11** was identified by NMR spectroscopy and GC/MS. As expected, the ^1H NMR spectrum for the precursor shows a large singlet for the six methyl protons at 1.7 ppm. Additionally, there is another upfield peak at 3.12 ppm for the two protons on the 9,10 phenanthrene bond. A large cluster of peaks in the aromatic region correspond to the phenanthrene protons. Similarly, for the ^{13}C NMR spectrum, two upfield peaks are seen again for the sp^3 carbon from the methyl groups, and the 9,10 phenanthrene carbons. The spectra also shows ten unique carbon environments, as one would expect

from the molecule. Additionally, the GC/MS showed a clear sharp peak at 11.7 minutes at $m/z = 232$ for the compound. A crystal structure was obtained for the molecule, which showed a C_s point group, which agrees with the number of carbon environments predicted in the molecule. All spectra along with a crystal structure are provided in the Appendix.

However, this “Takeda” method was not as reliable as “Petasis” method, as the reaction did not consistently yield **11**. The Takeda synthesis has worked well for cyclic ketones for other projects in the lab, suggesting, that it is somehow the acyclic nature of acetone that is affecting this reaction.

Another possible route to synthesizing the precursor **11** was explored, but was not fully executed. In this method of synthesis, the dibromo species **9** was reacted with *n*-butyllithium and acetone, to create a bromohydrin, **15**. This compound was then reacted with iodotrimethylsilane (TMSI) and hexamethyldisilazane (HMDS) to make **16**. The goal was to then remove the bromohydrin functionality to generate the required double bond, and make **11** (Figure 2.5).

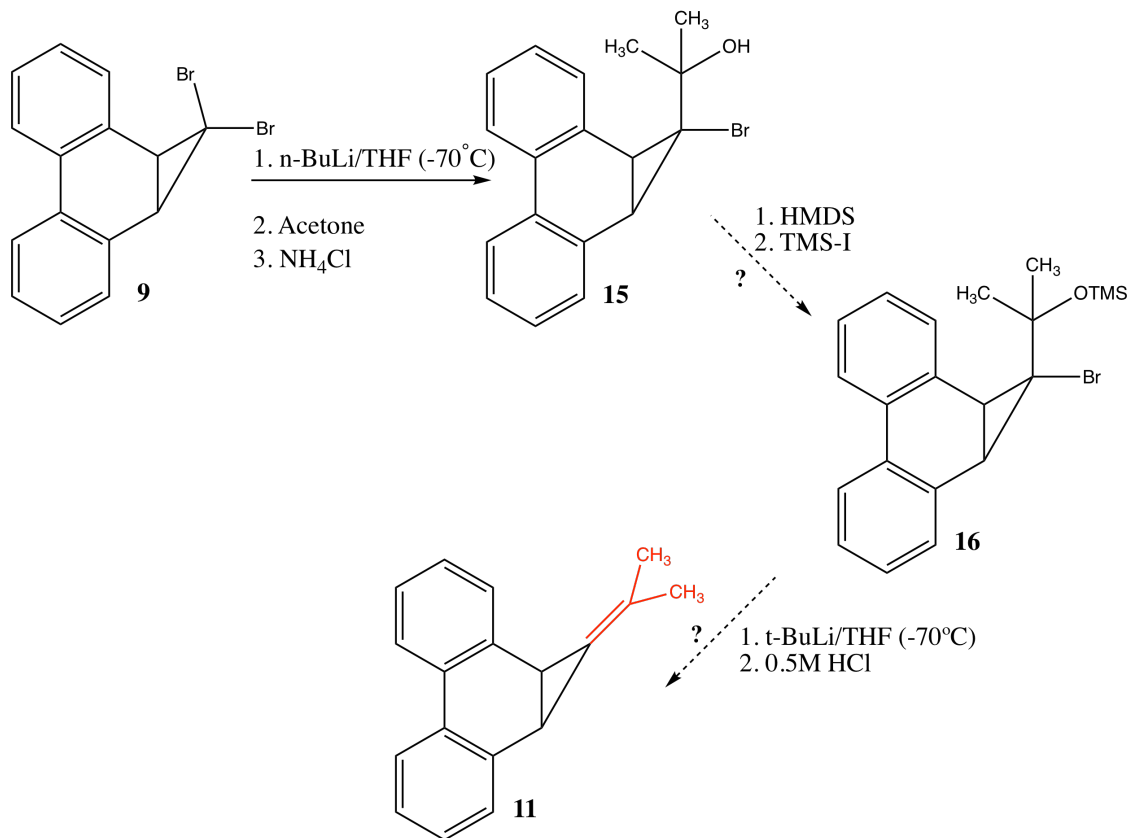


Figure 2.5: An alternative method of synthesizing the carbene precursor **11**.¹⁹

As shown in Figure 2.5, this method was not explored fully. While it is an additional step compared to the “Petasis” method, it has the advantage of not needing molar quantities of titanocene dichloride.

2.2 Photolysis of the Dimethylalkylidene Precursor

The dimethylalkylidene precursor, **11**, was photolyzed in the presence of the trapping agent cyclohexene. The carbene of interest, **3**, was generated that then proceeded to add across the double bond in cyclohexene. No internal rearrangement of the carbene was observed, such as the one to 2-butyne. The carbene was actually trapped! As discussed earlier, the driving force for the photolysis is the increased resonance stabilization energy of phenanthrene compared to that of two benzene rings (in **11**), in addition to the relief of ring strain.

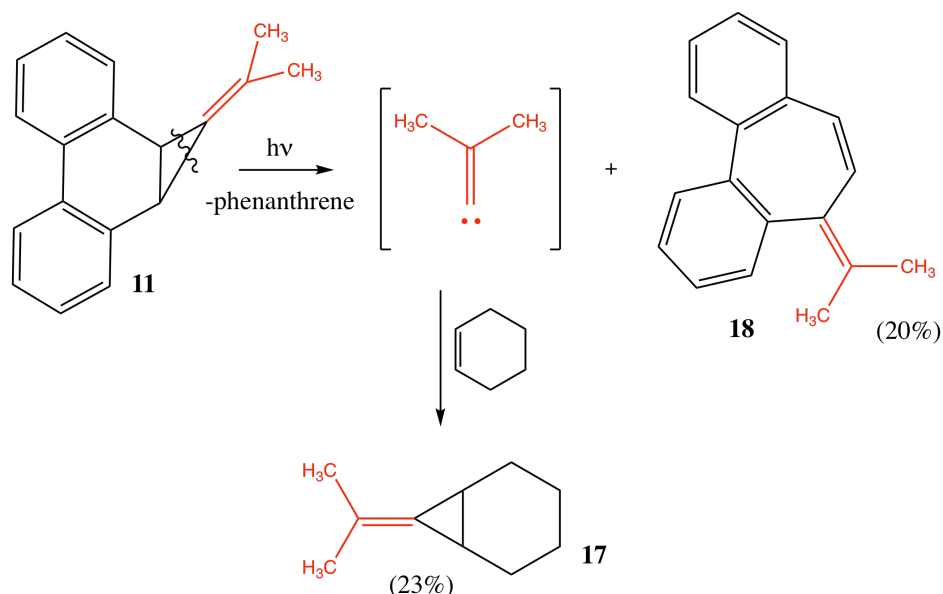


Figure 2.6: Photolysis of the dimethylalkylidene precursor **11**.

The precursor also underwent a rearrangement to form **18**. This process, shown in Figure 2.7, occurs via a 1,5-sigmatropic carbon shift that is photochemically driven. Being a photochemical [1,5] shift, it follows from the Woodward-Hoffman rules that this shift must be antarafacial. Followed by this shift, the cyclopropyl ring opens electrocyclically to relieve strain, to form a seven-member ring. This isomer is not photolabile, unlike **11**. This rearrangement is similar to what Dr. Sonoda and group proposed for their bicyclo triene derivatives.²⁰

The trapped product **17** was identified by NMR spectroscopy and GC/MS. The GC/MS showed a clear peak for $m/z = 136$ for the trapping. Additionally, the ^1H NMR spectrum shows six distinct environments, with appropriately aligned integrals for the molecule. Similarly, **18** was identified and characterized by NMR spectroscopy. Now, because of the asymmetric seven membered ring, the two methyl substituents were no longer homotopic. This can be seen by the presence of two upfield signals

(there are no other hydrogens bonded to sp^3 -hybridized carbons), that have roughly the same integral. The yield for the precursor was calculated by an internal standard of 2-methylnaphthalene. A known quantity of 2-methylnaphthalene was used, which has its distinct, single upfield peak. The integral of this peak was compared to the integral of one of the methyl signals from **18**, and the yield was calculated. For the rearranged product, a GC/MS peak was observed at $m/z = 232$ at a conspicuously different retention time. Neither molecule's crystal structure was obtained (**17** is an oil). All spectra are provided in the Appendix.

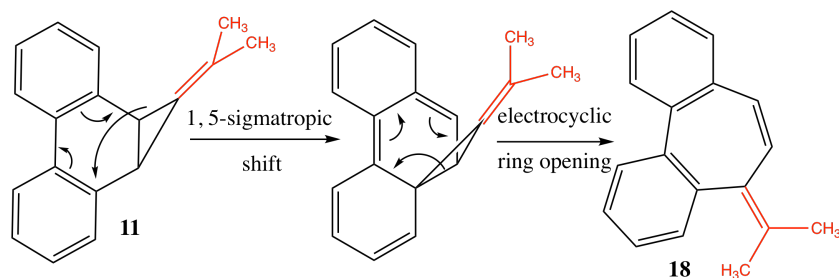


Figure 2.7: Rearrangement of the dimethylalkylidene precursor **11** to form a 7-member ring in **18**.

Dimethylalkylidene's lack of rearrangement may be attributed to the migratory aptitude of the two methyl groups. First, examining the work of Moore and Viduarri-Martinez, it is seen that for benzylidenecarbene, a hydrogen shift leads to formation of phenylacetylene.¹² A hydrogen shift has been attributed to its relative small size and propensity to tunnel. Similarly, in Yang and Languet's work on the α -methylbenzylidene carbene, it was not the smaller, seemingly more likely, methyl group that shifted. There was an exclusive phenyl shift, that can be justified by considering the stability of the transition state. The carbene carbon has an empty p orbital (on account on being a singlet), and the phenyl ring has π electron system. These electrons can donate to the empty p orbital to create a stable transition state with a temporary 3 member ring. In case of **11**, the methyl groups have neither the advantage of the tunneling from the hydrogen, nor the π stabilization from the phenyl groups. The transition state for the rearrangement is too high a barrier to cross, leading to **3** being trapped by cyclohexene to form **17**.

2.2.1 Neat Photolysis

A photolysis of **11** in the absence of any trapping agents was attempted. This was done to see if **3** did an internal rearrangement in the absence of competing intermolecular reactions. Note that the methyl migration is not conclusively disproven; it is just an unfavorable reaction pathway. The product of **3**'s rearrangement is 2-butyne. However, being a gas, the compound was very difficult to track and

identify over the course of the reaction.

For a possible attempt at capturing and isolating 2-butyne, the experiment would have to be conducted at low temperatures, with the photolysis being tracked by a low temperature NMR probe.

2.3 Computational Work

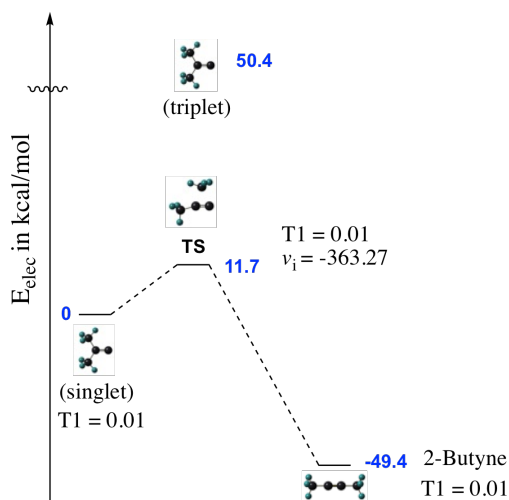


Figure 2.8: Energetics of the rearrangement of **3S** to 2-butyne. Calculations were performed at the CCSD(T)/cc-pVTZ//B3LYP/6-311++G** level. Note that the **3T** is 50.4 kcal/mol higher in energy than the “ground state” singlet.

Computational studies were performed on the dimethylalkylidene **3**, its precursor **11**, and the potential energy of possible reactions of this system (Figure 2.8). These calculations were performed at the CCSD(T)/cc-pVTZ//B3LYP/6-311++G** level. It was found that the triplet state energy for carbene **3** was 50.4 kcal/mol higher than the singlet state energy. This agrees with the understanding that alkylidenes prefer the singlet state since electrons are placed in a lower energy hybridized sp orbital with greater s -character than the p orbital. The transition state barrier for the alkyne rearrangement was 11.7 kcal/mol, while the alkyne was 49.4 kcal/mol more stable than the singlet carbene. The transition state for system was recognized by the presence of one imaginary frequency at -363.27 $1/\text{cm}$. The validity of coupled cluster calculations can be verified by the T1 diagnostic of 0.01 for the singlet, transition state, and 2-butyne calculations.

Moore et al.’s work on the benzylidene carbene showed that the transition state for the hydrogen shift was about 20 times more energetically favored than the phenyl shift (Figure 2.9). It was observed that the hydrogen shift required very little extra motion to “tip over” to the carbene carbon, since the hydrogen- π bond angle was reduced considerably.¹² Similarly, for Yang et al.’s work on the α -methylbenzylidene carbene, the methyl shift was about 4 times more unfavorable than the phenyl

shift. In this case as well, the triplet carbene was about 37 kcal/mol more unstable than the triplet.

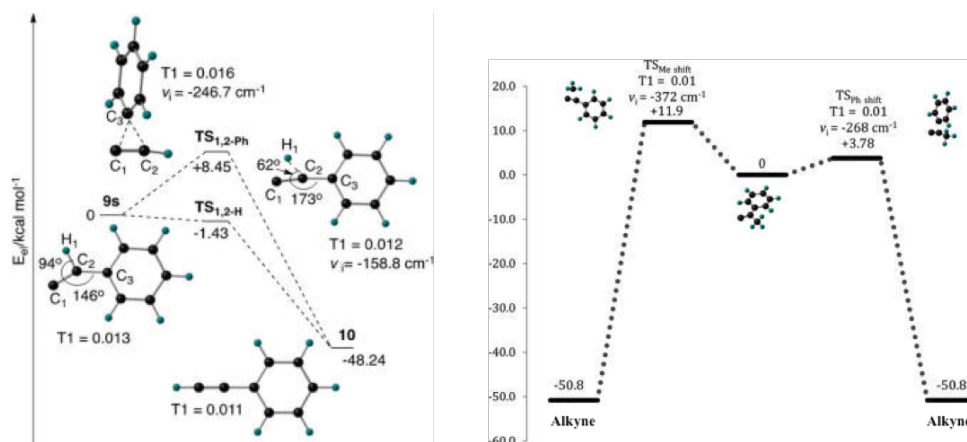


Figure 2.9: Energetics of the rearrangement of benzylidene carbene to phenylacetylene (CCSD(T)/cc-pVTZ//B3LYP/6-31+G**) (left). Energetics of the rearrangement of α-methylbenzylidene carbene to the alkyne (CCSD(T)/cc-pVTZ//B3LYP/6-311+G**) (right).^{12,13}

In both these previous studies, the numbers seem to indicate that the rearrangement of the alkyli-dene is solely dependent on kinetic factors, namely the height of the barrier for the transition state to the alkyne. However, there are other factors involved. Earlier this year, Maurer and Fan published a study on generating small cycloalkynes via photochemical generation of systems like **8** where the R₁ and R₂ groups were connected (Figure 2.10).

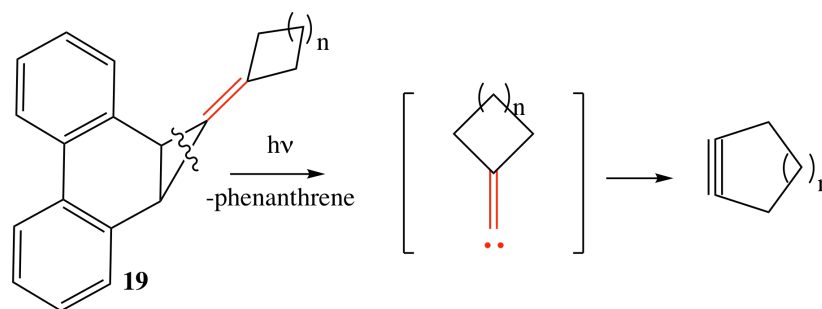


Figure 2.10: An overview of the generation of small cycloalkynes from phenanthrene based precursors. Maurer et al. explored systems with $n = 1, 2$.²¹

In their work, they found that the transition state for rearrangement to a cyclohexyne (from cyclopentylidene carbene) had a barrier of 9.1 kcal/mol while the transition state barrier to cyclopentyne from cyclobutylidene carbene was 1.6 kcal/mol (Figure 2.11). This is quite surprising, since the cyclobutylalkylidene is very similar to **3**: in fact, one can think of “tying” the two methyl groups in **3** with a carbon, to form the cyclobutylalkylidene carbene.

Modarelli et al. showed in 2001, that the transition state was kinetically so unfavorable because the *sp*³ carbon had to stretch to bond lengths of 1.7 Å (compared to 1.517 Å in the carbene), and

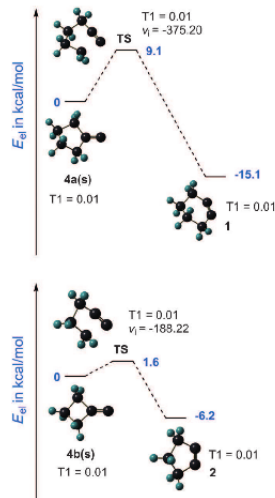


Figure 2.11: Energetics of the rearrangement of cyclic alkylidene carbenes to form cycloalkynes. Calculations were performed at the CCSD(T)/cc-pVTZ//B3LYP/6-31+G* level. Image from Maurer et al.²¹

the distance between the two forming C-C bonds was 1.821 Å, with 2.3 Å still to go. As shown in Figure 2.12, the non-migrating methyl group made an angle of 166° with the π system.⁸ While these calculations were performed over 15 years ago, they illustrate an important point. Methyl groups aren't prone to rearrangement because they have a terrible migratory aptitude, borne from a highly strained transition state.

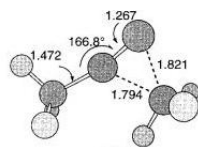


Figure 2.12: A schematic for the bond lengths and angles in the transition state for the methyl shift. Image from Modarelli et al.⁸

While Modarelli and group showed methyl's unwillingness to move in an Argon matrix at 14 K, this project here shows the first instance of the photochemical generation of the dimethylalkylidene carbene **3** in solution phase at room temperature, wherein methyl's resistance to shifting is observed again. Additionally, calculations on this system were outdated, and this project provides fresh calculations with extended basis sets for both density functional theory, and coupled cluster analysis.

2.4 Time-Resolved Laser Flash Photolysis

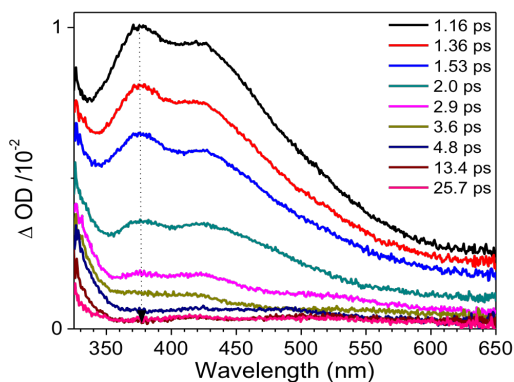


Figure 2.13: The change in absorbance of **12** over time. The shoulder at 325 nm indicates the generation of the benzylidene carbene.²²

Time-resolved laser flash photolysis analysis was performed on the precursor **11** in a collaboration with Professor David Lee Phillips from Hong Kong University. Extensive studies were performed on the benzylidene carbene, which track the kinetics and spectral properties of the precursor on femtosecond timescales. As shown in Figure 2.13, the compound **12** shows two strong peaks, that decline over about 20 ps. These peaks correspond to excitations in **12**. However, over time, a shoulder at 325 ps is seen that corresponds to the beginning of the generation of the carbene.

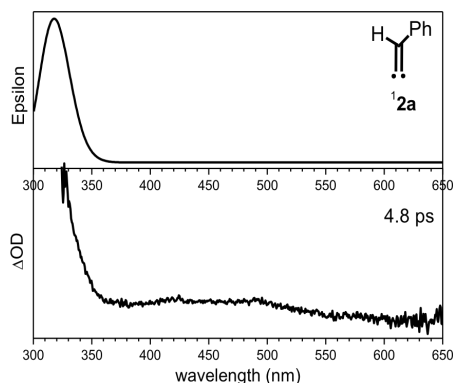


Figure 2.14: (top) Theoretical predicted spectrum for the benzylidene carbene using TD-DFT at the B3LYP/6-311G** level of theory. (bottom) Experimentally observed spectrum for the carbene.²²

When additional kinetic studies were performed, it was seen that the precursor generated the carbene in 4.8 ps, while it took another 11 ps for the carbene to rearrange to phenylacetylene. Figure 2.14 shows the absorbance of the carbene, as seen experimentally and predicted computationally.

It was hoped that dimethylalkylidene carbene **3**, would show similar definitive results providing an understanding of the kinetics of carbene generation. However, preliminary studies of the system

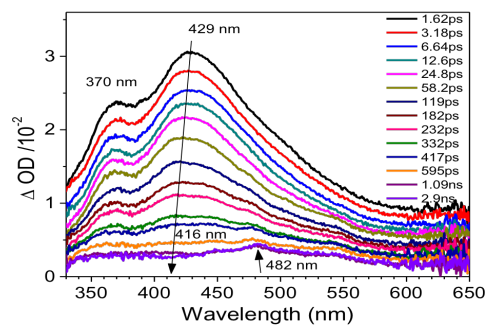


Figure 2.15: Absorbance spectrum for precursor **11**.²²

show that **3** doesn't have a strong absorbance in the region, because of the absence of a π system of electrons. Therefore work on this system is in its early stages, though it is hoped that kinetic analysis can provide a timeframe for the generation of this carbene.

Conclusion

This work provided a safe method of photochemically generating dimethylalkylidene **3** from a novel phenanthrene based precursor **11** in solution. Two different methods of synthesizing this precursor were examined: one is an adaptation from the “Petasis” method, while another is developed from the work of Takeda. Upon generation, the carbene reacted with cyclohexene to form adduct **17**. The precursor **11** also underwent a sigmatropic shift and a ring opening process to form **18**, an isomer (Figure 3.1). Unlike other alkylidenes, an internal rearrangement of **11** to yield 2-butyne was not observed. Computational studies using coupled cluster and density functional methods were performed. These showed that the triplet carbene was 50.4 kcal/mol more energetically unfavored than the singlet carbene. The transition state barrier for the rearrangement was 11.7 kcal/mol, with 2-butyne 49.4 kcal/mol more stable than the singlet carbene. Preliminary laser flash photolysis analysis on **11** showed that the carbene was not photoactive in the range of 325 - 650 nm.

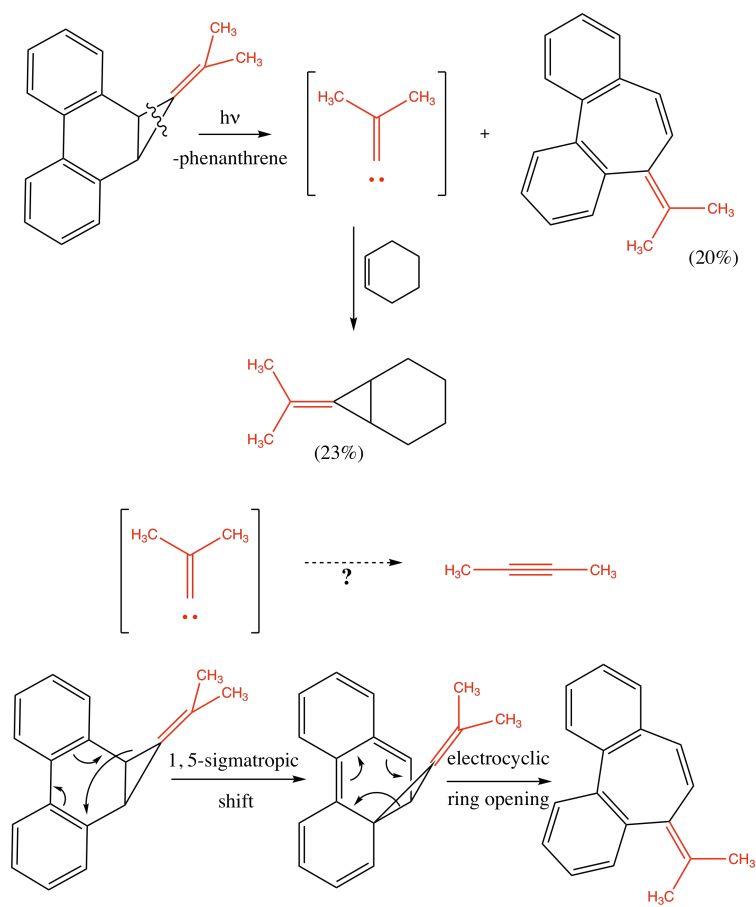


Figure 3.1: A summary of the work done on generating and trapping dimethylalkylidene.

3.1 Future Work

There are two main sources of future work in this area. Firstly, more extensive studies on the femtosecond timescale should provide a kinetic framework for the dimethylalkylidene carbene. The goal would be to understand how fast the carbene is generated, and how quickly it rearranges or adds.

Secondly, there is more work to be done on either capturing the carbene rearrangement product, 2-butyne or conclusively showing the impossibility of this rearrangement. This neat photolysis would have to be conducted at relatively low temperatures and monitored in a low temperature to actually track the progress of the generation of the alkyne.

Experimental Procedures

4.1 General Remarks

4.1.1 Reactions

Tetrahydrofuran was dried with activated alumina. The inert gas used was argon. All other chemicals were commercially bought and used as received. Flash chromatography was performed using a Combiflash instrument with “Gold” pre-packed columns on silica.

4.1.2 Spectra

All NMR spectra were collected in CDCl_3 at 500 MHz for ^1H and 125 MHz for ^{13}C . All chemical shifts were recorded in ppm. GC/MS were recorded on a capillary gas chromatograph coupled with a quadrupole, triple-axis mass selective detector operating in electron impact (EI) mode. IR spectra were collected using ATR-FTIR spectroscopy.

4.1.3 Photolysis

All photolysis experiments were performed using a Rayonet photochemical reactor equipped with 16 12-inch 8 W lamps with output in the range 315 to 400 nm.

4.1.4 Computational Studies

All calculations were run on Gaussian 09. Geometry optimization of **3** and **11** was done using density functional methods with the B3LYP method using the 6-311++G** basis set. Single point energy calculations were done using the CCSD(T) method at the cc-pVTZ level of theory.²³

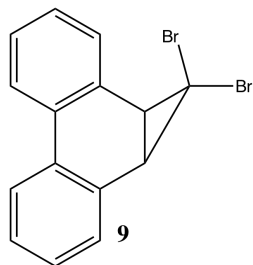
4.1.5 X-ray Structures

X-ray data were acquired at 173 K using a Bruker Smart Apex CCD diffractometer with graphite monochromated $\text{Mo K}\alpha$ radiation ($\lambda = 0.71073 \text{ \AA}$). Bruker Apex3 suite of programs was used to process the data²⁴ and the frames were integrated using the Bruker SAINT software.²⁵ The data was corrected for absorption effects using the multi-scan method SADABS.²⁶ Structure solution and refinement by least-squares on F^2 was done by using the Bruker SHELXTL software package.²⁷ Non-hydrogen atoms

were refined anisotropically and hydrogen atoms were calculated using a riding model. The .cif files were validated with the checkCIF/Platon facility using enCIFer.^{28,29}

4.2 1,1-dibromo-1a,9b-dihydro-1H-cyclopropa[l]phenanthrene

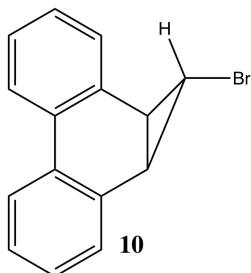
(9)¹⁴



To a slurry of 35.6 g (0.2 mol) phenanthrene, 0.5 g (0.002 mol) benzyltriethylammonium chloride, 40 mL dichloromethane, 40 mL (0.46 mol) bromoform and 1 mL ethanol, 80 mL 50% NaOH was added slowly while stirring. Over the course of the addition, the mixture turned dark orange, and was frothy. The reaction was left stirring loosely stoppered at room temperature for four days. The resultant mixture was combined with dichloromethane and water (100 mL each). The layers were separated, and the aqueous layer was extracted with dichloromethane (2×50 mL). All organic layers were combined and washed with 2 M HCl (2×100 mL), water (2×100 mL), and brine (100 mL). The solvent was allowed to evaporate from this organic suspension. Then, the resulting solid was recrystallized using chloroform. Vacuum filtration afforded the product, a white crystalline solid (22 g, 31.4%). NMR spectra agreed with literature spectra for the molecule.

4.3 1-Monobromo-1a,9b-dihydrocyclopropa[1]phenanthrene

(10)¹⁵

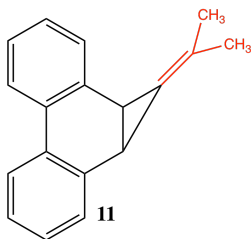


In an oven dried flask, 10.5 g (30 mmol) of **9** was dissolved in 160 mL dry THF under argon. The solution was cooled to -65°C using a dry ice/acetone bath and stirred. 14 mL of *n*-butyllithium solution (2.5 M in hexanes) was added dropwise over the course of 20 minutes, keeping the temperature below -65 °C throughout the addition. The reaction mixture was left stirring at -65 °C for 90 minutes before 10 mL of water was added slowly to quench the reaction. The ice bath was removed after 10 minutes, allowing the reaction mixture to come up to room temperature. The resulting solution was combined with 50 mL of water and separated. After the initial separation, the aqueous layer was extracted with diethyl ether (2 × 50 mL). All organic layers were then combined, and washed with water (2 × 40 mL) and brine (40 mL). The suspension was dried with sodium sulphate. The solid was recrystallized in hexanes. On vacuum filtration, a crystalline white product was obtained (3.7 g, 45.7%). Spectral data agreed with literature values for the molecule.

4.4 1-(propan-2-ylidene)-1a,9b-dihydrocyclopropa[1]phenanthrene

(11)

4.4.1 Method 1: Petasis¹⁶



In an oven dried flask, 13 mL *t*-butyllithium solution (1.7 M in pentane) was added dropwise to a stirred solution of **10** (2.7 g, 10 mmol) in anhydrous tetrahydrofuran (60 mL) at -70 °C under Argon. The reaction was stirred for 45 minutes before 1.0 g (4 mmol) of titanocene dichloride was added. The ice bath was changed to a regular ice/water bath after 15 more minutes of stirring. After 90 minutes of steady stirring where the temperature was maintained at or below 5 °C, 1.5 mL (2.04 mmol) of dry acetone was added. A water reflux was set up, and the reaction mixture was heated up to 70 °C after 20 minutes. The reflux was continued for 15-20 hours. The flask was then rinsed with diethyl ether (50 mL). The rinse was added to the reaction mixture. After solvent had evaporated, the remaining solid was recrystallized using hexanes. Vacuum

filtration afforded a fluffy white solid as the product (288 mg).

4.4.2 Method 2: Takeda¹⁷

From **9**:

In a flask, 935 mg of 4 Å molecular sieves and 445 mg (~ 18.29 mmol) of crushed magnesium were added and kept in an oven overnight. The flask was then cooled under argon, and 4.45 g (~ 17.9 mmol) of titanocene dichloride was added. 24 mL of dry THF and 6.5 mL (~ 36.79 mmol) of triethyl phosphite were added to the flask and the mixture was stirred for 3 hours. Then, 2.1440 g (6.02 mmol) of **9** was dissolved in 14 mL THF and added to the reaction mixture. After an hour, 210 µL of propanone was added to the mixture. After stirring for an hour at room temperature, the reaction mixture was filtered through cellite. The filtrate was left to evaporate. Upon evaporation, it was dissolved in a 1:1 mixture of hexanes and ethyl acetate and filtered through silica gel. The solvent was again allowed to evaporate and resultant solid was subsequently recrystallized in 190 proof ethanol. This afforded a light white solid.

Note: a similar synthesis is followed for using the dichloro variant of **9**, **14**.

IR (measured in 1/cm): 3030.93, 3066.85, 2926.77, 2970.10, 2909.57, 2849.64, 2712.90.

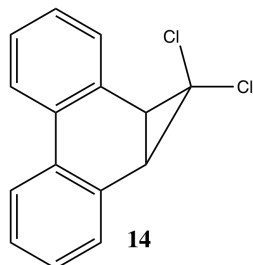
GC-MS: Retention time - 11.73 minutes; Fragments (in m/z): 232.1, 217.1, 202.1, 189.1, 178.1, 165.1.

NMR (in ppm): ¹H: δ = 1.70 (s, 6H), 3.12 (s, 2H), 7.26 (m, 4H), 7.41 (d, 2H), 7.97 (d, 2H); ¹³C: δ = 21.3, 22.3, 119.1, 122.2, 123.2, 125.8, 127.7, 128.8, 129.2, 134.0.

Melting point: 148°C - 151°C.

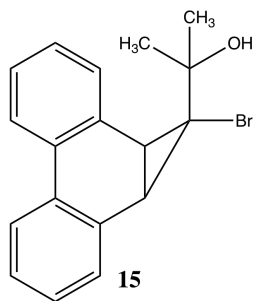
4.5 1,1-dichloro-1a,9b-dihydro-1H-cyclopropa[l]phenanthrene

(14)³⁰



To a flask with an attached condenser, 18.3 g (0.1 mol) phenanthrene, 0.278 g *n*-hexadecyltrimethyl ammonium chloride and 30 mL chloroform were added and stirred. 60 mL 50% NaOH was added to this mixture slowly. The reaction mixture was stirred at 50°C for about 36 hours. The resultant mixture was combined with 50 mL CH₂Cl₂ and 50 mL water. After an initial separation, the aqueous layer was extracted with dichloromethane (2 × 50 mL) and the extracts were added to the organic layer. The organic suspension was then washed with 5% HCl (2 × 75 mL), water (2 × 50 mL), and brine (2 × 75 mL). The solvent was allowed to evaporate from this organic suspension. The resulting solid was recrystallized using ethanol. Vacuum filtration afforded the product, a white crystalline solid. Spectra obtained agreed with literature spectra for the compound.

4.6 2-(1-bromo-1a,9b-dihydro-1H-cyclopropa[l]phenanthren-1-yl)propan-2-ol (18)¹⁹



In an oven dried flask, 3.534 g (~ 10 mmol) of **9** was dissolved in 50 mL of dry THF. While stirring, the mixture was cooled to -70°C in a dry ice/acetone bath, and 4.5 mL of *n*-butyllithium (2.5 M in hexanes) was added dropwise. The reaction turned green immediately. After about 2 hours of stirring, 0.7 mL (~ 10mmol) dry propanone was added slowly, upon which the reaction turned yellowish. After about 2.5 hours of stirring, the ice bath was removed, and the reaction was allowed to warm to room temperature. The reaction was quenched by 10 mL of ammonium chloride. The work up was as follows: the reaction mixture was separated with 75 mL dichloromethane and water each. The aqueous layer was extracted with CH₂Cl₂, and organic layers were combined. The organic layer was washed with water (2 × 50 mL) and brine (3 × 50 mL), and was dried with sodium sulfate. The mixture was separated by flash chromatography on an alumina column (hexanes → 10% ethyl acetate). Like fractions were combined and solvent was allowed to evaporate to give a solid (444.6 mg, 13.5%).

GC-MS: Retention time - 14.5 minutes; Fragments (in *m/z*): 310.0, 231.1, 215.1, 202.1.

4.7 Photolysis

232 mg of dry **11** was dissolved in 10 mL of cyclohexene in a vial. The vial was placed under an UV lamp with a range of 315-400 nm. The photolysis was discontinued after 18 hours, when on checking by GC-MS, there was no peak for the precursor. The solution was poured into a pre-packed silica column. Column chromatography was performed using hexanes, on a 40 g silica cartridge. Like fractions were combined. This gave the trapped carbene (31.6 mg), along with a rearrangement of the original precursor (47.76 mg).

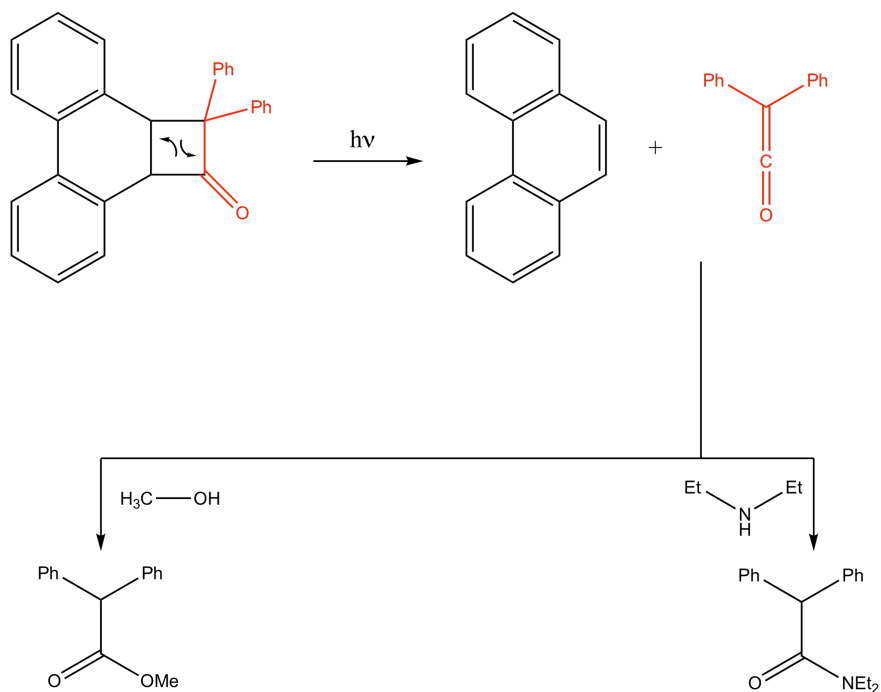
The trapped product was characterized as follows:

GC-MS: Retention time - 3.28 minutes; Fragments (in m/z): 136.1, 121.1, 107.1, 93.1, 79.1, 67.1
NMR: (in ppm) ¹H: δ = 1,19 (m, 4H), 1,5 (d, 2H), 1,69 (t, 4H), 1,79 (s, 6H); ¹³C: δ = 12.69, 21.47, 21.69, 22.64, 119.99, 125.63.

PART II: DIPHENYL KETENE

Abstract

Previous work has established various methods of photochemically generating ketenes. However these methods typically rely on the use of carcinogenic, highly reactive diazoketones. This work expands on a recent study that photochemically generated diphenyl ketene to include preliminary product studies. Diphenyl ketene was generated via the photolysis of a cyclobutyl-phenanthrene based precursor. It was subsequently trapped using methanol and diethylamine to form an ester and an amide respectively. A preliminary computational study on the energetics of the system has been done that shows the products to be 7 kcal/mol more stable than the starting precursor. Future plans include expanding the focus of the work to include other trapping pathways for the ketene, such as dimerization and cycloaddition. Extending recent laser flash photolysis (LFP) analysis to a broader range of reactions will provide more kinetic results on the behavior of ketenes. This is of interest to both experimentalists and theoreticians alike, since currently there is no thorough understanding of the reactivity of ketenes, and the intermediates that are formed in the process.



Introduction

5.1 A Brief History and Overview of Ketenes

Ketenes are derivatives of allenes where one of the terminal carbon atoms is replaced by an oxygen. The central carbon forms a double bond with an oxygen atom and a carbon atom, and is therefore sp hybridized. The remaining terminal carbon is sp^2 hybridized. Just like allenes, the two sets of π bonds are formed in two different planes, as shown in Figure 5.1. Similar to the story of the carbene, first attempts to recognize, isolate and understand ketenes stem from the efforts of Hermann Staudinger in Germany in the early 1900s. In 1905, working in Strasbourg, Staudinger was trying to isolate an α radical acid chloride, but ended up making diphenylketene ($R_1 = R_2 = \text{Ph}$ in Figure 5.1).³¹



Figure 5.1: The structure of a ketene and its bonding.

By 1908, Staudinger in Germany and Chick and Wilsmore in England had both described ketenes. Staudinger had in fact performed extensive studies on diphenylketene and produced a groundbreaking treatise on it.³²⁻³⁴ In 1912, Staudinger had written a book in German, “*Die Keten*” (The Ketene) and had established its reactivity. The cycloaddition reactions of ketenes were one of the first “no mechanism” reactions to be studied.³⁵

Ketenes are incredibly reactive, and because of this a large number of synthetic applications have been explored and developed. With Staudinger’s discovery of cycloaddition reactions, a wide variety of addition reactions were attempted. For instance, one of these is the synthesis of a β -lactam, which has applications as an antibiotic, in addition to being a synthon for broad range of compounds.³⁶ As described by Lectka et al., ketenes have these incredible applications since they provide a chiral center for asymmetric reactions, adding stereochemistry to syntheses.³¹ This leads to the creation of chiral auxiliaries, which are subsequently used to construct stereocenters.

5.2 Methods of Generation of Ketenes

One of the most common methods of generating ketenes is by reacting acid chlorides with a tertiary amine. Upon loss of the chloride, the carbonyl carbon forms an additional bond with the R substituent to form a ketene (Figure 5.2).

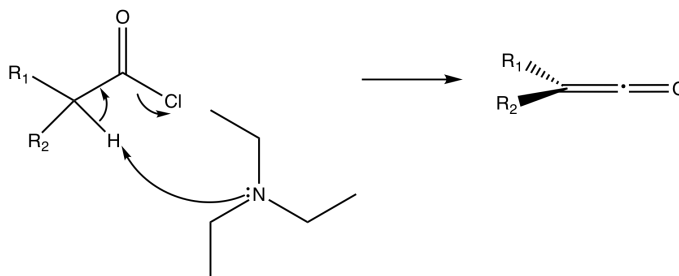


Figure 5.2: The synthesis of ketenes by reacting acid chlorides with a tertiary amine.

In recent years, many different routes to generating ketenes have been explored. For instance, in 2012, Hawker et al. showed a method of generating ketenes via thermal activation of Meldrum's acid derivatives in polymeric structures (Figure 5.3).³⁷ A more common pyrolytic method to generate ketenes is by thermally cracking cyclobutanones. Reacting acids with acid anhydrides followed by pyrolysis is another method of generating ketenes.³¹

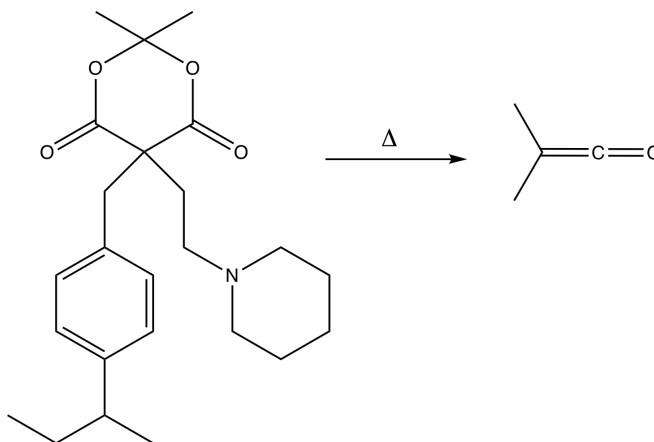


Figure 5.3: The synthesis of ketenes by reacting acid chlorides with a strong base.³⁷

One of the most common photochemical methods of generating ketenes is via the Wolff rearrangement. A diazoketone loses nitrogen gas upon photolysis, and rearranges to give the ketene. This mechanism could be via a ketocarbene, but this is not confirmed.⁷ It is possible that the ketene is formed directly (Figure 5.4). This method of generating ketenes has some issues though, since it involves the use of diazo compounds which are notoriously reactive, unstable, and carcinogenic.⁷

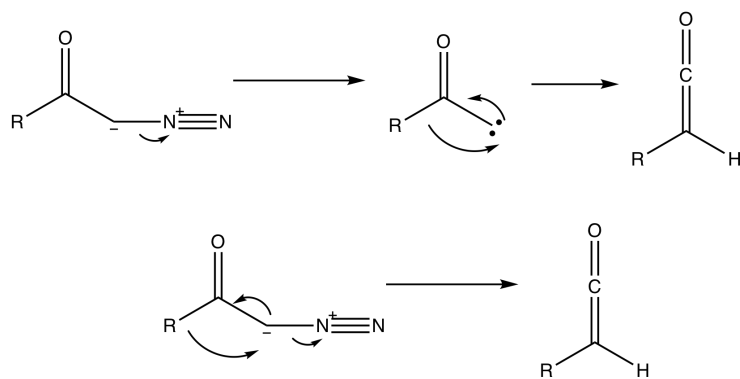


Figure 5.4: Wolff rearrangement is a photochemical route to generating ketenes. The first mechanism shows the possibility of the carbene intermediate while the second one doesn't.

In the last few decades there have been some new interesting photochemical routes to ketene generation as well. In 1982, Turro and Hacker photolysed 1-diazo naphthalenone compounds, which resulted in the formation of indan-based ketenes. This synthesis relied on the loss of nitrogen, leading to an internal rearrangement via a ring contraction, pushing one carbon out to form the ketene. A carbene intermediate is a possibility for this reaction.³⁸ A few years later, in 1997, Scaino et al. extended this method of generating ketenes to fluorenone-based systems (Figure 5.5). They studied the system and the generation of the ketene using laser flash photolysis with IR and UV detection to provide a kinetic analysis of the reactivity of the ketenes. This analysis showed that up to a nanosecond time scale, a carbene intermediate was not necessary for the reaction mechanism.³⁹

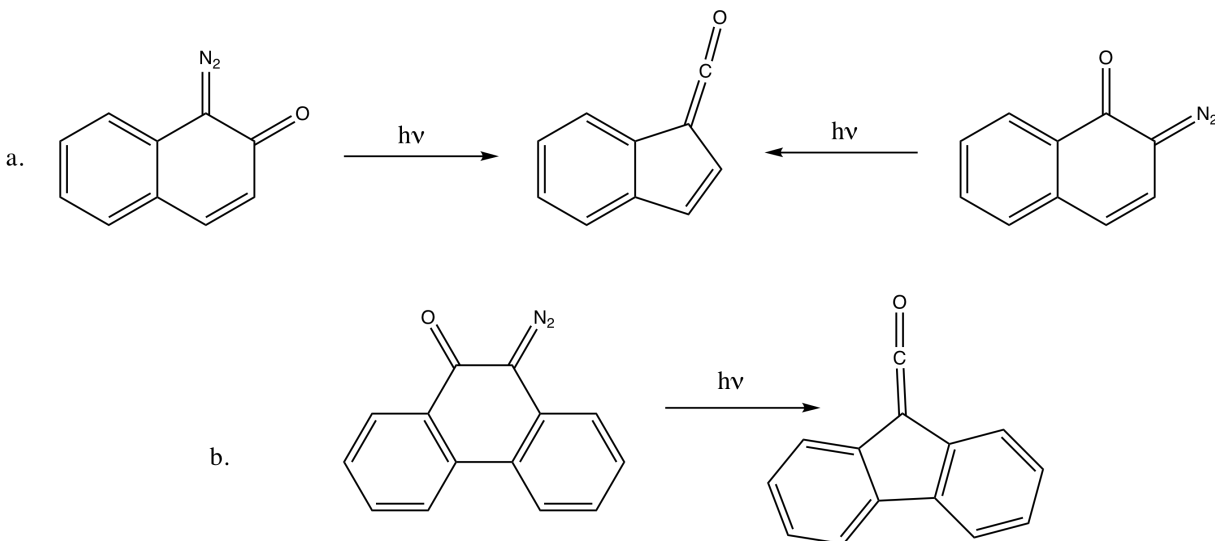


Figure 5.5: The synthesis of ketenes by photolysis of diazoketones. (a) The study by Hacker showing the rearrangement via ring contraction. Scaino studied a similar reaction with a fluorenone base (b).^{38,39}

Finally, in 1999, Furukawa et al. showed a method of photochemically generating ketenes that did not involve diazo precursors. In this method, they synthesized selenium and sulfur based naphthalene derivatives, which upon photolysis generated the ketene, which they proceeded to trap using alcohols and amines (Figure 5.6). Their final trapped products were an ester and an amide, respectively.⁴⁰

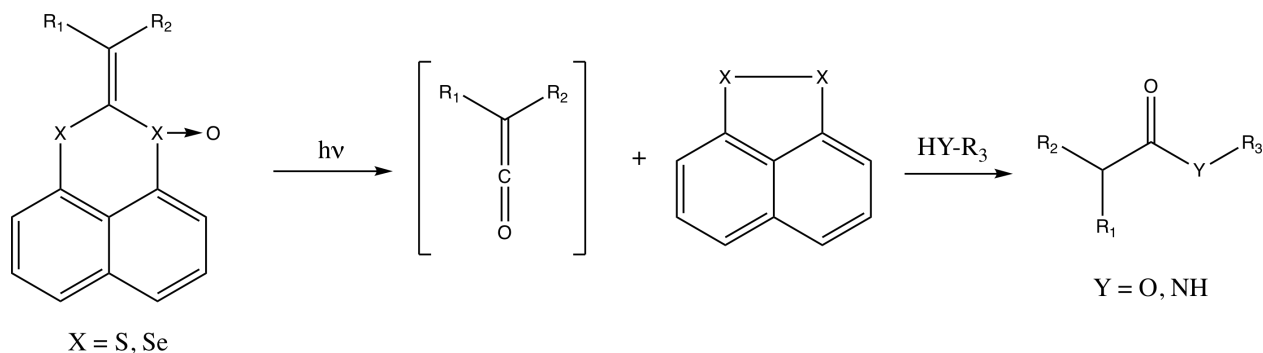


Figure 5.6: A summary of the synthesis of sulfur and selenium based precursors for ketene generation.⁴⁰

5.3 Reactivity of Ketenes

5.3.1 Some Characteristic Ketene Reactions

There are a few reactions that ketenes commonly perform. These are discussed below:

1. Nucleophilic attack on *sp* carbon

The central *sp* carbon in ketenes typically has a strong partial positive character. This is because of the polarization caused by the oxygen, and the other double carbon bond simply enhances this polarization. Figure 5.7 shows the electron density map for diphenyl ketene. This makes the central carbon very susceptible to attack from nucleophiles. For instance, Furukawa used alcohol and amines to trap their ketenes as esters and amides respectively. The mechanism for this nucleophilic attack is shown in Figure 5.8.

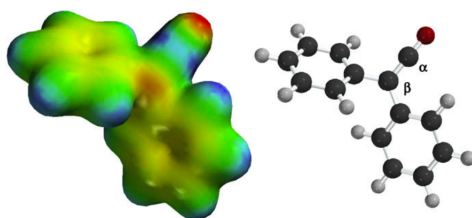


Figure 5.7: The electron density map for diphenylketene. The red portion shows electron rich regions. The two phenyl planes are orthogonal to each other. Image from Lectka et al.³¹

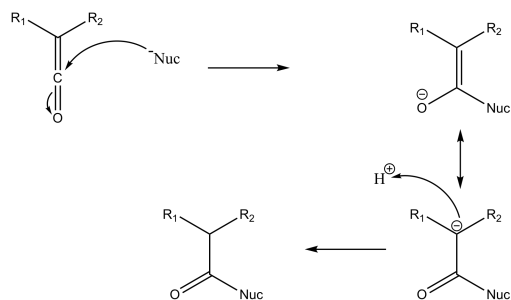


Figure 5.8: Mechanism of attack of nucleophiles on ketenes.

2. Cycloaddition reactions

Ketene cycloaddition was one of the first examples of a pericyclic reaction. These species can undergo [2+2], [3+2], and [4+2] cycloaddition reactions with a wide variety of substrates, including alkenes, dienes, enamines, enol ethers, and ketones.³⁴ These reactions are used to synthesize lactones, lactams, olefins, thiocarbonyl compounds, imides among other functional groups. Figure 5.9 provides examples of each of these additions.

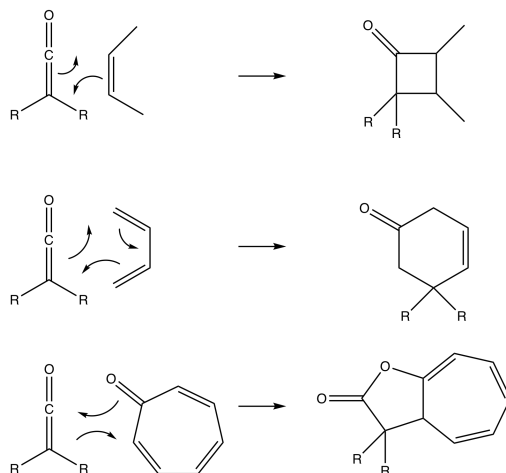


Figure 5.9: Examples of cycloadditions with ketenes. (top) [2+2], (middle) [3+2], (bottom) [4+2].³⁴

These two reaction types are some of the most common reactions that ketenes undergo.^{31,34} In their 2009 review, Lectka et al. presented a pictorial depiction of the scope of ketenes in synthetic chemistry (Figure 5.10).

5.3.2 Geometry and Orientation of Ketene Reactions

Ketene cycloadditions are remarkably different in how reactants approach each other, compared to those for other pericyclic processes, like the Diels Alder reaction. Instead of a top-bottom approach, the cycloaddition proceeds “orthogonally,” resulting in bulky groups ending up on the same side. Ketene

5.4 Where Are We Going? Where Have We Come From?

So, how did we get to ketenes from carbenes? Are the two projects actually related?^a

After the successful trapping of the dimethylalkylidene **3**, the natural question to ask was: how do other symmetric alkylidenes behave? Since Moore and Yang had worked on carbenes with phenyl, methyl, and hydrogen substituents, the diphenylalkylidene, **20**, seemed to be the next obvious system to study. Through Yang et al., it is known that phenyl groups have a propensity to move and rearrange to form alkynes. The question then was, how does the presence of the second phenyl group affect the overall behavior of the system?

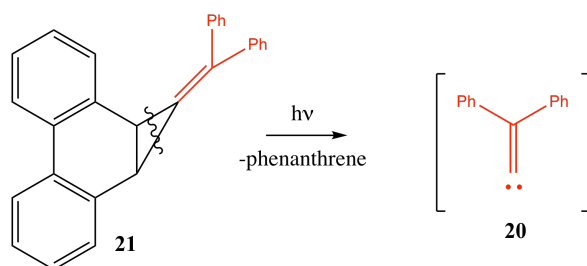


Figure 5.12: The diphenylalkylidene carbene **20**, generated by the photolysis of a phenanthrene-based precursor.

Similar to the process described in Part I of this work, the goal was to synthesize a phenanthrene-based precursor for **20**, which would generate the carbene upon photolysis (Figure 5.12). However, while attempting to synthesize this new precursor, **21**, a cyclobutyl derivative, **22** was instead obtained (Figure 5.13). The synthesis of **21** was attempted using the Takeda method as described in Part I (Figure 1.11).

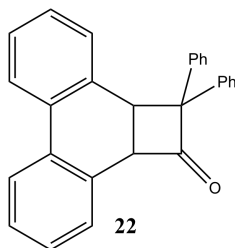


Figure 5.13: The alternate product obtained while trying to synthesize **21**.

While **22** was not the target molecule and ketenes were not initially targeted in this study, the system presented very interesting opportunities to pursue. In 2016, Tippmann et al. synthesized **22**, and photolyzed it to generate diphenyl ketene, **24** (Figure 6.1). Their work focuses on analyzing the mechanism of the reaction via LFP and IR studies on the system. They observed that their reaction

^aThe title for this section is inspired by a story by Joyce Carol Oates titled "Where Are You Going? Where Have You Been?"

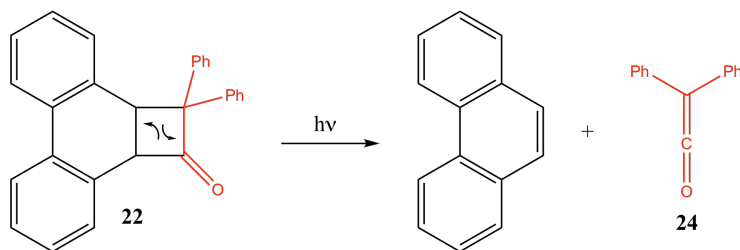


Figure 5.14: The photolysis of cyclobutanone **22** results in phenanthrene and diphenyl ketene **24** being formed.

rate constants were consistent with those for diphenyl ketene.⁴¹

This work, now in its preliminary stages, should to extend Tippmann's work on the diphenyl ketene system and further understanding of the behavior and reactivity of the ketene (Figure 5.14).

Results and Discussion

6.1 Synthesis of Phenanthrene-based Precursor

This project stemmed from an attempt to synthesize the phenanthrene-based precursor for diphenylalkylidene, **21**. As discussed earlier in Part I, there were three principle pathways to synthesize this molecule: the Petasis reaction, the Takeda reaction, and the bromohydrin synthesis. However, since the Petasis reaction necessarily meant the loss of 50% of starting material, that pathway was not attempted.

Instead, the Takeda method was attempted. Starting with phenanthrene, first a dihalogenated cyclopropyl ring is constructed. Then, titanocene dichloride, triethyl phosphite, magnesium are used to make the precursor **21** (Figure 6.1). Benzophenone is used as the ketone. This reaction was attempted with both the dibromo and dichloro substituted compounds (**9** and **14**). The reaction did not generate the desired product but instead made large quantities of the dihydrogen derivative, **27** (Figure 6.2).

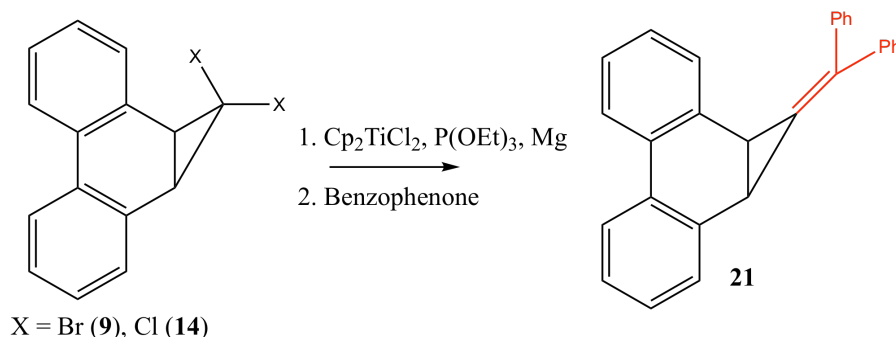


Figure 6.1: The proposed method of synthesizing **21**.

While there are many possible factors that contributed to the generation of **27** instead of **21**, one possibility is that phenyl is too bulky of a substituent. Therefore, during the course of the reaction, titanium complex may not have been able to approach the benzophenone. Note that with cyclopentadienyl rings, the titanium complex is reasonably sterically hindered in itself.

Since the Petasis and Takeda methods were now out of question, the bromohydrin method of synthesizing **21** was explored. This method, as discussed earlier, begins by synthesizing the bromohydrin, **23**, from the dibromo substituent **9** as shown in Figure 6.3.¹⁹ For the mechanism, *n*-butyllithium removes a bromine group via a halogen-lithium exchange. The driving force for this reaction is the increased stability of the **9** anion compared to the *n*-butyl anion. This cyclopropyl anion proceeds to at-

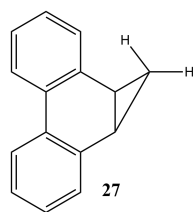


Figure 6.2: This compound was the product of the Takeda reaction with benzophenone.

tack the carbonyl carbon in benzophenone, creating the enolate ion. Upon quenching with ammonium chloride, the bromohydrin **23** is formed.

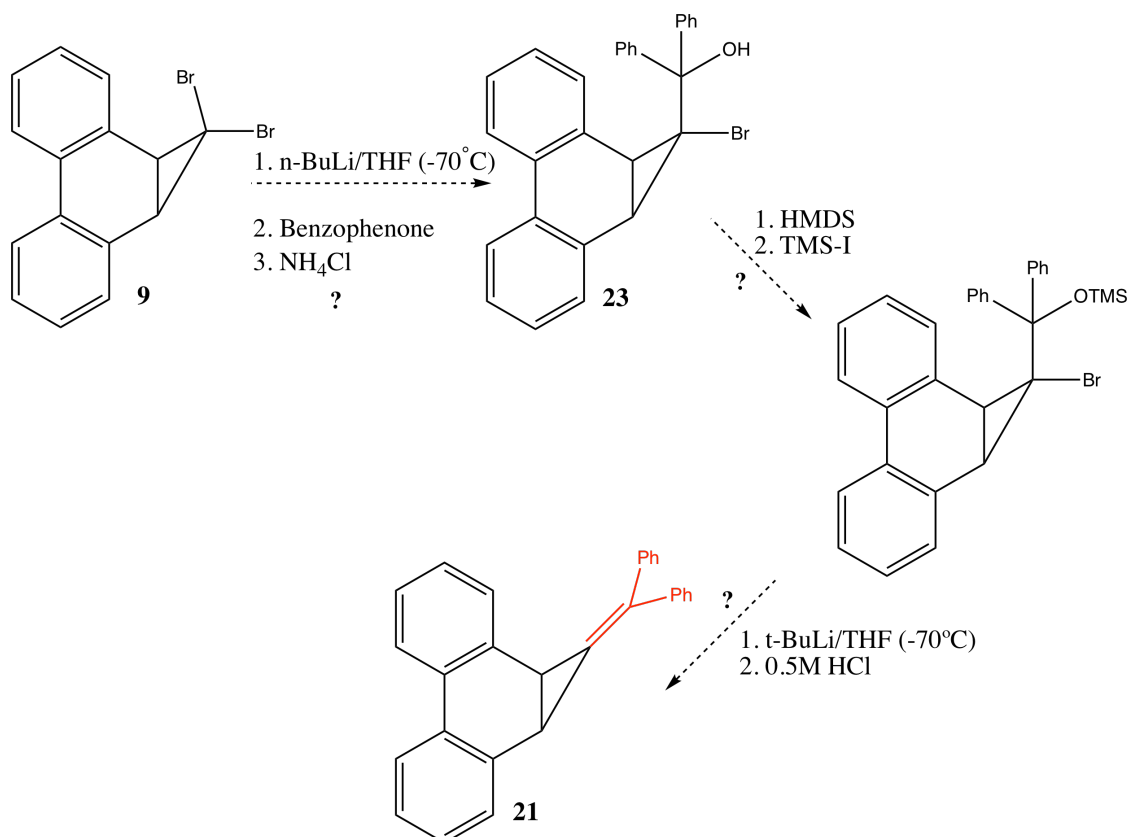


Figure 6.3: An overview of the proposed synthesis of **21** via the bromohydrin **21**.

After the first reaction and the subsequent work up, the resultant product was characterized by NMR spectroscopy. The IR spectrum for this compound was taken, and a large broad peak was expected that corresponded to the hydroxyl group. No such peak was found. Instead, a strong peak that was observed was at 1771 $1/\text{cm}$, which corresponds to a carbonyl stretch. The reaction had formed the cyclobutyl product **22** shown in Figure 6.4.

This product was further characterized by GC/MS and NMR spectroscopy. The ^1H NMR spectrum showed two peaks in the aliphatic region. These two protons correspond to the 9,10 bond in the

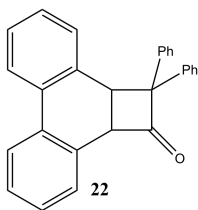


Figure 6.4: The molecule that was synthesized from **9**.

phenanthrene. They are not homotopic to each other, since cyclobutyl ring is not symmetric with its substituents. All the protons in the aromatic region (6-8 ppm) integrate to 18, which is the number of all the phenyl protons. In the ^{13}C NMR spectrum, the carbonyl carbon is clearly identified, at 207 ppm, while the benzylic carbon is at 85 ppm. There are two other distinct aliphatic carbons, from the 9,10 phenanthrene bond. However, the GC/MS doesn't show a molecular ion peak for the compound at 372 m/z as we would expect. Instead, two separate peaks at 194 m/z and 178 m/z are seen. This is because **22** undergoes a thermal electrocyclic ring opening reaction when injected into the GC port (at 250° C). This reaction will be discussed further in later sections.

Seebach et al. have studied this cyclobutanone formation, where the enolate anion, instead of being protonated, loses the halide and is trapped as an epoxide. A mechanism for this reaction is shown in Figure 6.5. A crucial step was the stability of the cation, marked **a** in the figure. In this case, the cation is benzylic and it is stabilized by resonance with both the phenyl rings. Tippmann et al. noted that when the reaction was run with fluorenone as the ketone, the corresponding cyclobutyl product was not isolated. Instead, the reaction stopped at the epoxide, as shown in Figure 6.6. This is because the rearrangement cannot proceed since the cationic intermediate would be antiaromatic with 4π electrons (Figure 6.7).

However, it is difficult to predict the outcome of this *n*-butyllithium reaction since there are more factors at play than cation stability. The same reaction was attempted with di-*t*-butyl ketone. It was predicted that since the tertiary carbocation would be stable, this reaction would proceed to the rearrangement and form the cyclobutanone. However, that did not happen.⁴²

6.2 Photolysis

The compound **22** was photolyzed in the presence of various trapping agents. Upon photolysis, the cyclobutanone went through a ring opening pericyclic reaction to give phenanthrene and diphenyl ketene. Interestingly, this ring opening is both photochemically and thermally driven. The thermal reaction was observed when it was injected into the GC port, and two products were seen in the GC

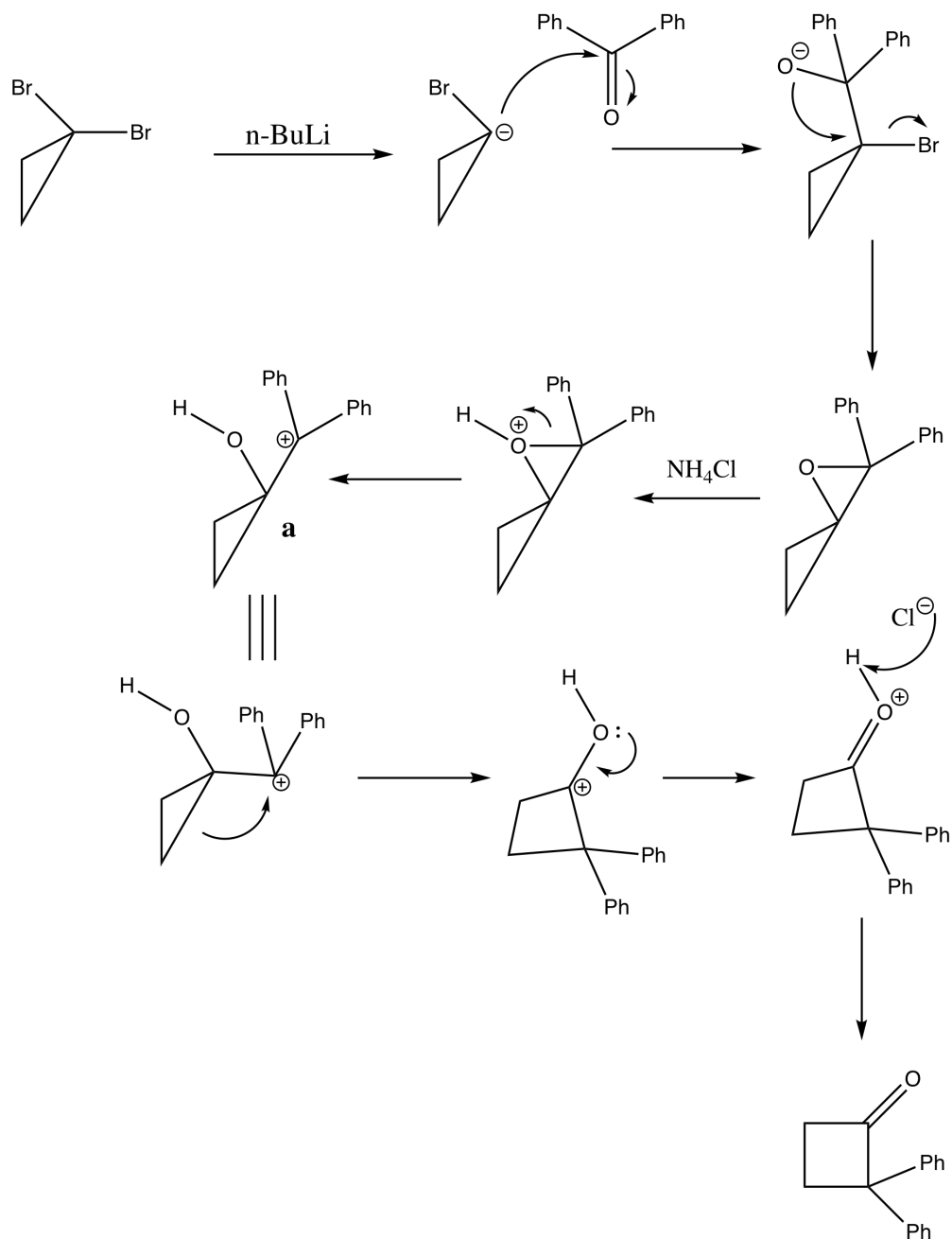


Figure 6.5: The mechanism for the formation of **22**. Note that phenanthrene system is not shown for clarity, but is connected to the cyclopropyl ring.

trace, instead of a single product peak. The driving force for this ring opening is the loss of ring strain from the cyclobutyl ring and the higher resonance stabilization energy of phenanthrene compared to the precursor **22**. Because ketenes can undergo nucleophilic additions to the sp carbon and cycloadditions, photolysis was attempted in the presence of trapping agents (methanol, diethylamine, and 2,3-dimethyl 2-butene) to understand the reactivity of **24**.

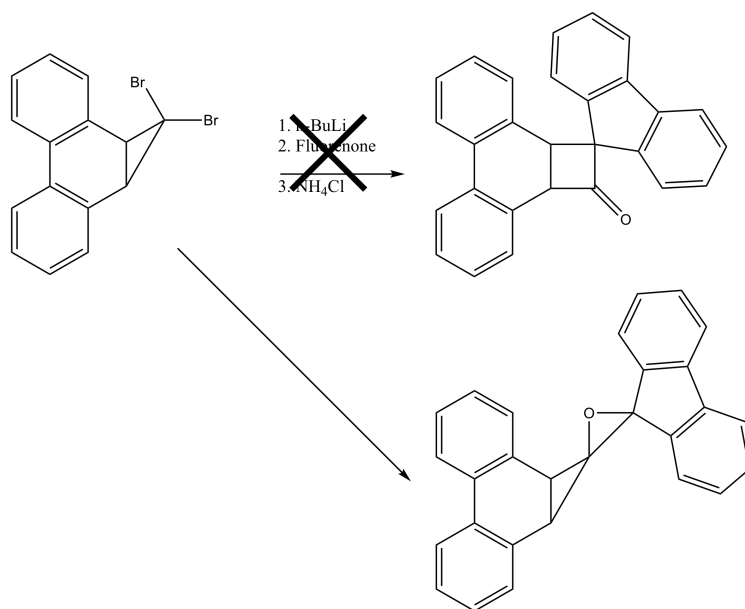


Figure 6.6: When dibromo substituent **9** is reacted with fluorenone, the epoxide is formed instead of the cyclobutanone product.⁴¹

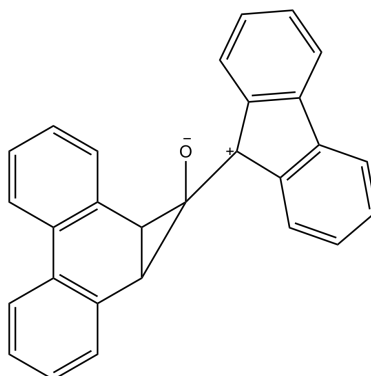


Figure 6.7: The above intermediate is anti-aromatic and prevents the fluorenone system from proceeding to the cyclobutanone.⁴¹

6.2.1 Photolysis with Methanol

When **22** was photolyzed with methanol, the ketene reacted with the alcohol to form an ester. The photolysis was monitored by GC/MS was continued until the starting material peak disappeared. Since the precursor fragmented in the GC into phenanthrene and **24** and phenanthrene was a product of the photolysis that was not being further reacted, the **24** peak was used to track reaction progress. Most of the ketene reacted with the methanol to form **25** (Figure 5.14). Some of the ketene lost carbon monoxide to form the diphenyl carbene. The solution was not degassed prior to photolysis, due to operator error. Therefore, the diphenyl carbene reacted with oxygen in the tube to form benzophenone, which is also seen in the GC/MS.

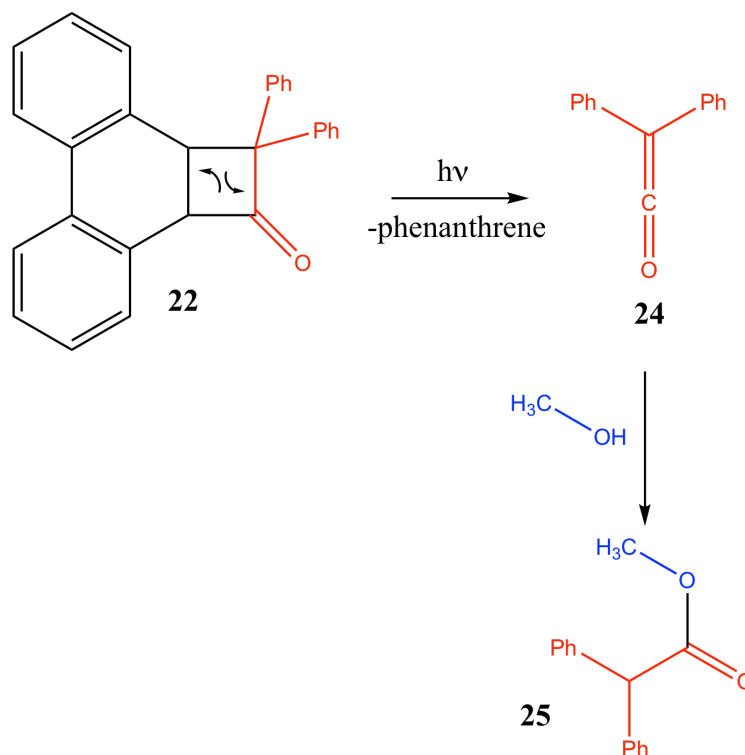


Figure 6.8: The photolysis of **22** with methanol produces an ester **25**.

6.2.2 Photolysis with Diethylamine

Precursor **22** was also photolyzed with diethylamine as a trapping agent. This reaction produced the secondary amide **26** (Figure 6.9). Just like in the first case, the photolysis was monitored by GC/MS and continued until the ketene peak no longer showed (Figure 6.9). The photolysis took 12 hours.

6.2.3 Photolysis 2,3-dimethyl 2-butene

Precursor **22** was photolyzed with 2,3-dimethyl 2-butene. The goal was for both reactants to undergo a [2+2] addition to form **28** (Figure 6.10). However, this product was not observed. It is clear that the ketene is undergoing some reaction, since the ketene peak decreases over time. While products from the photolysis have not been isolated and identified, a NIST MS Search 2.0 was used to potentially identify these compounds. According to the search program, the photolysis may have resulted in the formation of 2,2-diphenylacetic acid among other products. More work is needed to understand the reactions occurring here.

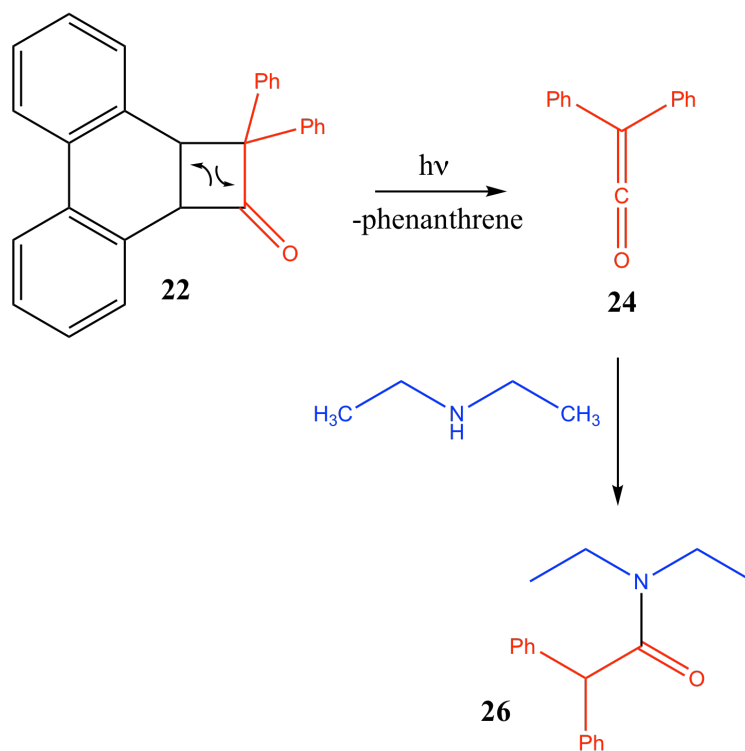


Figure 6.9: The photolysis of **22** with an amine produces an amide **26**.

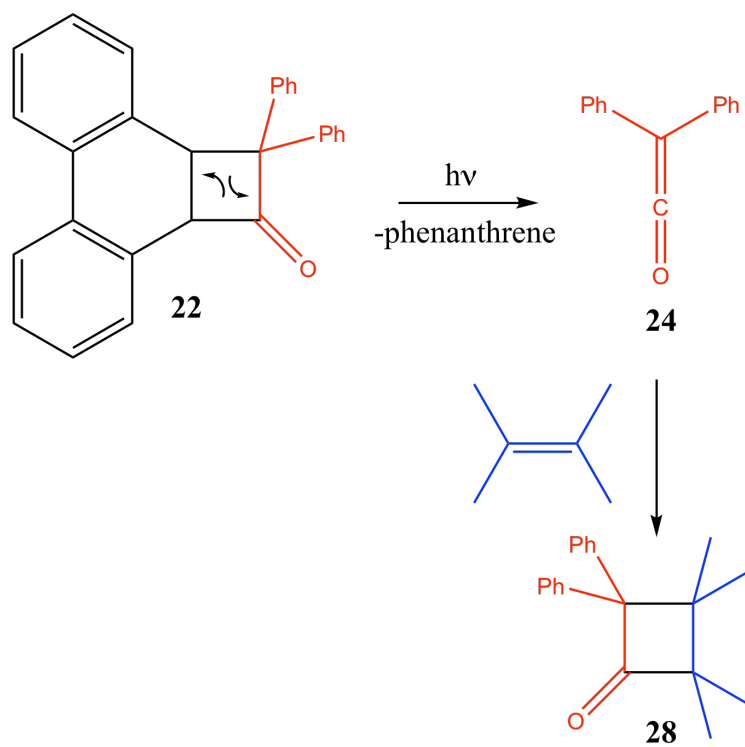


Figure 6.10: The photolysis of **22** with an alkene, should have produced cyclobutane **28**.

6.2.4 Neat Photolysis

The neat photolysis of the precursor **22** was also attempted. Precursor **22** was dissolved in benzene, and no additional chemical was added. It was predicted that the ketene would be formed, and would undergo a dimerization reaction with a [2+2] cycloaddition to form **29**. However, this was not observed. Just as with the alkene, it was clear that the system was being photolyzed, since the precursor peak was decreasing over time. Part of the ketene definitely reacted with oxygen to form benzophenone. There could be a variety of reasons for the dimerization is not observed. One possibility is that the dimer is not stable, and breaks down again to give the ketene. Additional experiments need to be done on this system to understand the behavior of the ketene.

6.3 Computational Studies

Preliminary computational studies were performed on the precursor **22** and the ketene **24**. The density functional method, B3LYP, was used at the 6-31G(d) level of theory for these calculations. The products of the photolysis (phenanthrene and the ketene) are 7 kcal/mol more stable than the starting material.

Conclusion

This work used a safe method of generating ketenes photochemically using a phenanthrene-based precursor. The ketene of interest, diphenyl ketene (**20**), was subsequently trapped with methanol and diethylamine (Figure 7.1). A crystal structure for this compound **22** was identified. Preliminary calculations on this system were performed that showed the photolyzed products (phenanthrene and diphenylketene) to be 7 kcal/mol more stable than the starting material.

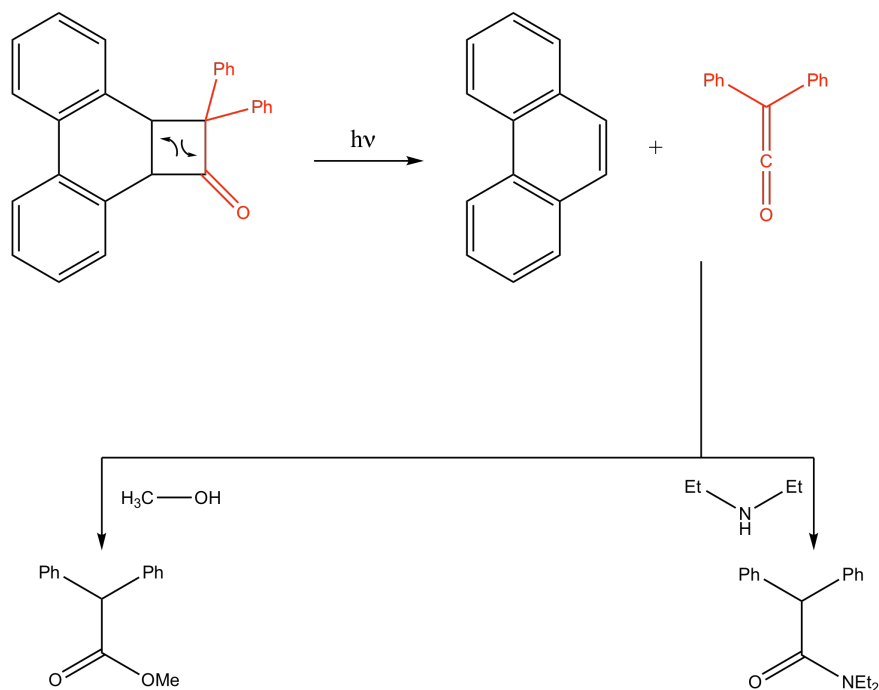


Figure 7.1: A summary of the photolysis experiments of compound **22**.

7.1 Future Work

Since this project is in its very early stages, much work remains to be done on this system. Firstly, more ketene reactions could be explored to “trap” the ketene. This includes a neat photolysis, trying to get the ketene to dimerize. Other reactions could be done to give evidence for the ketene by reacting with a good diene for a Diels-Alder reaction or another alkene for a [2+2] reaction.

An important aspect would be to understand the mechanism of the synthesis of **22** better, with the intention of predicting when the cyclobutyl substituent is formed versus the cyclopropyl one. This reaction goes through an epoxide intermediate, and carbocation stability appears to play an important

role: these factors could be studied via kinetic studies to predict the outcome of the synthesis better. Additionally, it is proposed that the ketene formation goes through a radical mechanism. Future projects could use LFP and IR studies to examine how the ketene is actually formed. Finally, additional computational work is required to better understand the transition state of the system, to better model the reaction pathway and potential energy surface of these ketene reactions.

Experimental Procedures

8.1 General Remarks

8.1.1 Reactions

Tetrahydrofuran was dried with activated alumina. The inert gas used was argon. All other chemicals were commercially bought and used as received. Flash chromatography was performed using a Combiflash instrument with “Gold” pre-packed columns on silica.

8.1.2 Spectra

All NMR spectra were collected in CDCl_3 at 500 MHz for ^1H and 125 MHz for ^{13}C . All chemical shifts were recorded in ppm. GC/MS were recorded on a capillary gas chromatograph coupled with a quadrupole, triple-axis mass selective detector operating in electron impact (EI) mode. IR spectra were collected using ATR-FTIR spectroscopy.

8.1.3 Photolysis

All photolysis experiments were performed under a Rayonet photochemical reactor equipped with 16 12-inch 8 W lamps with output in the range 315 to 400 nm.

8.1.4 Computational Studies

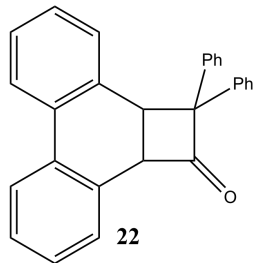
All calculations were run on Gaussian 09. Geometry optimization of **3** and **11** was done using density functional methods with the B3LYP method using the 6-31G* basis set.²³

8.1.5 X-ray Structures

X-ray data were acquired at 173 K using a Bruker Smart Apex CCD diffractometer with graphite monochromated $\text{Mo K}\alpha$ radiation ($\lambda = 0.71073 \text{ \AA}$). Bruker Apex3 suite of programs was used to process the data²⁴ and the frames were integrated using the Bruker SAINT software.²⁵ The data was corrected for absorption effects using the multi-scan method SADABS.²⁶ Structure solution and refinement by least-squares on F^2 was done by using the Bruker SHELXTL software package.²⁷ Non-hydrogen atoms

were refined anisotropically and hydrogen atoms were calculated using a riding model. The .cif files were validated with the checkCIF/Platon facility using enCIFer.^{28,29}

8.2 2,2-diphenyl-2a,10b-dihydrocyclobuta[1]phenanthren-1(2H)-one (**22**)^{19,41,43}



In an oven dried flask, 3.542 g (~ 10 mmol) of compound **9** was dissolved in 40 mL dry THF. The reaction mixture was cooled to -70°C while stirring and 4.2 mL n-butyllithium (2.5 M in hexanes) was added dropwise. After 90 minutes of stirring at -70°C , 1.826 g (~ 10 mmol) of dry benzophenone was added to the reaction. The dry ice bath was removed after 90 minutes of stirring. When the reaction had come to rt, 10 mL of ammonium chloride was used to quench the reaction. The mixture was separated with 50 mL of dichloromethane and 50 mL of water. The aqueous layer was extracted with dichloromethane (2×50 mL), and organic layers were combined. The organic layer was washed with water (2×50 mL), brine (2×50 mL), and dried with sodium sulfate. The solid obtained after rotary evaporation was recrystallized in hexanes and minimal ethyl acetate. This afforded a solid (1.049 g, 28%).

GC-MS: Retention time: 8.569 minutes (194), Fragments (in m/z): 194.1, 165.1, 139.1, 82.3.

NMR: (in ppm) ^1H : δ = 7.70 (td, 2H), 7.67 (m, 2H), 7.4 (dm, 1H), 7.33 (m, 2H), 7.25 (dm, 2H), 7.17 (dtd, 2H), 6.8 (tt, 2H), 6.79 (tt, 2H), 6.47 (m, 2H), 4.93 (d, 1H), 4.80 (d, 1H). ^{13}C : δ = 207.27, 140.83, 138.61, 132.49, 131.84, 131.34, 130.73, 128.63, 128.59, 128.16, 128.05, 128.05, 127.55, 127.51, 127.34, 127.11, 127.11, 126.97, 126.17, 123.15, 122.99, 85.80, 77.16, 58.09, 39.89.

IR (measured in $1/\text{cm}$): 3060.38, 1771.45, 1597.48, 1489.35, 1443.90.

Melting point: 144°C - 148°C .

8.3 Photolysis

8.3.1 With Methanol

92.2 mg (~ 0.25 mmol) of **22** was dissolved in 4 mL benzene and 1 mL methanol in a vial that was then sealed. It was photolyzed with UV lamps in the range 315-400nm. The photolysis was discontinued after 21.5 hours, when on checking by GC-MS, there was no peak for the precursor.

GC-MS: Retention time: 9.827 minutes, Fragments (in m/z): 226.1, 167.1, 152.1.

8.3.2 With Diethylamine

93.9 mg (~ 0.25 mmol) of **22** was dissolved in 4 mL benzene and 1 mL diethylamine in a vial that was then sealed. It was photolyzed with UV lamps in the range 315-400 nm. The photolysis was discontinued after 12 hours, when on checking by GC-MS, there was no peak for the precursor. The solution was poured into a pre-packed silica column. Column chromatography was performed using hexanes, followed by 20% ethyl acetate over time, on a 24 g silica cartridge. Good separation was not achieved.

GC-MS: Retention time: 12.339 minutes, Fragments (in m/z): 267.1, 165.1, 100.1, 72.1.

8.3.3 With 2,3-dimethyl 2-butene

92.3 mg (~ 0.25 mmol) of **22** was dissolved in 4 mL benzene and 2 mL 2, 3-dimethyl 2-butene in a vial that was then sealed. It was photolyzed with UV lamps in the range 315-400nm. The photolysis was discontinued after 38 hours.

8.3.4 Neat Photolysis

187.6 mg (~ 0.5 mmol) of **22** was dissolved in 6.5 mL benzene in a vial that was then sealed. It was photolyzed with UV lamps in the range 315-400 nm. The photolysis was discontinued after 23.5 hours.

Bibliography

- [1] Kirmse, W. *Carbene Chemistry*; Academic Press, 1964; Vol. 1.
- [2] Doering, W.; Buttery, R.; Laughlin, R.; Chaudhari, N. *J. Am. Chem. Soc.* **1956**, *78*, 3234.
- [3] Hine, J. *J. Am. Chem. Soc.* **1950**, *72*, 2438.
- [4] Bertrand, G., Ed. *Carbene Chemistry: From Fleeting Intermediates to Powerful Reagents*; Marcel Dekker Inc, 2002.
- [5] Igau, A.; Grutzmacher, H.; Baceiredo, A.; Bertrand, G. *J. Am. Chem. Soc.* **1988**, *110*, 6463.
- [6] Arduengo, A. J. I.; Harlow, R.; Kline, M. *J. Am. Chem. Soc.* **1991**, *113*, 361.
- [7] Jr., M. J.; Fleming, S. A. *Organic Chemistry*, 5th ed.; W. W. Norton And Co., 2010.
- [8] Reed, S. C.; Capitosti, G. J.; Zhu, Z.; Modarelli, D. A. *J. Org. Chem.* **2001**, *66*, 287.
- [9] Yao, K.; Geng, Z. Y.; Wang, Y. C.; Jia, B. L. *J. Mol. Struct. THEOCHEM* **2007**, *821*.
- [10] Richardson, D. B.; Durrett, L. R.; Jr., J. M. M.; Putnam, W. E.; Slaymaker, S. C.; Dvoretzky, I. *J. Am. Chem. Soc.* **1965**, *87*, 2763.
- [11] Chateaufneuf, J. E.; Johnson, R. P.; Kirchhoff, M. M. *J. Am. Chem. Soc.* **1990**, *112*, 3217.
- [12] Moore, K. A.; Vidaurri-Martinez, J. S.; Thamattoor, D. M. *J. Am. Chem. Soc.* **2012**, *134*, 20037.
- [13] Yang, X.; Languet, K.; Thamattoor, D. M. *J. Org. Chem.* **2016**, *81*, 8194.
- [14] Nguyen, J. M.; Thamattoor, D. M. *Synthesis* **2007**, *14*, 2093.
- [15] Graves, K. S.; Thamattoor, D. M.; Rablen, P. R. *J. Org. Chem.* **2011**, *76*, 1584.
- [16] Petasis, N. A.; Bzowej, E. I. *Tetrahedron Lett.* **1993**, *34*, 943.
- [17] Takeda, T.; Sasaki, R.; Fujiwara, T. *J. Org. Chem.* **1998**, *63*, 7286.
- [18] Woodworth, R. C.; Skell, P. S. *J. Am. Chem. Soc.* **1956**, *78*, 4496.
- [19] Hassig, R.; Siegel, H.; Seebach, D. *Chem. Ber.* **1982**, *115*, 1990.
- [20] Tobe, Y.; Iwasa, N.; Umeda, R.; Sonoda, M. *Tetrahedron Lett.* **2001**, *42*, 5485.
- [21] Maurer, D. P.; Fan, R.; Thamattoor, D. M. *Angew. Chem. Int. Ed.* **2017**, *56*, 4499.
- [22] Lu, L.; Yang, X.; Moore, K. A.; Lan, X.; Coldren, W. H.; Hadad, C. M.; Phillips, D. L.; Thamattoor, D. M. *Manuscript in Preparation*
- [23] Frisch, M. J. et al. Gaussian 09 Revision A.1. Gaussian Inc. Wallingford CT 2009.
- [24] APEX3; Bruker AXS Inc. Madison, Wisconsin, USA.
- [25] SAINT; Bruker AXS Inc. Madison, Wisconsin, USA.
- [26] SADABS; G. M. Sheldrick, University of Gottingen, Germany; Bruker AXS Inc. Madison, Wisconsin, USA.
- [27] XPREP; XS; XL; G. M. Sheldrick, University of Gottingen, Germany; Bruker AXS Inc. Madison, Wisconsin, USA.
- [28] Allen, F. H.; Johnson, O.; Shields, G. P.; Smith, B. R.; Towler, M. *J. Appl. Crystallogr.* **2004**, *37*, 335.
- [29] Maurer, D. P. Chemistry Honors Thesis. 2016.
- [30] Takeuchi, D.; Okada, T.; Kuwabara, J.; Osakada, K. *Macromol. Chem. Phys.* **2006**, *207*, 1546.
- [31] Paull, D. H.; Weatherwax, A.; Lectka, T. *Tetrahedron* **2009**, *65*, 6771.

- [32] Staudinger, H. *Justus Liebigs Ann. Chem* **1907**, 356, 51.
- [33] Chick, F.; Wilsmore, N. T. M. *J. Chem. Soc. Trans.* **1908**, 93, 946.
- [34] Hyatt, J. A.; Reynolds, P. W. others.; et al. , Eds.; Wiley And Sons, 1994; Vol. 45.
- [35] Doering, W.; Roth, W. R. *Tetrahedron* **1962**, 18.
- [36] Fu, N.; Tidwell, T. T. *Tetrahedron* **2008**, 64, 10465.
- [37] Leibfarth, F. A.; Wolffs, M.; Campos, L. M.; Delany, K.; Treat, N.; Kade, M. J.; Moon, B.; Hawker, C. J. *Chem. Sci.* **2012**, 3, 766.
- [38] Hacker, N. P.; Turro, N. J. *Tetrahedron Lett.* **1982**, 23, 1771.
- [39] de Lucas, N. C.; Netto-Ferreira, J. C.; Andraos, J.; Lusztyk, J.; Wagner, B. D.; Scaiano, J. C. *Tetrahedron Lett.* **1997**, 38, 5147.
- [40] Kobayashi, K.; Shinhara, S.; Moriyama, M.; Fujii, T.; Horn, E.; Yabe, A.; Furukawa, N. *Tetrahedron Lett.* **1999**, 40, 5211.
- [41] Tippmann, E. M.; Curtis, R. *Tetrahedron Letters* **2016**, 57, 4785.
- [42] Le, T. Unpublished results.
- [43] Braun, M.; Seebach, D. *Angew. Chem.* **1974**, 86, 279.

Appendix A: Spectra

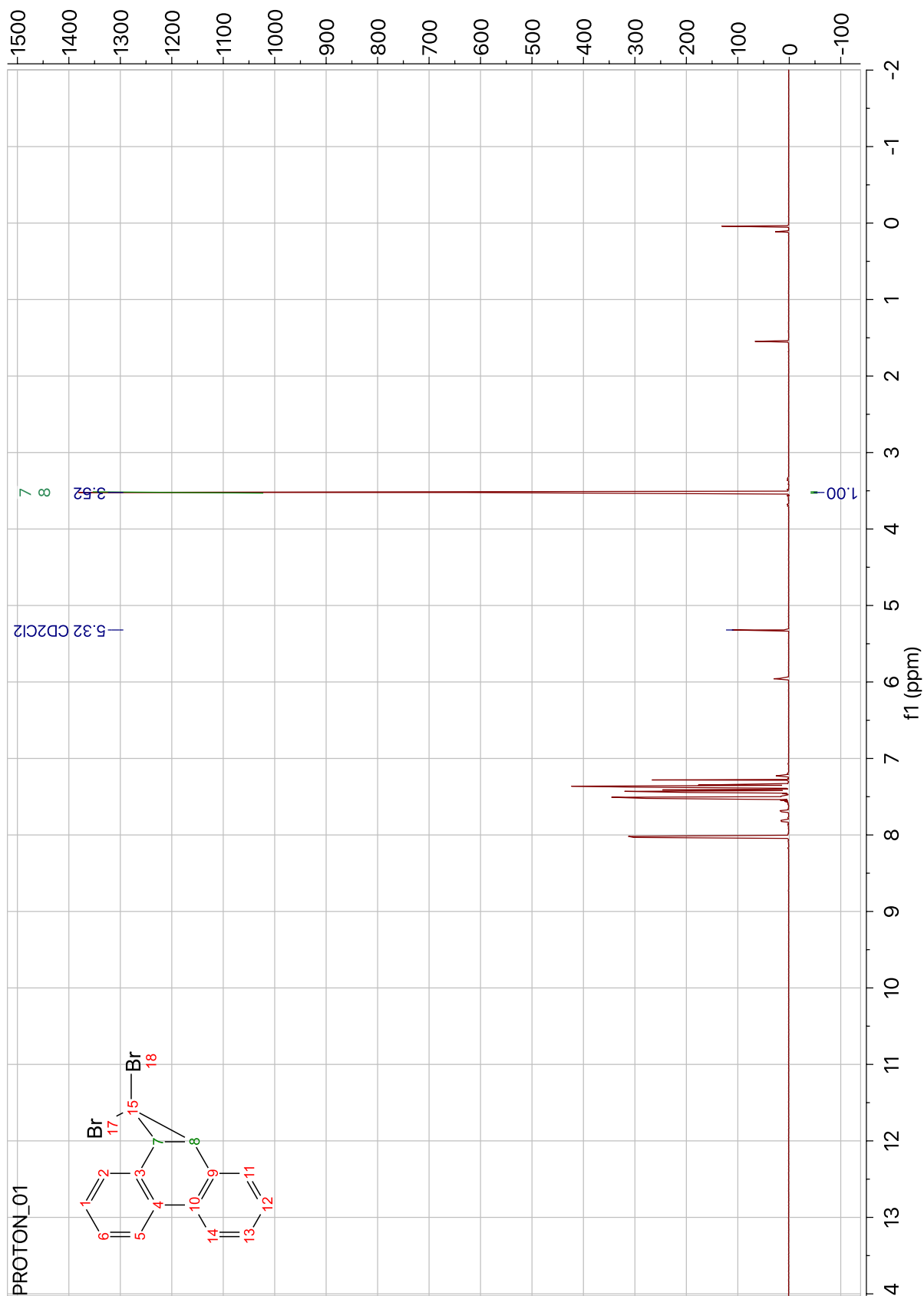


Figure 9.1: ^1H NMR spectrum for **9**

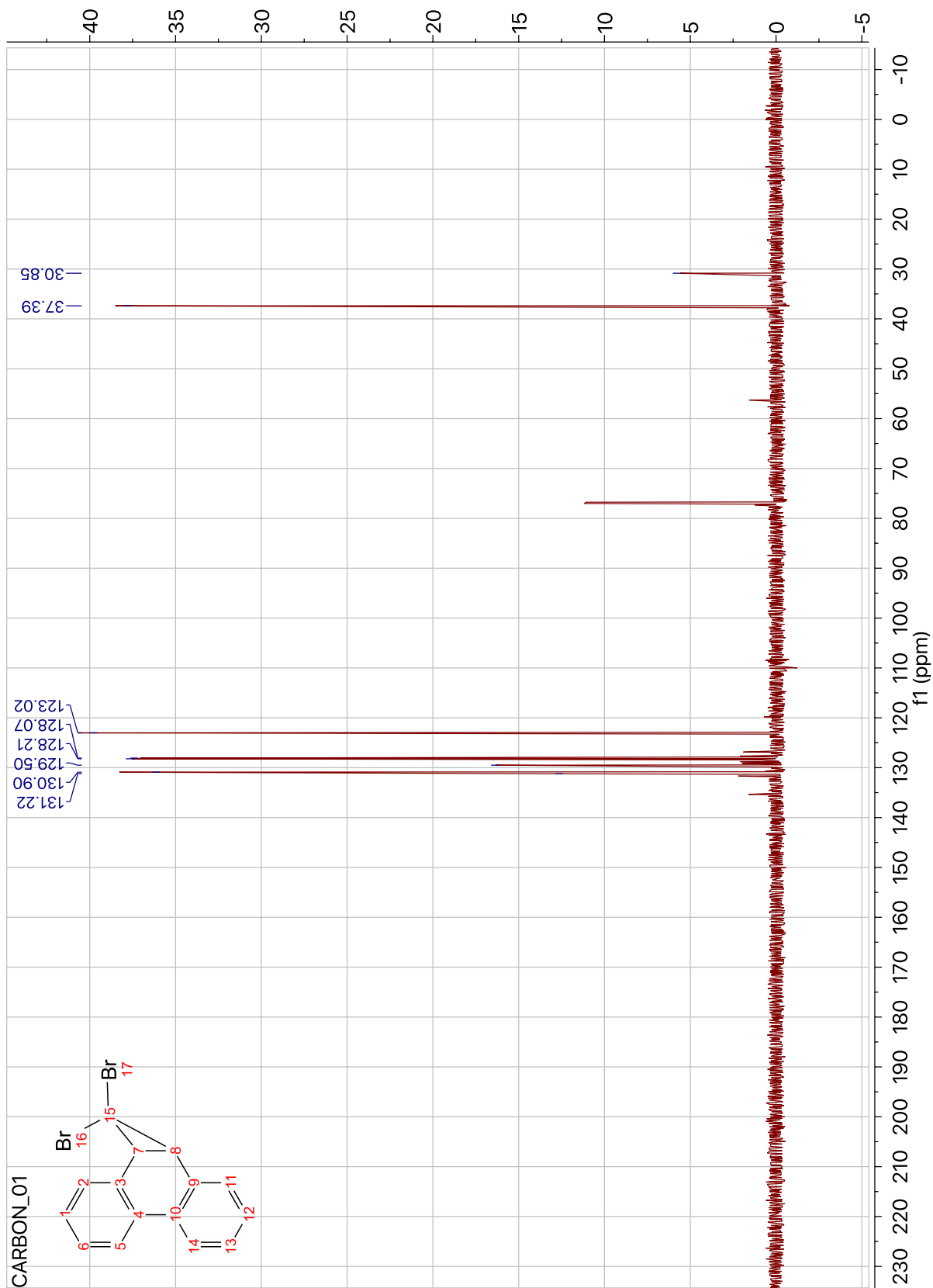


Figure 9.2: ^{13}C NMR spectrum for **9**

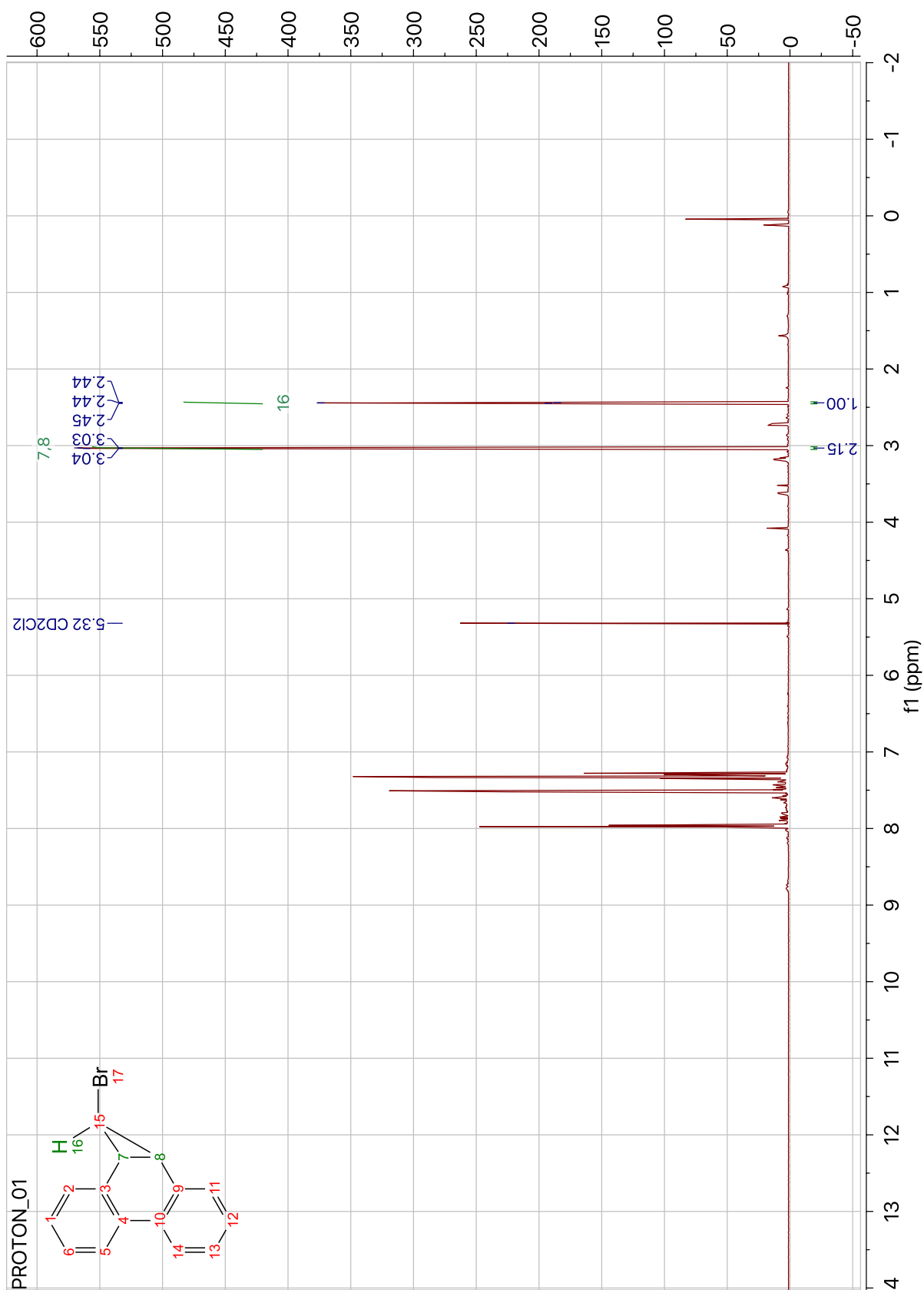


Figure 9.3: ^1H NMR spectrum for **10**

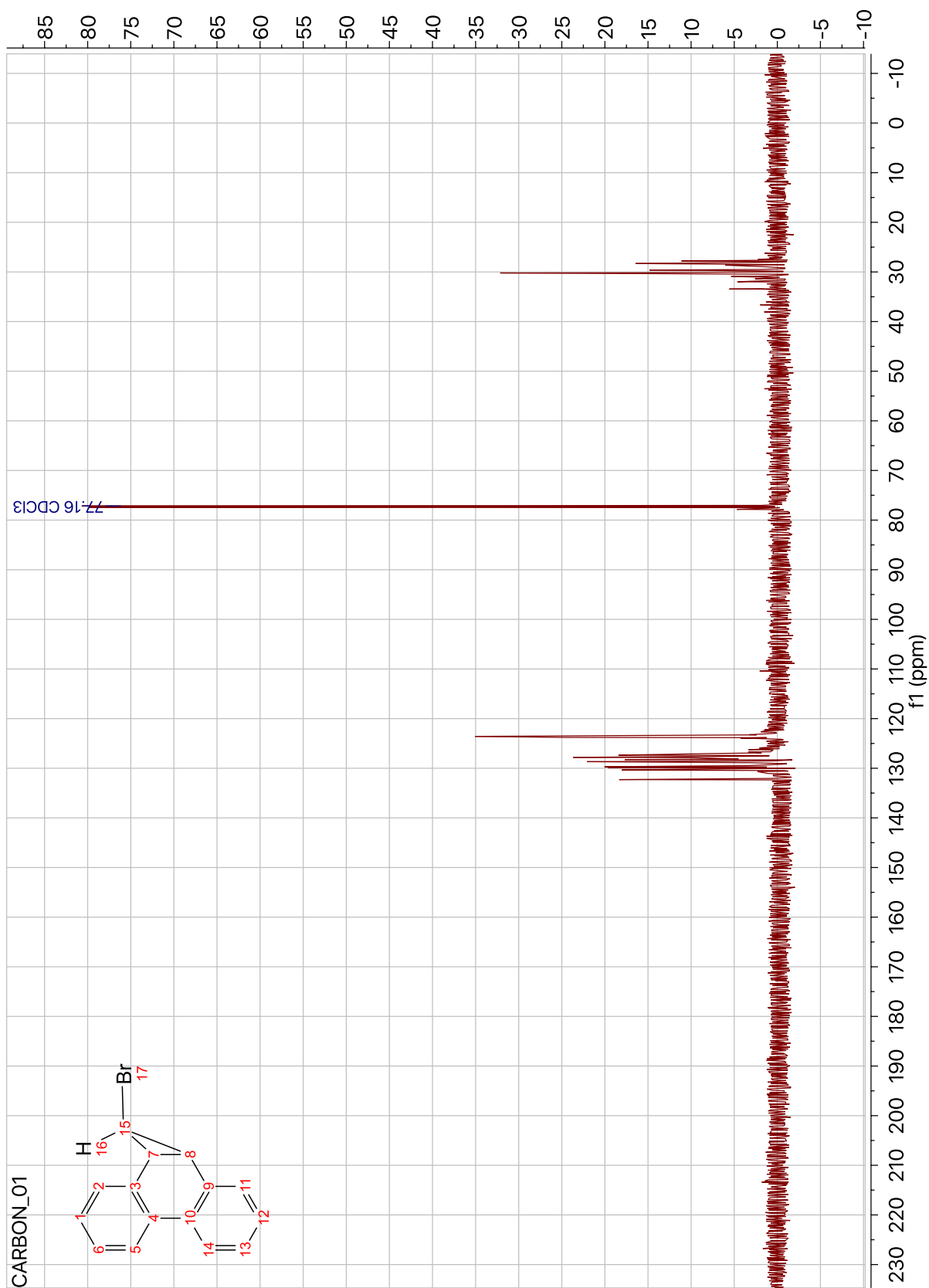


Figure 9.4: ¹³C NMR spectrum for 10

File :D:\1\data\Tarini\TH071115002.D
Operator : Tarini
Acquired : 11 Jul 2015 12:36 using AcqMethod DASLAB3MIN.M
Instrument : GCMS1
Sample Name: monobr chk
Misc Info :
Vial Number: 1

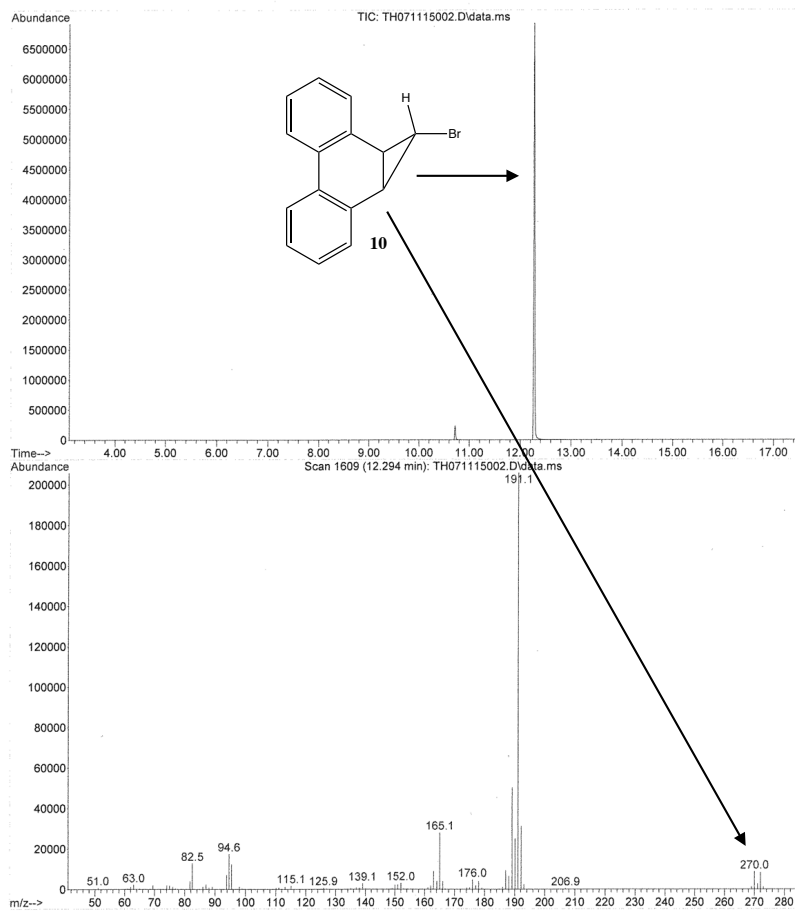


Figure 9.5: GC/MS data for 10

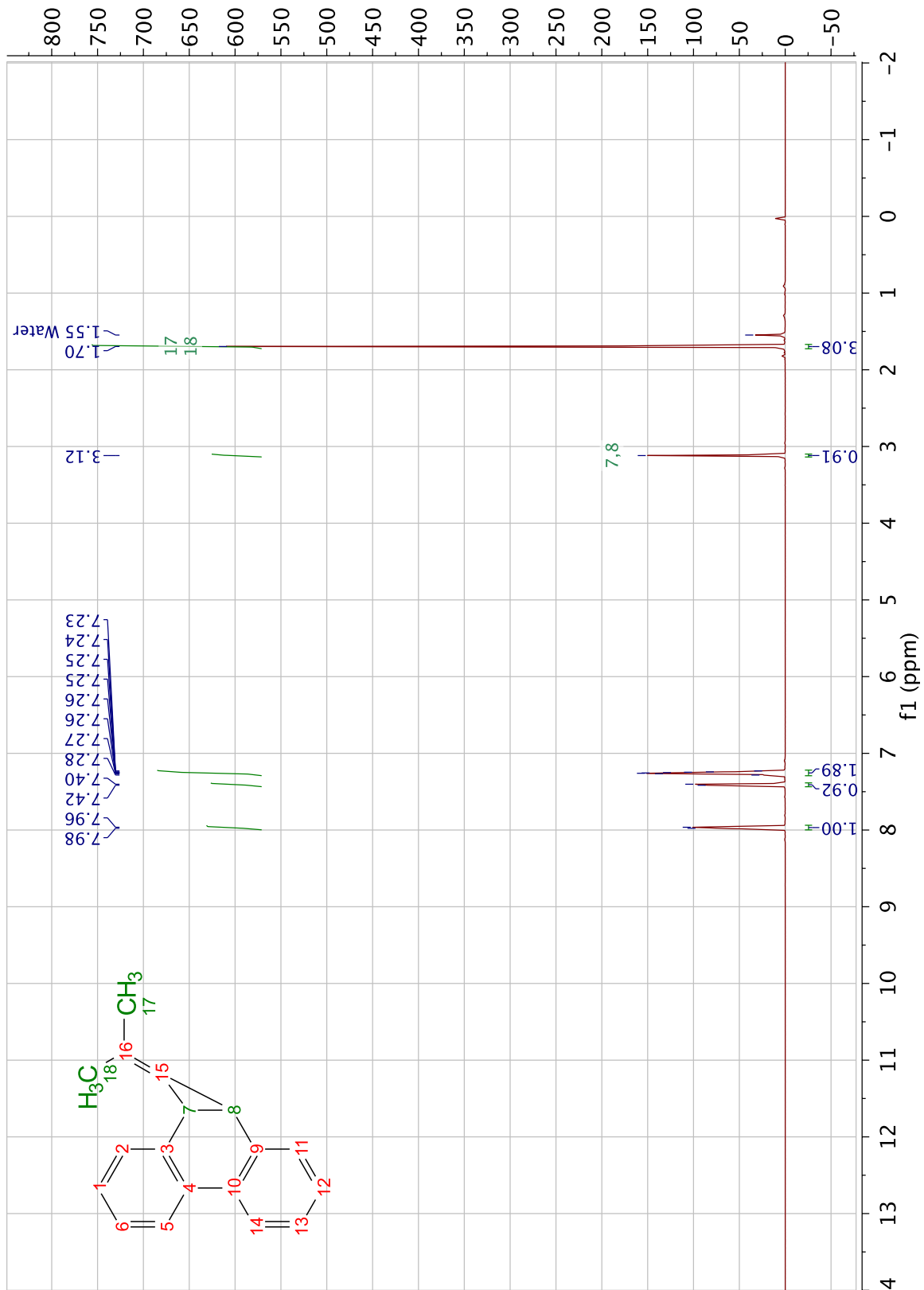


Figure 9.6: ^1H NMR spectrum for **11**

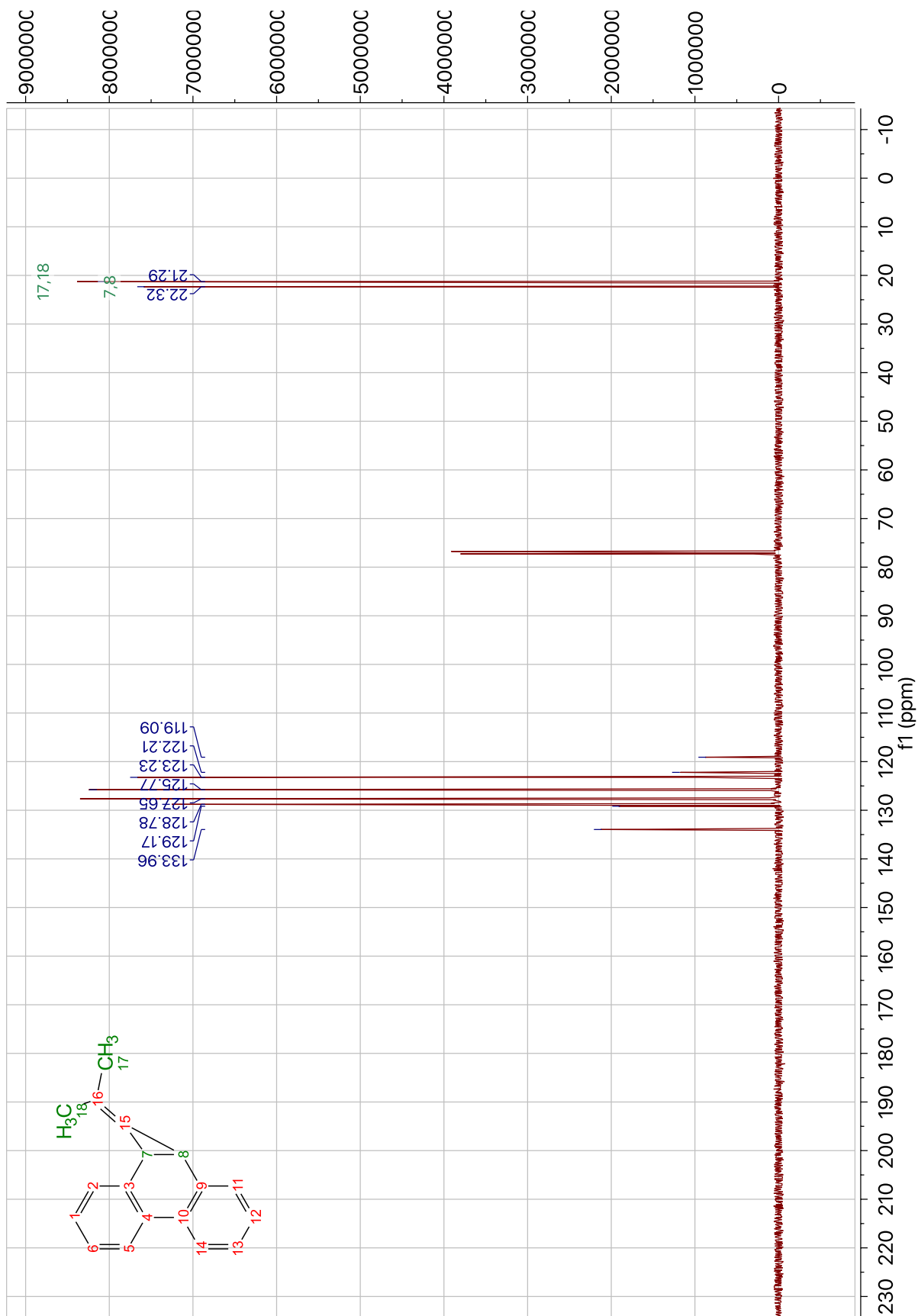


Figure 9.7: ^{13}C NMR spectrum for **11**

File :D:\1\data\Tarini\TH080615006.D
Operator : Tarini
Acquired : 6 Aug 2015 12:47 using AcqMethod DASLAB3MIN.M
Instrument : GCMS1
Sample Name: DMV Prec
Misc Info :
Vial Number: 1

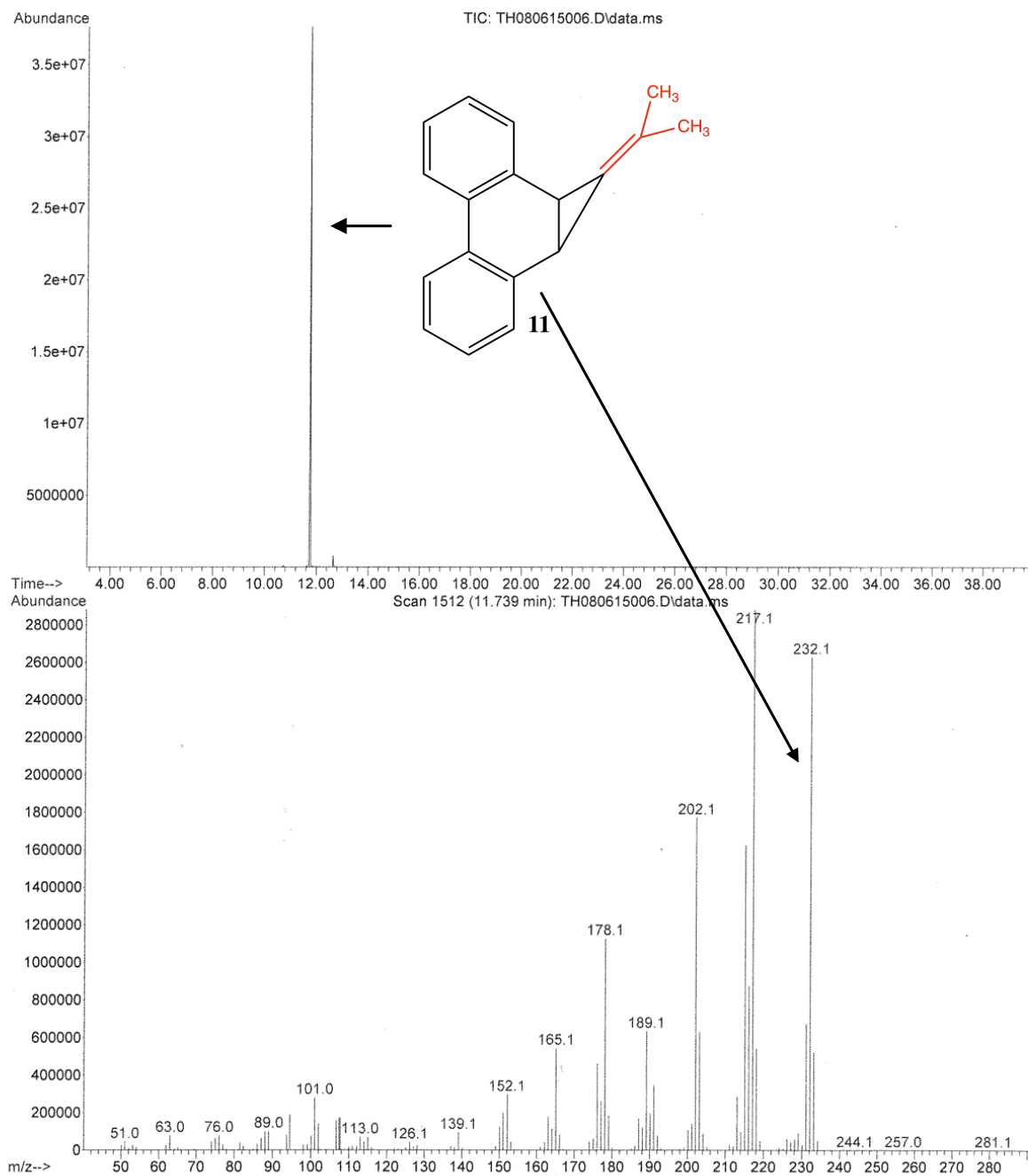


Figure 9.8: GC/MS data for **11**



c:\pel_data\spectra\ch242-2005\th_dmvp\precursor.sp

Figure 9.9: IR spectrum for 11

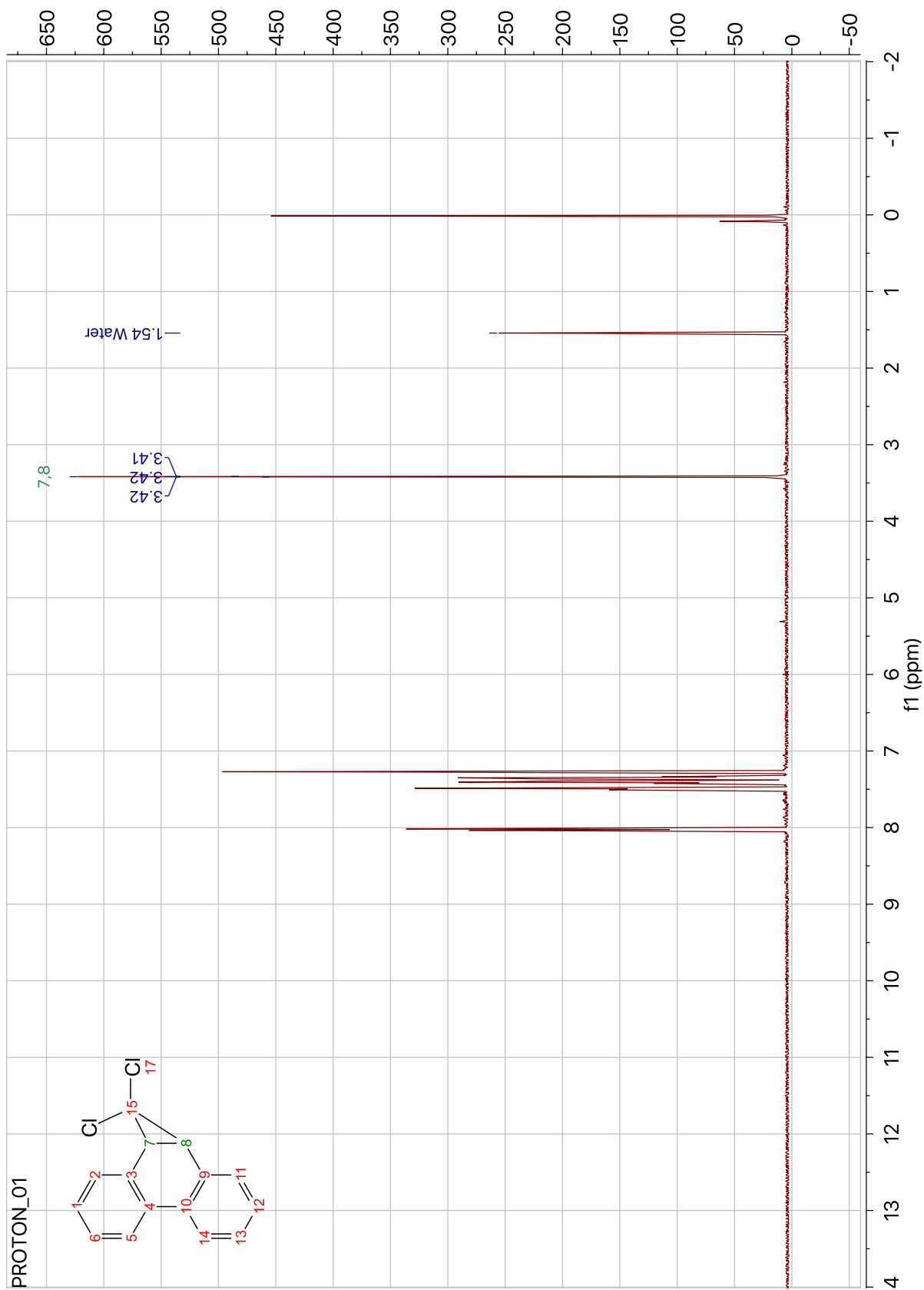


Figure 9.10: ^1H NMR spectrum for 14

File :D:\1\data\Tarini\TH041716003.D
Operator : Tarini
Acquired : 17 Apr 2016 21:26 using AcqMethod DASLAB3MIN.M
Instrument : GCMS1
Sample Name : dichloro
Misc Info :
Vial Number: 1

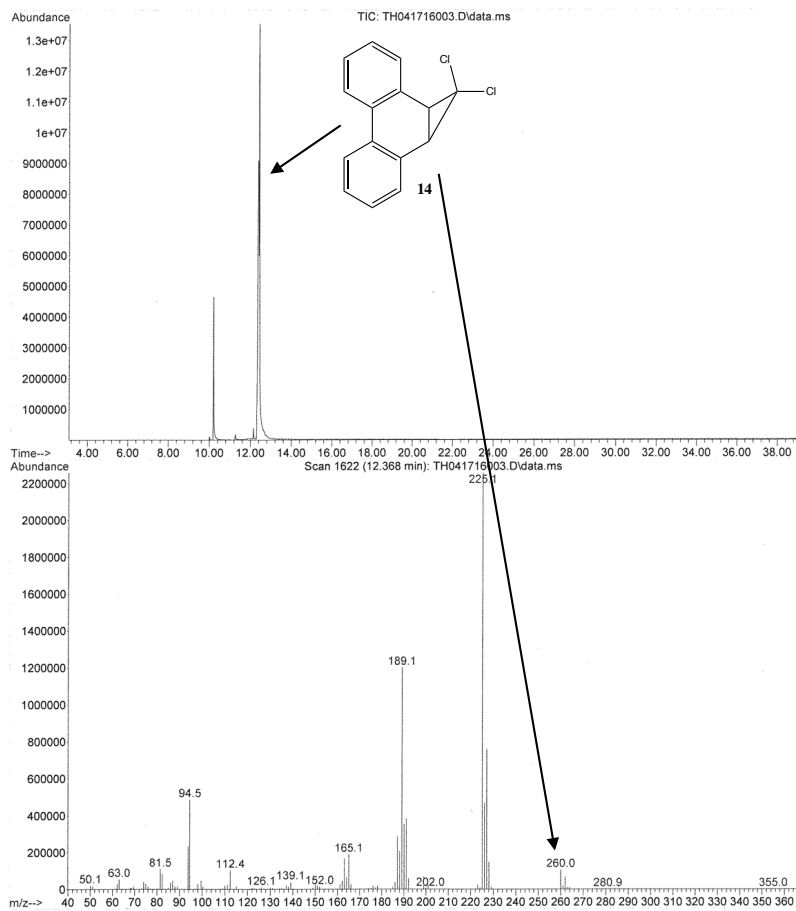


Figure 9.11: GC/MS data for 14

File :D:\1\data\Tarini\TH030617002.D
Operator : Tarini
Acquired : 6 Mar 2017 19:12 using AcqMethod DASLAB3MIN.M
Instrument : GCMS1
Sample Name: Alcohol reaction with acetone
Misc Info : frac 68
Vial Number: 1

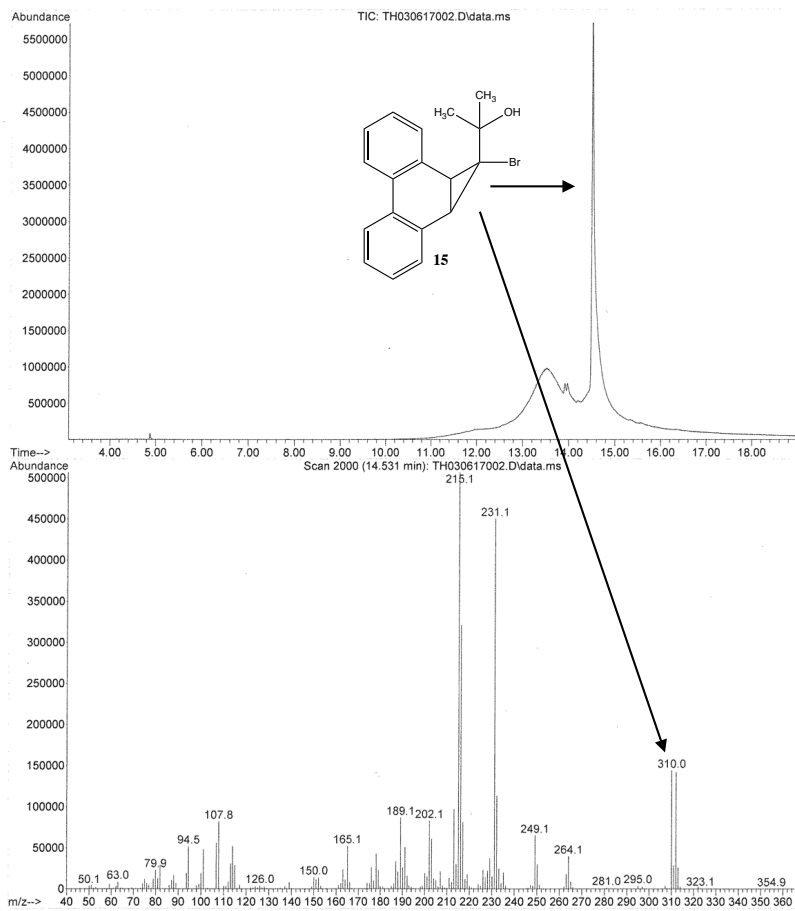


Figure 9.12: GC/MS data for 15

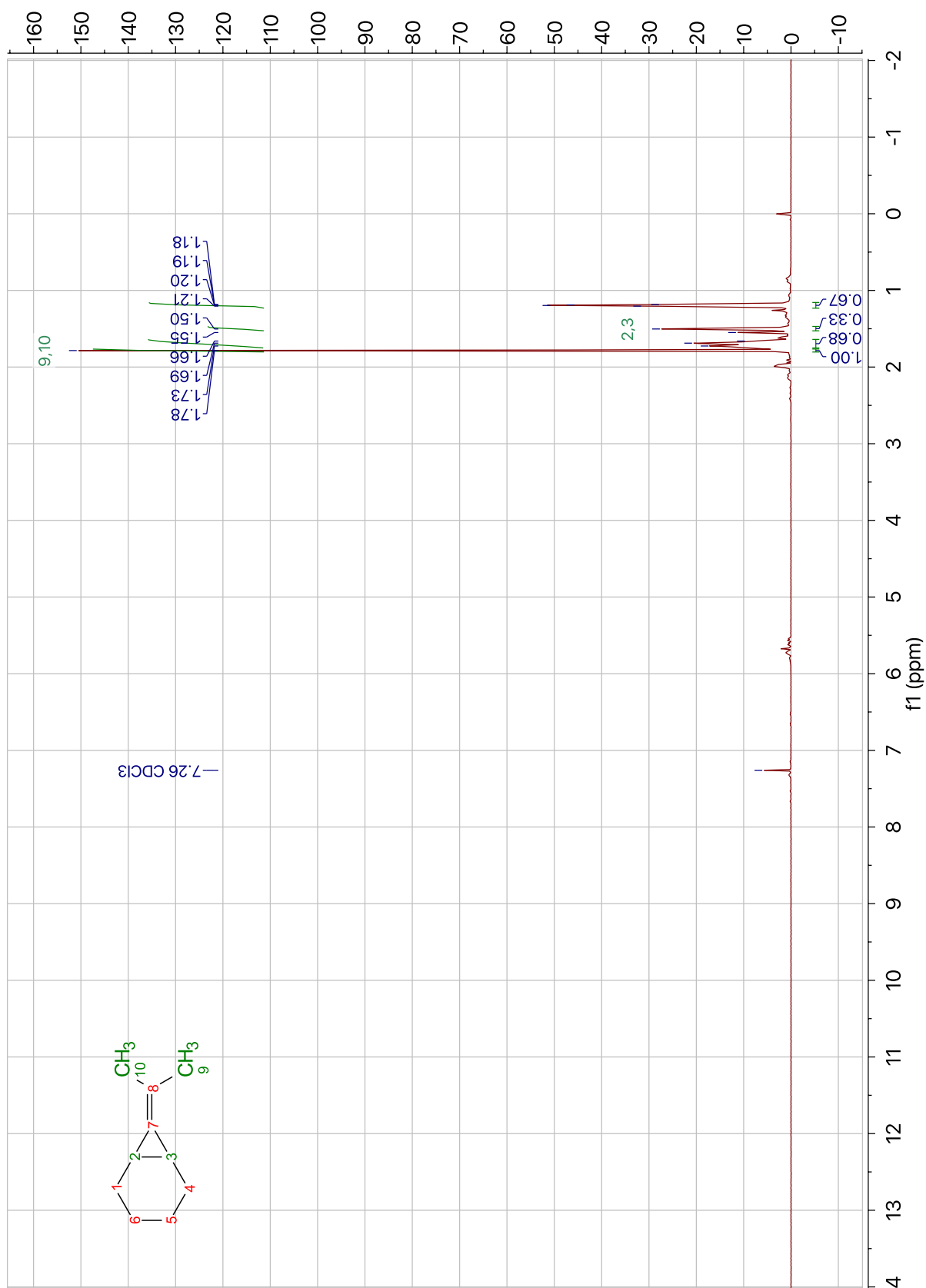


Figure 9.13: ¹H NMR spectrum for **17**

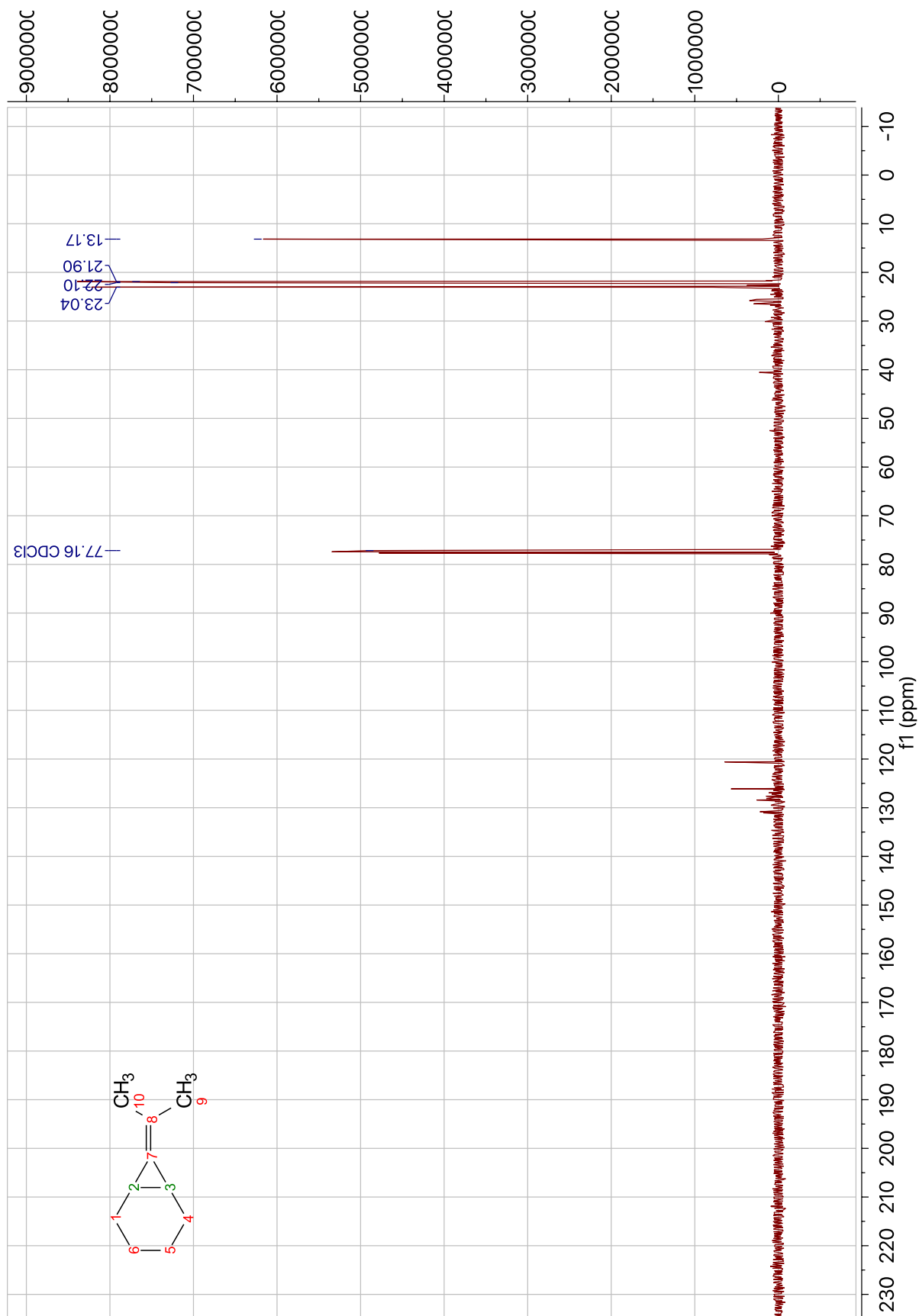


Figure 9.14: ^{13}C NMR spectrum for 17

File :D:\1\data\Tarini\TH080615016.D
Operator : Tarini
Acquired : 7 Aug 2015 14:29 using AcqMethod DASLAB3MIN.M
Instrument : GCMS1
Sample Name: DMV (hopefully) post photo
Misc Info : fraction 9
Vial Number: 1

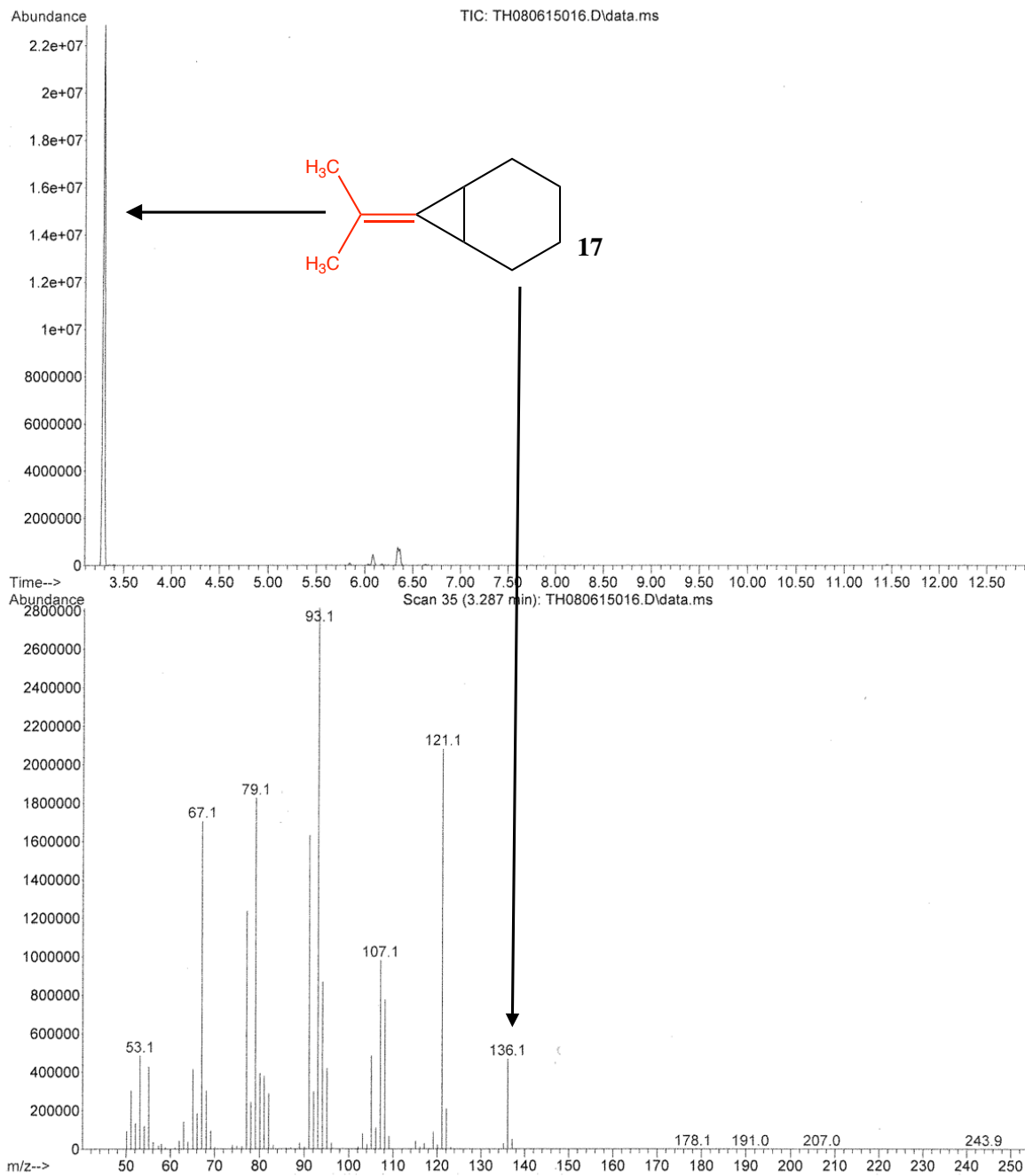


Figure 9.15: GC/MS data for 17

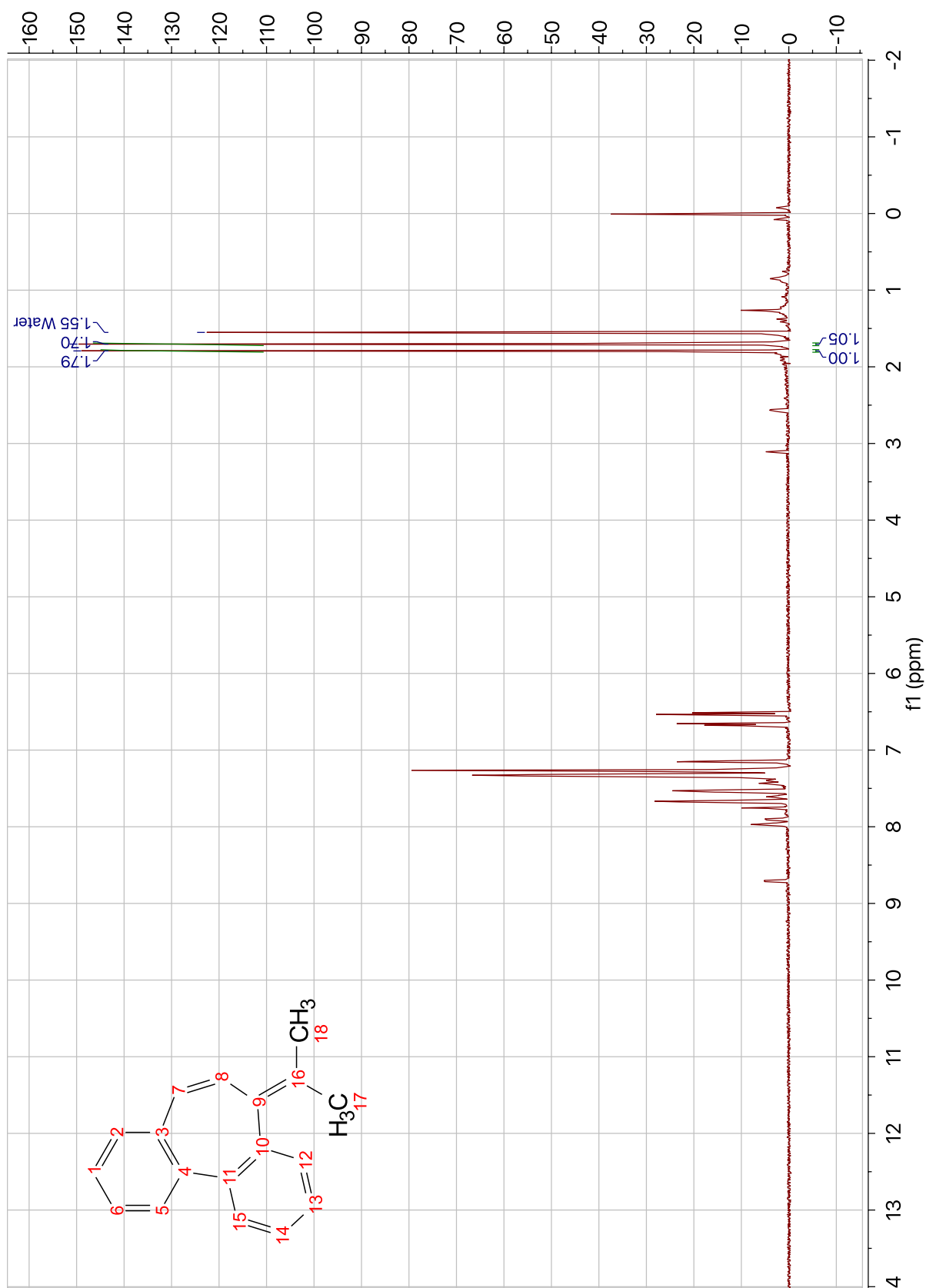


Figure 9.16: ^1H NMR spectrum for **18**

File :D:\1\data\Tarini\TH081015011.D
Operator : Tarini
Acquired : 10 Aug 2015 16:52 using AcqMethod DASLAB3MIN.M
Instrument : GCMS1
Sample Name: DMV prec photo
Misc Info : frac 29
Vial Number: 1

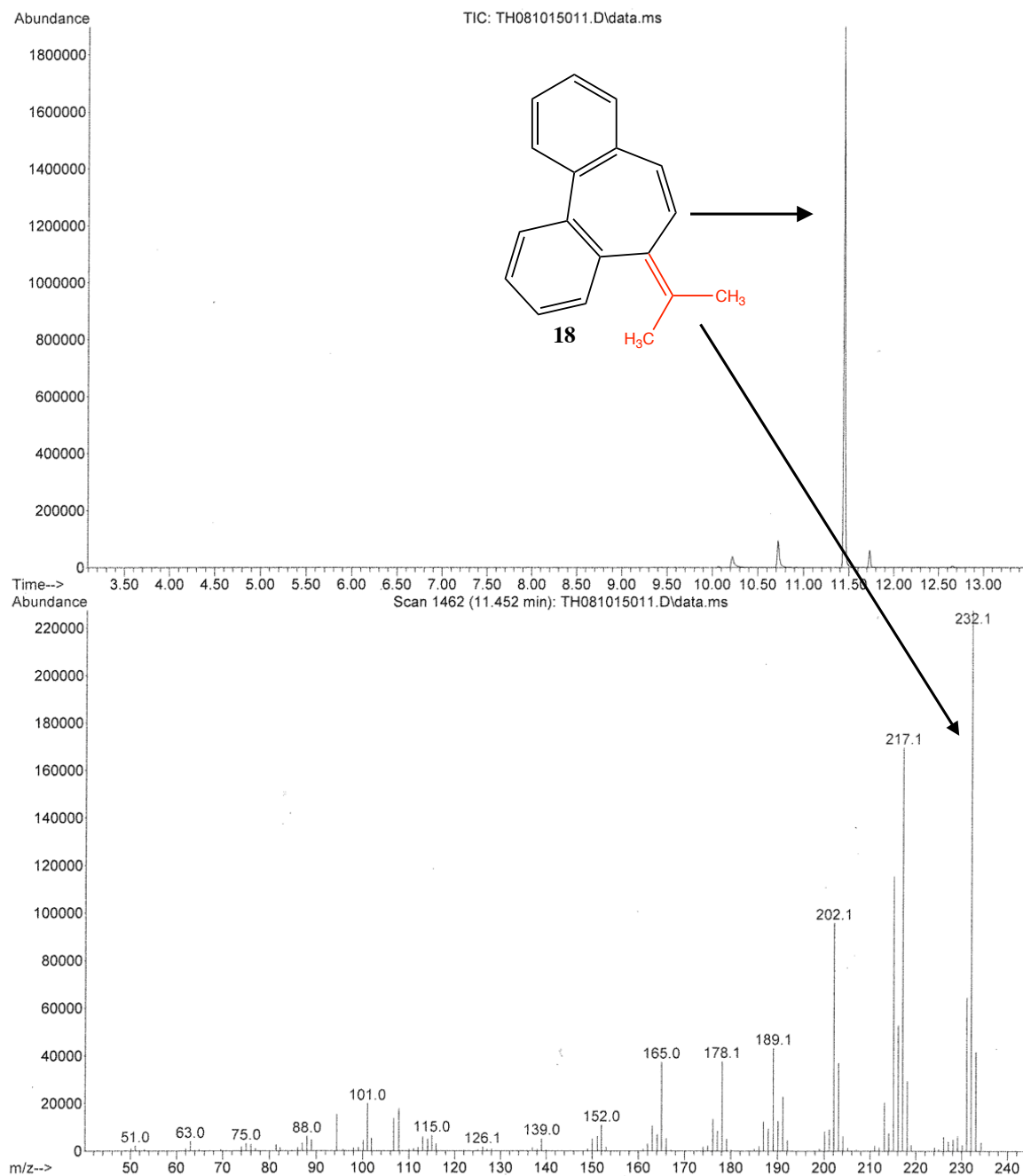


Figure 9.17: GC/MS data for 18

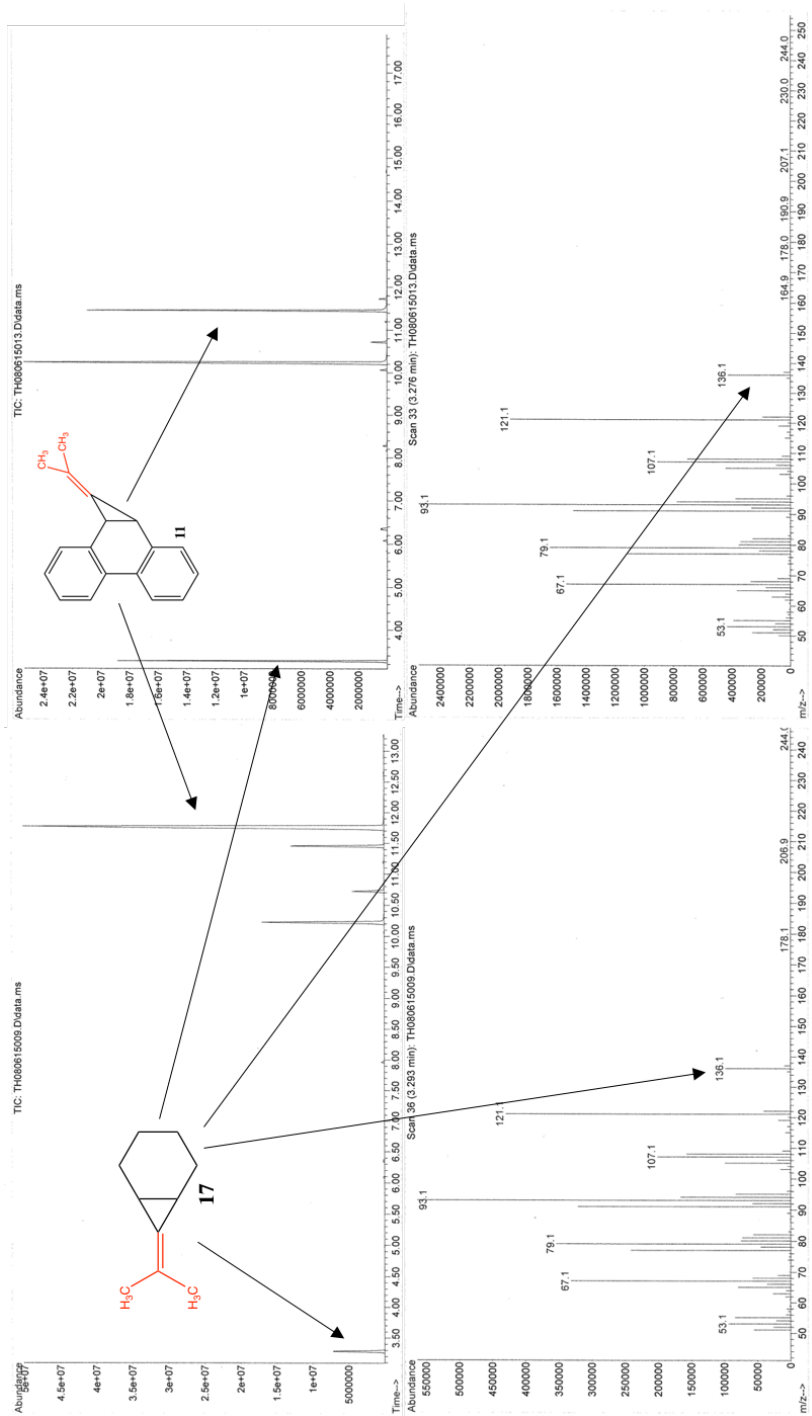


Figure 9.18: Change in peak for **11** over time as the photolysis progresses. (left) is 2 hours of photolysis, while the (right) is 18 hours of photolysis.

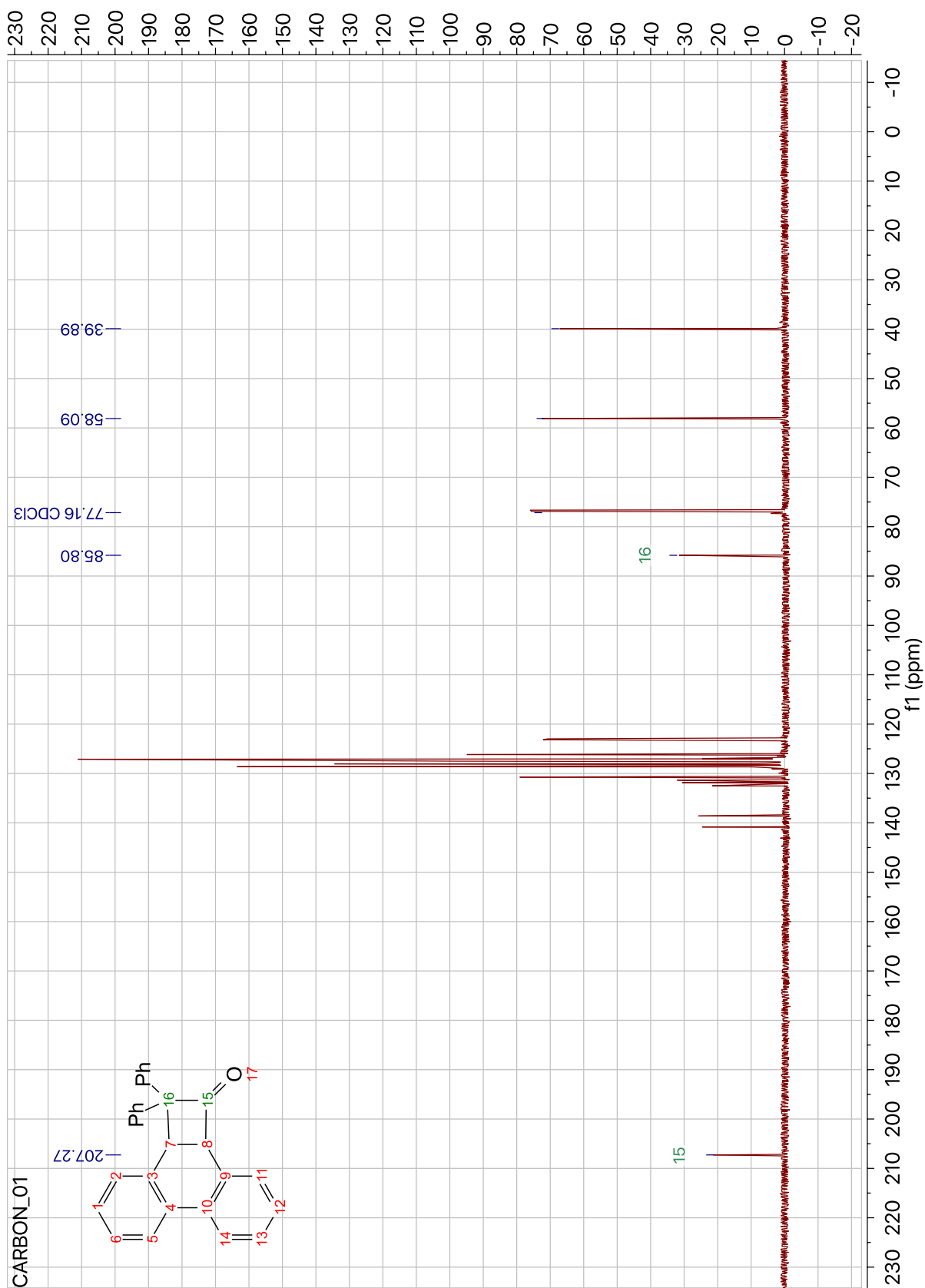


Figure 9.20: ^{13}C NMR spectrum for **22**

File :D:\1\data\Tarini\TH021817001.D
 Operator : Tarini
 Acquired : 18 Feb 2017 17:13 using AcqMethod DASLAB3MIN.M
 Instrument : GCMS1
 Sample Name: Alcohol rxn-cyclobutyl product
 Misc Info : Pre-photolysis
 Vial Number: 1

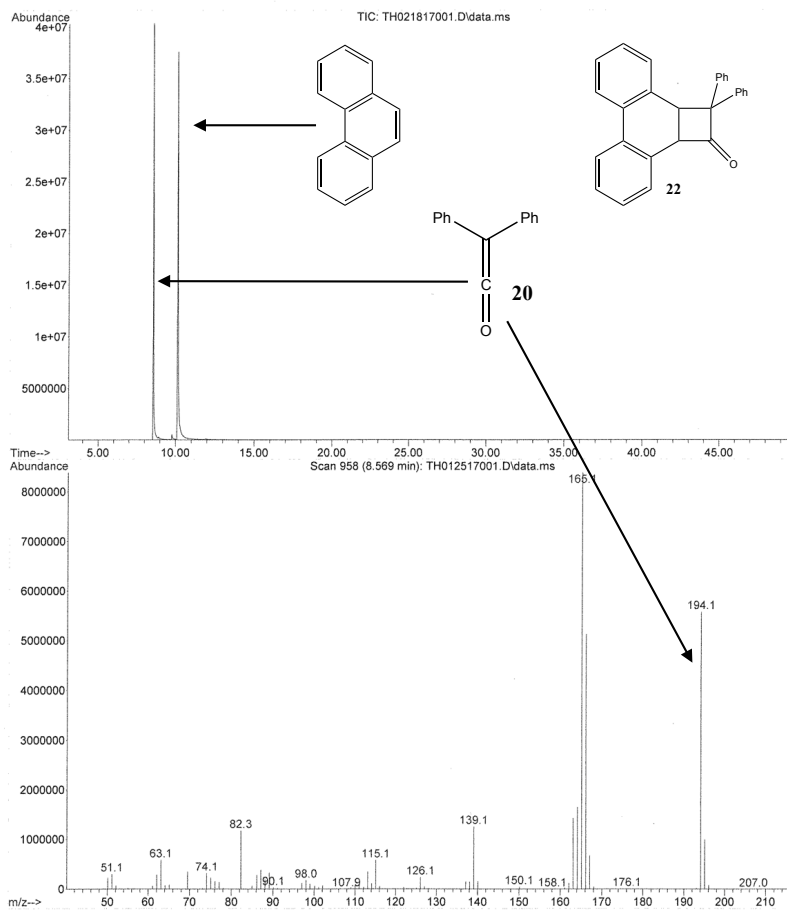


Figure 9.21: GC/MS data for **22**

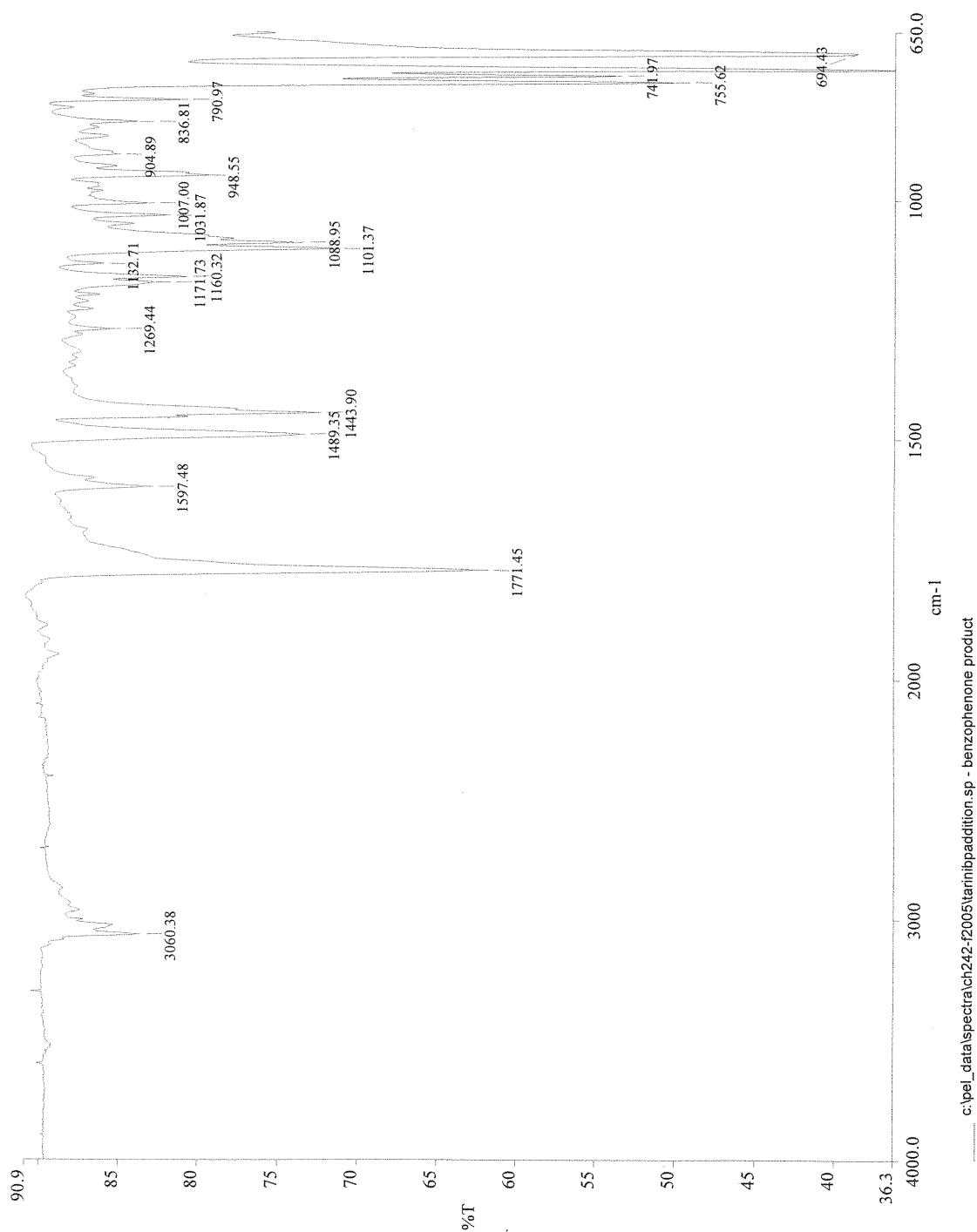


Figure 9.22: IR spectrum for **22**

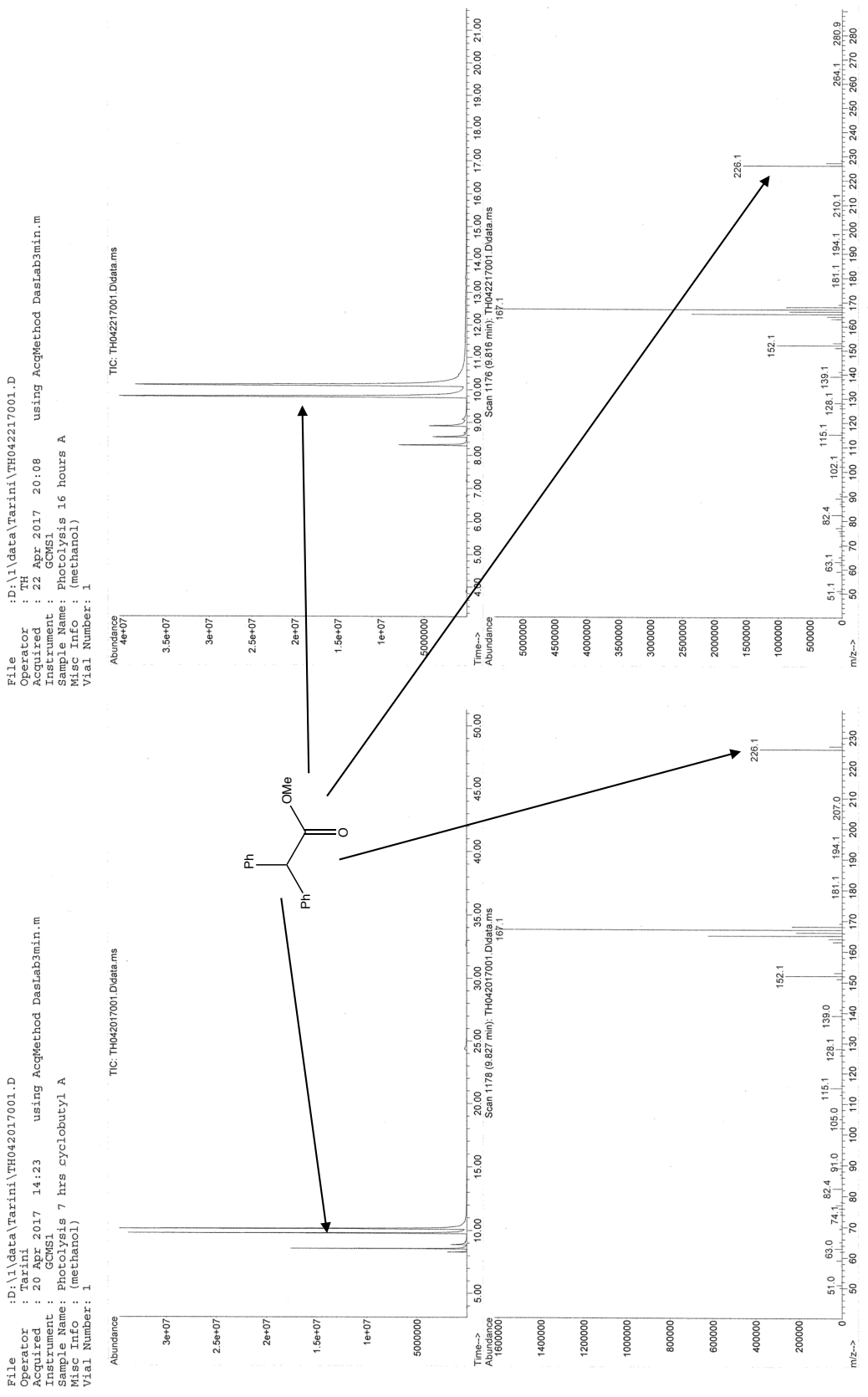


Figure 9.23: Change in peak for **25** over time as the photolysis progresses. (left) is 7 hours of photolysis, while the (right) is 16 hours of photolysis.

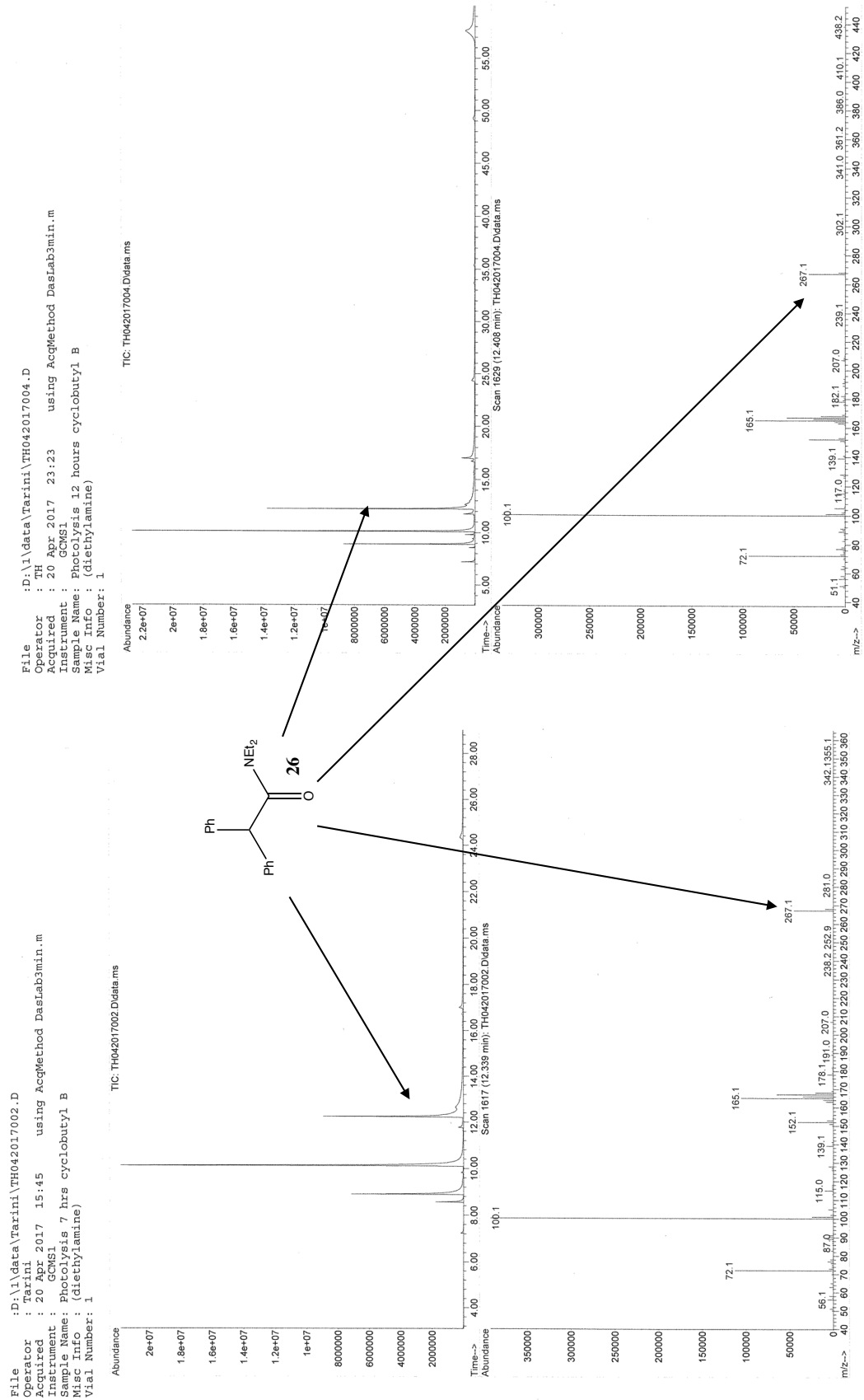
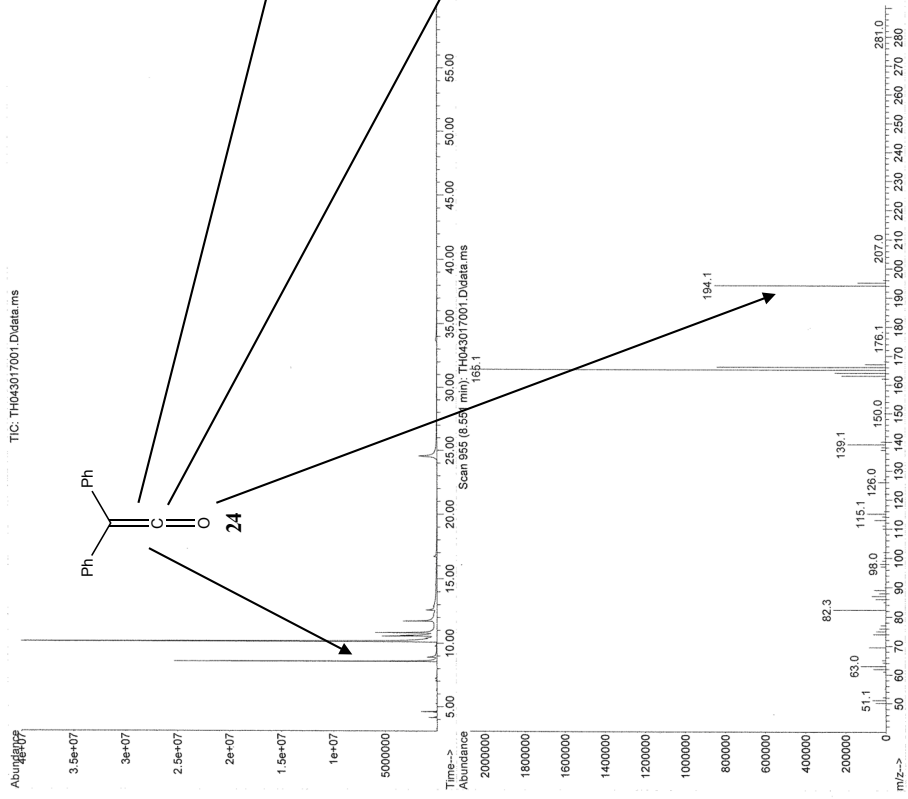


Figure 9.24: Change in peak for **26** over time as the photolysis progresses. (left) is 7 hours of photolysis, while the (right) is 12 hours of photolysis.

File : D:\1\data\Tarini\TH043017001.D
 Operator : TH
 Acquired : 30 Apr 2017 13:15 using AcqMethod DasLab3min.m
 Instrument : GCMS1
 Sample Name : Photolysis C 19 hrs
 Misc Info : (2,3-dimethyl 2-butene)
 Vial Number: 1



File : D:\1\data\Tarini\TH050317001.D
 Operator : TH
 Acquired : 3 May 2017 12:11 using AcqMethod DASLAB3MIN.M
 Instrument : GCMS1
 Sample Name : Photolysis C 38 hrs
 Misc Info : (2,3 2-butene)
 Vial Number: 1

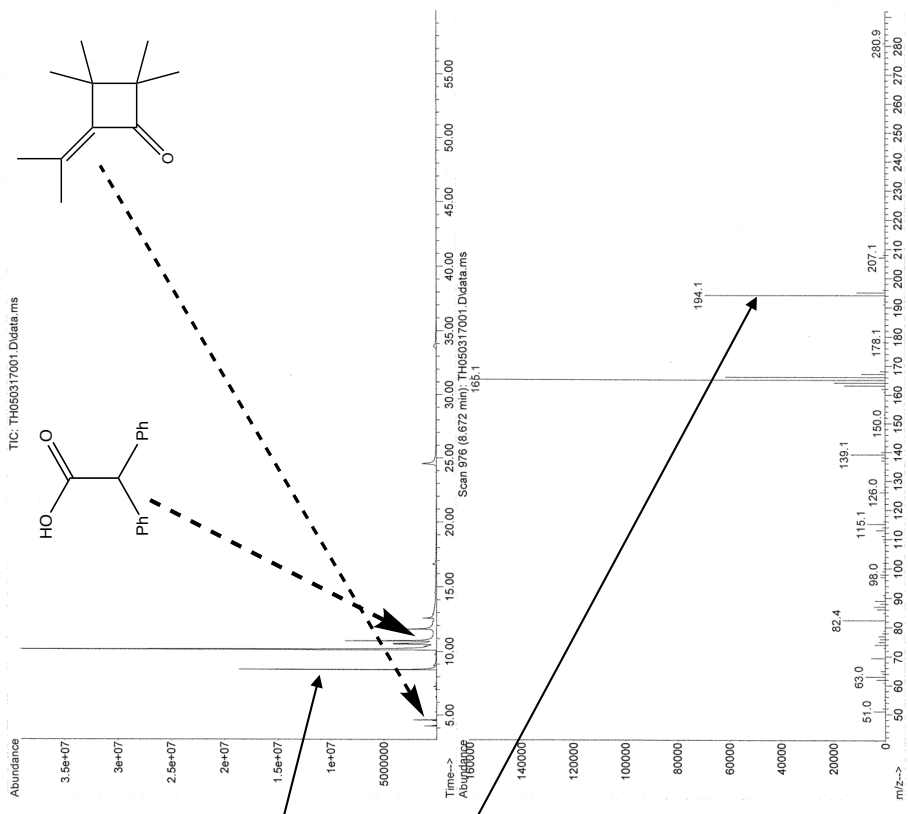


Figure 9.25: Change in peak for **24** over time as the photolysis progresses. (left) is 19 hours of photolysis, while the (right) is 38 hours of photolysis.

File :D:\1\data\Tarini\TH042117004.D
Operator : TH
Acquired : 21 Apr 2017 23:08 using AcqMethod DasLab3min.m
Instrument : GCMS1
Sample Name: Photolysis 16 hours D
Misc Info : (neat)
Vial Number: 1

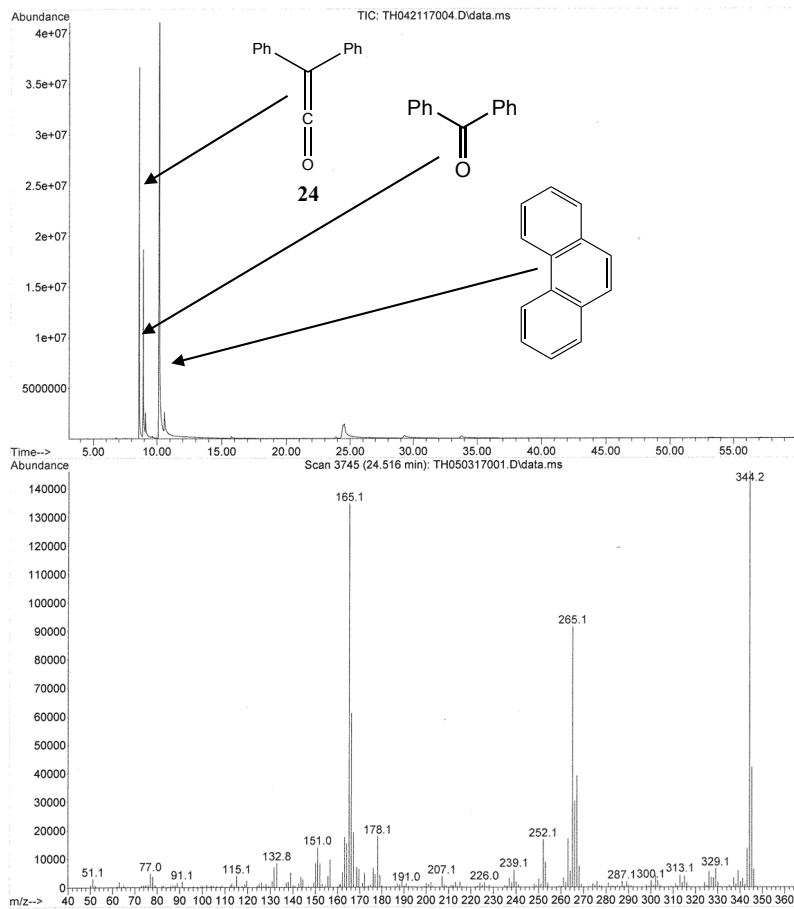


Figure 9.26: GC/MS for neat photolysis of **22** at time 16 hours.

Appendix B: Computational Studies

Cartesian coordinates and energies for (R/U)B3LYP/6-311++G** optimized structures

Dimethylvinylidene singlet (3s)

Charge = 0 Multiplicity = 1

C,0,0.,0.,0.23193823
C,0,0.,0.,1.53348223
C,0,0.,-1.31534078,-0.52241931
H,0,-0.88827931,-1.3772535,-1.15795013
H,0,0.88827931,-1.3772535,-1.15795013
H,0,0.,-2.17195706,0.15329334
C,0,0.,1.31534078,-0.52241931
H,0,0.88827931,1.3772535,-1.15795013
H,0,-0.88827931,1.3772535,-1.15795013
H,0,0.,2.17195706,0.15329334

Zero-point correction=	0.082514 (Hartree/Particle)
Thermal correction to Energy=	0.088079
Thermal correction to Enthalpy=	0.089023
Thermal correction to Gibbs Free Energy=	0.055601
Sum of electronic and zero-point Energies=	-155.863361
Sum of electronic and thermal Energies=	-155.857796
Sum of electronic and thermal Enthalpies=	-155.856852
Sum of electronic and thermal Free Energies=	-155.890274

Cartesian coordinates and energies for (R/U)B3LYP/6-311++G** optimized structures

Dimethylvinylidene triplet (3t)

Charge = 0 Multiplicity = 3

C,0,0.,0.,0.2523588765
C,0,0.,0.,1.6821295947
C,0,0.,1.2799478229,-0.526683016
H,0,0.8766111351,1.3250232135,-1.1867424577
H,0,-0.8766111351,1.3250232135,-1.1867424577
H,0,0.,2.1483090954,0.1308946958
C,0,0.,-1.2799478229,-0.526683016
H,0,-0.8766111351,-1.3250232135,-1.1867424577
H,0,0.8766111351,-1.3250232135,-1.1867424577
H,0,0.,-2.1483090954,0.1308946958

Zero-point correction=	0.078825 (Hartree/Particle)
Thermal correction to Energy=	0.083511
Thermal correction to Enthalpy=	0.084455
Thermal correction to Gibbs Free Energy=	0.051185
Sum of electronic and zero-point Energies=	-155.794873
Sum of electronic and thermal Energies=	-155.790187
Sum of electronic and thermal Enthalpies=	-155.789243
Sum of electronic and thermal Free Energies=	-155.822513

S**2 before annihilation 2.0052, after 2.0000

Cartesian coordinates and energies for (R/U)B3LYP/6-311++G** optimized structures

TS 3s to 2-butyne

Charge = 0 Multiplicity = 1

C,0,0.1413234811,0.2559672611,0.2738308758
C,0,0.431054162,-0.5560044522,1.193378364
C,0,-0.1452733304,1.4417170112,-0.5436431086
H,0,0.5568569373,1.5452874149,-1.3759895762
H,0,-1.163873095,1.4288402313,-0.9421898744
H,0,-0.0441022748,2.3228349848,0.094264805
C,0,0.0919490364,-1.4186765313,-0.3835334781
H,0,-0.1930375333,-0.9963877171,-1.3542386732
H,0,1.0320153801,-1.9466235268,-0.508833139
H,0,-0.7069127632,-2.0769546759,-0.0571041953

Zero-point correction=	0.081217 (Hartree/Particle)
Thermal correction to Energy=	0.086531
Thermal correction to Enthalpy=	0.087476
Thermal correction to Gibbs Free Energy=	0.053776
Sum of electronic and zero-point Energies=	-155.845910
Sum of electronic and thermal Energies=	-155.840596
Sum of electronic and thermal Enthalpies=	-155.839652
Sum of electronic and thermal Free Energies=	-155.873351

Cartesian coordinates and energies for (R/U)B3LYP/6-311++G** optimized structures

2-Butyne

Charge = 0 Multiplicity = 1

C,0,0.,-0.0000000007,0.60211377
C,0,0.,-0.0000000007,-0.60211377
C,0,0.,-0.0000000007,2.06091377
H,0,-0.8835572321,-0.5101220064,2.45597782
H,0,0.8835572321,-0.5101220064,2.45597782
H,0,0.,1.0202440109,2.45597782
C,0,0.,-0.0000000007,-2.06091377
H,0,0.8835572321,-0.5101220064,-2.45597782
H,0,-0.8835572321,-0.5101220064,-2.45597782
H,0,0.,1.0202440109,-2.45597782

Zero-point correction=	0.083804 (Hartree/Particle)
Thermal correction to Energy=	0.089549
Thermal correction to Enthalpy=	0.090493
Thermal correction to Gibbs Free Energy=	0.056981
Sum of electronic and zero-point Energies=	-155.943053
Sum of electronic and thermal Energies=	-155.937307
Sum of electronic and thermal Enthalpies=	-155.936363
Sum of electronic and thermal Free Energies=	-155.969876

Summary output of (R/U)CCSD(T)/cc-pVTZ//B3LYP/6-311++G** calculations

Dimethylvinylidene singlet (3s)

```
1\1\GINC-NSCC-N2\SP\RCCSD(T)-FC\CC-pVTZ\C4H6\TSHARDIK\04-Aug-2015\0\#\#
rccsd=(t,tldiag)/cc-pvtz geom=connectivity\Dimethylvinylidene single
t DFT C2v CCSD\0,1\C,0,0.,0.,0.231996\C,0,0.,0.,1.53354\C,0,0.,1.3153
41,-0.522362\H,0,0.888279,1.377254,-1.157893\H,0,-0.888279,1.377254,-1
.157893\H,0,0.,2.171957,0.153351\C,0,0.,-1.315341,-0.522362\H,0,-0.888
279,-1.377254,-1.157893\H,0,0.888279,-1.377254,-1.157893\H,0,0.,-2.171
957,0.153351\Version=EM64L-G09RevA.02\State=1-A1\HF=-154.8975278\MP2=
-155.5276528\MP3=-155.5682496\MP4D=-155.5843304\MP4DQ=-155.5675345\MP4
SDQ=-155.5729674\CCSD=-155.5733742\CCSD(T)=-155.6029264\RMSD=1.526e-09
\PG=C02V [C2(C1C1),SGV(C2H2),X(H4)]\@
```

Dimethylvinylidene triplet (3t)

```
1\1\GINC-NSCC-N2\SP\UCCSD(T)-FC\CC-pVTZ\C4H6(3)\TSHARDIK\04-Aug-2015\0
\#\# uccsd=(t,tldiag)/cc-pvtz geom=connectivity\Dimethylvinylidene tri
plet C2v ccsd\0,3\C,0,0.,0.,0.22564\C,0,0.,0.,1.655411\C,0,0.,1.27994
8,-0.553401\H,0,0.876611,1.325023,-1.213461\H,0,-0.876611,1.325023,-1.
213461\H,0,0.,2.148309,0.104176\C,0,0.,-1.279948,-0.553401\H,0,-0.8766
11,-1.325023,-1.213461\H,0,0.876611,-1.325023,-1.213461\H,0,0.,-2.1483
09,0.104176\Version=EM64L-G09RevA.02\State=3-A2\HF=-154.851176\MP2=-1
55.4447249\MP3=-155.4916315\MP4D=-155.5060655\MP4DQ=-155.4913556\PUHF=
-154.854157\PMP2-0=-155.4465617\PMP3-0=-155.4926533\MP4SDQ=-155.495986
9\CCSD=-155.4966448\CCSD(T)=-155.5226684\S2=2.015325\S2-1=2.003517\S2A
=2.000086\RMSD=9.205e-09\PG=C02V [C2(C1C1),SGV(C2H2),X(H4)]\@
```

2-Butyne

```
1\1\GINC-NSCC-N2\SP\RCCSD(T)-FC\CC-pVTZ\C4H6\TSHARDIK\04-Aug-2015\0\#\#
rccsd=(t,tldiag)/cc-pvtz geom=connectivity\2-Butyne D3H CCSD\0,1\C,
0,0.,0.,0.602114\C,0,0.,0.,-0.602114\C,0,0.,0.,2.060914\H,0,0.,1.02024
4,2.455978\H,0,-0.883557,-0.510122,2.455978\H,0,0.883557,-0.510122,2.4
55978\C,0,0.,0.,-2.060914\H,0,-0.883557,-0.510122,-2.455978\H,0,0.,1.0
20244,-2.455978\H,0,0.883557,-0.510122,-2.455978\Version=EM64L-G09Rev
A.02\State=1-A1'\HF=-154.9647988\MP2=-155.6192823\MP3=-155.6471479\MP4
D=-155.6633604\MP4DQ=-155.6458361\MP4SDQ=-155.6515112\CCSD=-155.650654
1\CCSD(T)=-155.681652\RMSD=3.181e-09\PG=D03H [C3(C1C1.C1C1),3SGV(H2)]\
\@
```

TS 3s to 2-butyne

```
1\1\GINC-NSCC-N2\SP\RCCSD(T)-FC\CC-pVTZ\C4H6\TSHARDIK\04-Aug-2015\0\#\#
rccsd=(t,tldiag)/cc-pvtz geom=connectivity\TS CCSD(T)\0,1\C,0,0.227
333,0.367423,-0.001134\C,0,-0.779057,1.126361,0.000443\C,0,1.576853,-0
.211538,0.000254\H,0,1.760517,-0.821095,0.889761\H,0,1.762542,-0.82142
9,-0.888623\H,0,2.295977,0.610893,0.000901\C,0,-1.266201,-0.636744,0.0
00276\H,0,-0.629437,-1.529064,-0.010144\H,0,-1.865126,-0.660928,0.9051
83\H,0,-1.878037,-0.651391,-0.896111\Version=EM64L-G09RevA.02\State=1
-A\HF=-154.8638797\MP2=-155.5178053\MP3=-155.548664\MP4D=-155.5650701\
MP4DQ=-155.5462573\MP4SDQ=-155.5517616\CCSD=-155.5512107\CCSD(T)=-155.
5842393\RMSD=7.932e-09\PG=C01 [X(C4H6)]\@
```

Cartesian coordinates and energies for (R/U)B3LYP/6-31G* optimized structures

Diphenyl Ketene (24)

Charge = 0 Multiplicity = 1
C, 0, -0.077205553, 1.593384799, -0.3315005219
C, 0, 1.0255469291, 2.0186200339, -0.9416847294
O, 0, -1.0484871077, 1.218883981, 0.2059817332
C, 0, 1.7717689854, 1.0486023544, -1.7899222956
C, 0, 2.39861389, 1.4773857051, -2.97278316
C, 0, 1.8471220922, -0.3123695328, -1.4477775
C, 0, 3.0800769005, 0.5708789986, -3.7827791743
H, 0, 2.3452668898, 2.52405165, -3.2560906334
C, 0, 2.5121323392, -1.2193651035, -2.2714768935
H, 0, 1.3902461719, -0.6588988833, -0.5238722593
C, 0, 3.1363914153, -0.7821319839, -3.4406806847
H, 0, 3.5604332398, 0.9233729037, -4.6918686214
H, 0, 2.5552871674, -2.2677867858, -1.9883998623
H, 0, 3.6647892184, -1.4869083066, -4.0766307344
C, 0, 1.4359527067, 3.4347825153, -0.7334448023
C, 0, 2.7978773765, 3.7729363631, -0.6509860508
C, 0, 0.4824634322, 4.4570753369, -0.5895683773
C, 0, 3.188789395, 5.0929676252, -0.4343157812
H, 0, 3.5482479684, 2.9950633192, -0.7533591719
C, 0, 0.8773692638, 5.7727925837, -0.3522958102
H, 0, -0.5751986323, 4.2195523209, -0.675349097
C, 0, 2.2324055263, 6.0988672414, -0.2783237506
H, 0, 4.2471400806, 5.3338076254, -0.3766312298
H, 0, 0.1224199452, 6.5467080195, -0.241434075
H, 0, 2.5404493293, 7.1262326999, -0.1051933268

Zero-point correction=	0.196318
(Hartree/Particle)	
Thermal correction to Energy=	0.208257
Thermal correction to Enthalpy=	0.209201
Thermal correction to Gibbs Free Energy=	0.156466
Sum of electronic and zero-point Energies=	-614.511947
Sum of electronic and thermal Energies=	-614.500008
Sum of electronic and thermal Enthalpies=	-614.499064
Sum of electronic and thermal Free Energies=	-614.551799

Cartesian coordinates and energies for (R/U)B3LYP/6-31G* optimized structures

Diphenyl Ketene Precursor (22)

Charge = 0 Multiplicity = 1

C,0,-4.2585616628,-2.9273288004,2.3136392582
C,0,-3.9168957888,-3.1501501281,0.9831159499
C,0,-3.4728563384,-2.1022252687,0.1676492997
C,0,-3.3749245064,-0.7918543145,0.6803963243
C,0,-3.7035976286,-0.5944282045,2.0349140274
C,0,-4.1402836521,-1.640026675,2.8413527106
C,0,-3.065302507,-2.4220125324,-1.2538957332
C,0,-2.9650829931,0.3357904979,-0.1972201453
C,0,-2.4336453989,0.0900867696,-1.4830488247
C,0,-2.263236961,-1.3145086359,-1.9935191808
C,0,-2.1027668068,1.1698779761,-2.3102524342
H,0,-1.7152600197,0.9717519035,-3.307039301
C,0,-2.2624029138,2.4874199359,-1.8899040551
C,0,-2.7858146265,2.736427983,-0.6210867543
C,0,-3.1392502299,1.6730538622,0.2032060438
H,0,-4.5993418586,-3.7505571043,2.9353428112
H,0,-3.9720934795,-4.1521012242,0.5654981661
H,0,-3.5987581959,0.3899548298,2.4777936148
H,0,-4.3832369863,-1.4496409866,3.8832477305
H,0,-1.9943677803,3.3083373133,-2.5492720778
H,0,-2.9347058173,3.7566147141,-0.2778728357
H,0,-3.5821499497,1.8942167752,1.1680239817
C,0,-0.8926596101,-2.1292668751,-1.7743250509
C,0,-1.8019203809,-3.2925589929,-1.290329712
O,0,-1.6052126574,-4.4610749146,-1.0758489918
H,0,-3.9045234689,-2.8541428438,-1.8129270299
H,0,-2.5033459955,-1.338696174,-3.0591278935
C,0,0.03769517,-1.584645023,-0.6849224661
C,0,0.1767358392,-2.205971639,0.5625064131
C,0,0.7971481244,-0.4334289533,-0.9464508059
C,0,1.0426259445,-1.6830913487,1.5266827959
H,0,-0.382351046,-3.1074736089,0.7897973066
C,0,1.6573292982,0.0897081171,0.0158283837
H,0,0.7202678213,0.0506922204,-1.9150941443
C,0,1.7833183545,-0.5336584948,1.2597267206
H,0,1.1354592822,-2.182814839,2.4873514196
H,0,2.233838839,0.9833818771,-0.2084841325
H,0,2.4570255999,-0.128314761,2.0099816877
C,0,-0.0965229063,-2.4882591415,-3.0278531364
C,0,-0.1548859832,-1.738855864,-4.2086518381
C,0,0.7495601124,-3.6090533792,-2.9893935157
C,0,0.6125150437,-2.0933169932,-5.3216654667
H,0,-0.7977772629,-0.8664404421,-4.2717993196
C,0,1.5072744164,-3.9680737251,-4.1017633365
H,0,0.7994963226,-4.2056451023,-2.0845530785
C,0,1.4445642127,-3.210073172,-5.2737483832
H,0,0.5543147521,-1.49269529,-6.2257642214
H,0,2.149842046,-4.8432563211,-4.0524130479
H,0,2.0389379235,-3.4885820123,-6.1397718624

Cartesian coordinates and energies for (R/U)B3LYP/6-31G* optimized structures

Phenanthrene

Charge = 0 Multiplicity = 1

```
C, 0, -4.2703595388, -3.3191373308, -0.0040454425
C, 0, -2.8897291181, -3.3087893114, -0.0051296704
C, 0, -2.1679192133, -2.0923280644, -0.0037076279
C, 0, -2.8744985462, -0.85261956, -0.0010519947
C, 0, -4.2886356539, -0.8976780674, -0.0000492926
C, 0, -4.9730220953, -2.099525516, -0.0015031544
C, 0, -0.73258189, -2.0931988878, -0.0049568218
C, 0, -2.1189323191, 0.3941343605, 0.0004739362
C, 0, -0.6929755919, 0.3414759704, -0.0009183593
C, 0, -0.0279641636, -0.9305093165, -0.0036715894
C, 0, 0.0513562332, 1.5442919773, 0.0004857143
H, 0, 1.1372650493, 1.4832125535, -0.0006298177
C, 0, -0.5783915055, 2.7729707274, 0.0032247377
C, 0, -1.9847275283, 2.8314572086, 0.004672793
C, 0, -2.7334193465, 1.6685838903, 0.0033273663
H, 0, -0.2184856219, -3.0514250031, -0.0069863112
H, 0, -4.8124966808, -4.2607625425, -0.0051584354
H, 0, -2.3330533222, -4.2431544927, -0.0071253423
H, 0, -4.8590184898, 0.0250061468, 0.0018491566
H, 0, -6.059720282, -2.1003649118, -0.000698053
H, 0, 1.059392358, -0.9428002558, -0.0046945914
H, 0, 0.0054455876, 3.6893251251, 0.0042825193
H, 0, -2.4868723581, 3.7951789704, 0.0068806975
H, 0, -3.8153172029, 1.7472076499, 0.0045545831
```

Zero-point correction=
(Hartree/Particle)

0.194848

Thermal correction to Energy=

0.204282

Thermal correction to Enthalpy=

0.205226

Thermal correction to Gibbs Free Energy=

0.160019

Sum of electronic and zero-point Energies=

-539.343808

Sum of electronic and thermal Energies=

-539.334374

Sum of electronic and thermal Enthalpies=

-539.333430

Sum of electronic and thermal Free Energies=

-539.378638

Appendix C: Crystal Structure Determination

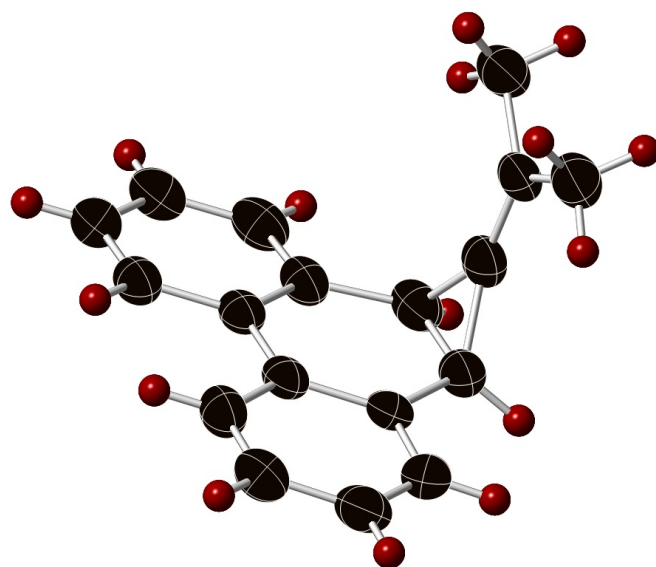


Figure 11.1: Crystal structure for the dimethylalkylidene precursor **11**

Crystal Structure Report for THdmvprec

A clear colourless block-like specimen of $C_{18}H_{16}$, approximate dimensions 0.090 mm x 0.160 mm x 0.370 mm, was used for the X-ray crystallographic analysis. The X-ray intensity data were measured.

The total exposure time was 10.27 hours. The frames were integrated with the Bruker SAINT software package using a narrow-frame algorithm. The integration of the data using a monoclinic unit cell yielded a total of 5599 reflections to a maximum θ angle of 26.82° (0.79 \AA resolution), of which 2681 were independent (average redundancy 2.088, completeness = 98.6%, $R_{\text{int}} = 1.64\%$, $R_{\text{sig}} = 2.61\%$) and 2287 (85.30%) were greater than $2\sigma(F^2)$. The final cell constants of $a = 10.69(3) \text{ \AA}$, $b = 4.895(6) \text{ \AA}$, $c = 12.40(4) \text{ \AA}$, $\beta = 93.43(12)^\circ$, volume = $648.(3) \text{ \AA}^3$, are based upon the refinement of the XYZ-centroids of 1840 reflections above $20 \sigma(I)$ with $4.905^\circ < 2\theta < 50.67^\circ$. Data were corrected for absorption effects using the Multi-Scan method (SADABS). The ratio of minimum to maximum apparent transmission was 0.852. The calculated minimum and maximum transmission coefficients (based on crystal size) are 0.9760 and 0.9940.

The final anisotropic full-matrix least-squares refinement on F^2 with 165 variables converged at $R1 = 4.32\%$, for the observed data and $wR2 = 11.65\%$ for all data. The goodness-of-fit was 1.024. The largest peak in the final difference electron density synthesis was $0.162 \text{ e}^-/\text{\AA}^3$ and the largest hole was $-0.112 \text{ e}^-/\text{\AA}^3$ with an RMS deviation of $0.033 \text{ e}^-/\text{\AA}^3$. On the basis of the final model, the calculated density was 1.191 g/cm^3 and $F(000)$, 248 e^- .

Table 1. Sample and crystal data for THdmvprec.

Identification code	THdmvprec	
Chemical formula	$C_{18}H_{16}$	
Formula weight	232.31 g/mol	
Temperature	173(2) K	
Wavelength	0.71073 \AA	
Crystal size	0.090 x 0.160 x 0.370 mm	
Crystal habit	clear colourless block	
Crystal system	monoclinic	
Space group	P 1 21 1	
Unit cell dimensions	$a = 10.69(3) \text{ \AA}$	$\alpha = 90^\circ$
	$b = 4.895(6) \text{ \AA}$	$\beta = 93.43(12)^\circ$
	$c = 12.40(4) \text{ \AA}$	$\gamma = 90^\circ$
Volume	$648.(3) \text{ \AA}^3$	
Z	2	
Density (calculated)	1.191 g/cm^3	
Absorption coefficient	0.067 mm^{-1}	

Table 2. Data collection and structure refinement for THdmvprec.

Theta range for data collection	1.65 to 26.82°	
Index ranges	-13<=h<=13, -6<=k<=6, -15<=l<=15	
Reflections collected	5599	
Independent reflections	2681 [R(int) = 0.0164]	
Coverage of independent reflections	98.6%	
Absorption correction	Multi-Scan	
Max. and min. transmission	0.9940 and 0.9760	
Refinement method	Full-matrix least-squares on F ²	
Refinement program	SHELXL-2014/7 (Sheldrick, 2014)	
Function minimized	$\Sigma w(F_o^2 - F_c^2)^2$	
Data / restraints / parameters	2681 / 1 / 165	
Goodness-of-fit on F ²	1.024	
Δ/σ_{\max}	0.002	
Final R indices	2287 data; I>2 σ (I)	R1 = 0.0432, wR2 = 0.1065
	all data	R1 = 0.0526, wR2 = 0.1165
Weighting scheme	$w=1/[\sigma^2(F_o^2)+(0.0636P)^2+0.0425P]$ where $P=(F_o^2+2F_c^2)/3$	
Absolute structure parameter	-2.3(10)	
Largest diff. peak and hole	0.162 and -0.112 eÅ ⁻³	
R.M.S. deviation from mean	0.033 eÅ ⁻³	

Table 3. Atomic coordinates and equivalent isotropic atomic displacement parameters (Å²) for

THdmvprec.

U(eq) is defined as one third of the trace of the orthogonalized U_{ij} tensor.

	x/a	y/b	z/c	U(eq)
C1	0.0134(2)	0.6063(7)	0.1995(2)	0.0573(7)
C2	0.8886(2)	0.5152(5)	0.14932(19)	0.0469(6)
C3	0.8134(2)	0.3532(5)	0.2012(2)	0.0489(6)
C4	0.6875(2)	0.2297(6)	0.2066(2)	0.0514(6)
C5	0.5769(2)	0.4132(5)	0.21282(19)	0.0454(6)
C6	0.4829(2)	0.4122(6)	0.1290(2)	0.0543(7)
C7	0.3814(2)	0.5887(6)	0.1288(2)	0.0563(7)
C8	0.3722(2)	0.7699(6)	0.2134(2)	0.0540(7)
C9	0.8527(2)	0.6245(7)	0.03810(19)	0.0567(7)
C10	0.7855(2)	0.2245(6)	0.3049(2)	0.0504(6)
C11	0.7633(2)	0.4049(5)	0.39828(19)	0.0446(6)
C12	0.6613(2)	0.5896(5)	0.39521(19)	0.0415(5)
C13	0.5667(2)	0.5935(4)	0.30097(18)	0.0418(5)
C14	0.4629(2)	0.7709(5)	0.2985(2)	0.0486(6)
C15	0.6505(2)	0.7645(5)	0.4843(2)	0.0473(6)
C16	0.7357(2)	0.7560(6)	0.5730(2)	0.0525(6)
C17	0.8340(2)	0.5713(6)	0.5762(2)	0.0541(7)
C18	0.8465(2)	0.3959(6)	0.4899(2)	0.0530(6)

Table 4. Bond lengths (Å) for THdmvprec.

C1-C2	1.506(5)	C1-H14	0.98
C1-H13	0.98	C1-H1	0.98
C2-C3	1.323(4)	C2-C9	1.507(5)
C3-C10	1.478(5)	C3-C4	1.480(5)
C4-C5	1.490(4)	C4-C10	1.559(5)
C4-H7	1.0	C5-C6	1.402(5)
C5-C13	1.414(4)	C6-C7	1.386(5)
C6-H6	0.95	C7-C8	1.382(5)
C7-H5	0.95	C8-C14	1.389(5)
C8-H2	0.95	C9-H16	0.98
C9-H15	0.98	C9-H3	0.98

C10-C11	1.487(5)	C10-H12	1.0
C11-C18	1.401(5)	C11-C12	1.415(4)
C12-C15	1.408(4)	C12-C13	1.499(5)
C13-C14	1.408(4)	C14-H4	0.95
C15-C16	1.386(5)	C15-H8	0.95
C16-C17	1.385(4)	C16-H9	0.95
C17-C18	1.385(5)	C17-H11	0.95
C18-H10	0.95		

Table 5. Bond angles (°) for THdmvprec.

C2-C1-H14	109.5	C2-C1-H13	109.5
H14-C1-H13	109.5	C2-C1-H1	109.5
H14-C1-H1	109.5	H13-C1-H1	109.5
C3-C2-C1	121.7(3)	C3-C2-C9	121.9(3)
C1-C2-C9	116.3(3)	C2-C3-C10	147.0(3)
C2-C3-C4	147.9(3)	C10-C3-C4	63.6(2)
C3-C4-C5	118.8(3)	C3-C4-C10	58.1(2)
C5-C4-C10	117.8(2)	C3-C4-H7	116.5
C5-C4-H7	116.5	C10-C4-H7	116.5
C6-C5-C13	119.3(3)	C6-C5-C4	119.7(3)
C13-C5-C4	121.0(2)	C7-C6-C5	121.7(3)
C7-C6-H6	119.2	C5-C6-H6	119.2
C8-C7-C6	119.3(3)	C8-C7-H5	120.3
C6-C7-H5	120.3	C7-C8-C14	120.1(3)
C7-C8-H2	120.0	C14-C8-H2	120.0
C2-C9-H16	109.5	C2-C9-H15	109.5
H16-C9-H15	109.5	C2-C9-H3	109.5
H16-C9-H3	109.5	H15-C9-H3	109.5
C3-C10-C11	118.3(3)	C3-C10-C4	58.2(2)
C11-C10-C4	117.9(3)	C3-C10-H12	116.5
C11-C10-H12	116.5	C4-C10-H12	116.5
C18-C11-C12	119.5(3)	C18-C11-C10	119.3(3)
C12-C11-C10	121.1(2)	C15-C12-C11	117.8(2)
C15-C12-C13	121.4(2)	C11-C12-C13	120.8(2)
C14-C13-C5	117.7(2)	C14-C13-C12	121.2(2)
C5-C13-C12	121.0(2)	C8-C14-C13	121.8(3)

C8-C14-H4	119.1	C13-C14-H4	119.1
C16-C15-C12	121.6(3)	C16-C15-H8	119.2
C12-C15-H8	119.2	C17-C16-C15	120.2(3)
C17-C16-H9	119.9	C15-C16-H9	119.9
C16-C17-C18	119.4(3)	C16-C17-H11	120.3
C18-C17-H11	120.3	C17-C18-C11	121.4(3)
C17-C18-H10	119.3	C11-C18-H10	119.3

Table 6. Torsion angles (°) for THdmvprec.

C1-C2-C3-C10	11.7(5)	C9-C2-C3-C10	-
			166.7(3)
C1-C2-C3-C4	168.1(4)	C9-C2-C3-C4	-10.3(6)
C2-C3-C4-C5	-59.3(5)	C10-C3-C4-C5	106.6(3)
C2-C3-C4-C10	-	C3-C4-C5-C6	116.7(3)
	165.9(5)		
C10-C4-C5-C6	-	C3-C4-C5-C13	-61.7(3)
	176.3(2)		
C10-C4-C5-C13	5.3(3)	C13-C5-C6-C7	1.7(4)
C4-C5-C6-C7	-	C5-C6-C7-C8	-0.2(4)
	176.8(2)		
C6-C7-C8-C14	-1.1(4)	C2-C3-C10-C11	59.3(5)
C4-C3-C10-C11	-	C2-C3-C10-C4	166.3(4)
	107.0(3)		
C5-C4-C10-C3	-	C3-C4-C10-C11	107.7(3)
	108.3(3)		
C5-C4-C10-C11	-0.6(3)	C3-C10-C11-C18	-
			115.9(3)
C4-C10-C11-C18	177.1(2)	C3-C10-C11-C12	62.7(3)
C4-C10-C11-C12	-4.3(3)	C18-C11-C12-C15	2.1(3)
C10-C11-C12-C15	-	C18-C11-C12-C13	-
	176.5(2)		176.7(2)
C10-C11-C12-C13	4.8(3)	C6-C5-C13-C14	-1.8(3)
C4-C5-C13-C14	176.7(2)	C6-C5-C13-C12	176.4(2)
C4-C5-C13-C12	-5.1(3)	C15-C12-C13-C14	-0.5(3)
C11-C12-C13-C15	178.1(2)	C15-C12-C13-C5	-

C14			178.7(2)
C11-C12-C13-C5	0.0(3)	C7-C8-C14-C13	0.9(4)
C5-C13-C14-C8	0.5(3)	C12-C13-C14-C8	177.7(2)
C11-C12-C15-C16	-0.6(3)	C13-C12-C15-C16	178.1(2)
C12-C15-C16-C17	-0.5(4)	C15-C16-C17-C18	0.2(4)
C16-C17-C18-C11	1.3(4)	C12-C11-C18-C17	-2.4(3)
C10-C11-C18-C17	176.1(2)		

Table 7. Anisotropic atomic displacement parameters (\AA^2) for THdmvprec.

The anisotropic atomic displacement factor exponent takes the form: $-2\pi^2 [h^2 a^{*2} U_{11} + \dots + 2 h k a^* b^* U_{12}]$

	U_{11}	U_{22}	U_{33}	U_{23}	U_{13}	U_{12}
C1	0.0457(13)	0.0725(19)	0.0546(14)	0.0015(14)	0.0104(11)	0.0026(14)
C2	0.0420(12)	0.0506(14)	0.0497(13)	0.0049(11)	0.0148(10)	0.0022(11)
C3	0.0462(13)	0.0471(14)	0.0550(14)	0.0049(12)	0.0155(11)	0.0038(11)
C4	0.0494(13)	0.0443(13)	0.0623(15)	0.0074(12)	0.0188(11)	0.0059(12)
C5	0.0447(12)	0.0414(13)	0.0517(13)	0.0024(11)	0.0170(10)	0.0101(11)
C6	0.0509(14)	0.0595(17)	0.0538(14)	0.0085(13)	0.0138(11)	0.0140(14)
C7	0.0447(14)	0.0713(18)	0.0532(15)	0.0036(15)	0.0059(11)	0.0111(14)
C8	0.0448(13)	0.0597(16)	0.0582(15)	0.0047(13)	0.0087(11)	0.0033(13)
C9	0.0530(14)	0.0679(16)	0.0501(14)	0.0022(13)	0.0100(11)	0.0003(14)
C10	0.0498(13)	0.0416(12)	0.0617(14)	0.0045(12)	0.0189(11)	0.0038(12)
C11	0.0426(12)	0.0394(13)	0.0535(13)	0.0085(11)	0.0169(10)	0.0015(11)
C12	0.0389(12)	0.0367(12)	0.0504(12)	0.0043(10)	0.0144(9)	0.0034(10)

	U ₁₁	U ₂₂	U ₃₃	U ₂₃	U ₁₃	U ₁₂
C13	0.0395(11)	0.0391(12)	0.0482(12)	0.0021(11)	0.0141(9)	⁻ 0.0041(11)
C14	0.0466(13)	0.0479(14)	0.0526(14)	0.0001(12)	0.0124(11)	0.0033(12)
C15	0.0449(12)	0.0430(13)	0.0550(14)	⁻ 0.0004(11)	0.0125(11)	⁻ 0.0012(11)
C16	0.0540(14)	0.0525(15)	0.0518(14)	⁻ 0.0018(13)	0.0103(11)	⁻ 0.0046(13)
C17	0.0501(14)	0.0611(17)	0.0515(14)	0.0110(13)	0.0056(11)	⁻ 0.0049(13)
C18	0.0466(13)	0.0525(15)	0.0609(15)	0.0154(13)	0.0119(11)	0.0044(13)

Table 8. Hydrogen atomic coordinates and isotropic atomic displacement parameters (\AA^2) for THdmprec.

	x/a	y/b	z/c	U(eq)
H14	1.0245	0.5346	0.2732	0.086
H13	1.0165	0.8064	0.2014	0.086
H1	1.0806	0.5372	0.1565	0.086
H7	0.6730	0.0533	0.1671	0.062
H6	0.4888	0.2875	0.0709	0.065
H5	0.3188	0.5851	0.0711	0.068
H2	0.3038	0.8939	0.2134	0.065
H16	0.7705	0.5520	0.0133	0.085
H15	0.9154	0.5680	-0.0119	0.085
H3	0.8489	0.8244	0.0407	0.085
H12	0.8270	0.0451	0.3218	0.06
H4	0.4546	0.8948	0.3566	0.058
H8	0.5833	0.8914	0.4836	0.057
H9	0.7266	0.8773	0.6318	0.063
H11	0.8922	0.5649	0.6371	0.065
H10	0.9130	0.2668	0.4928	0.064

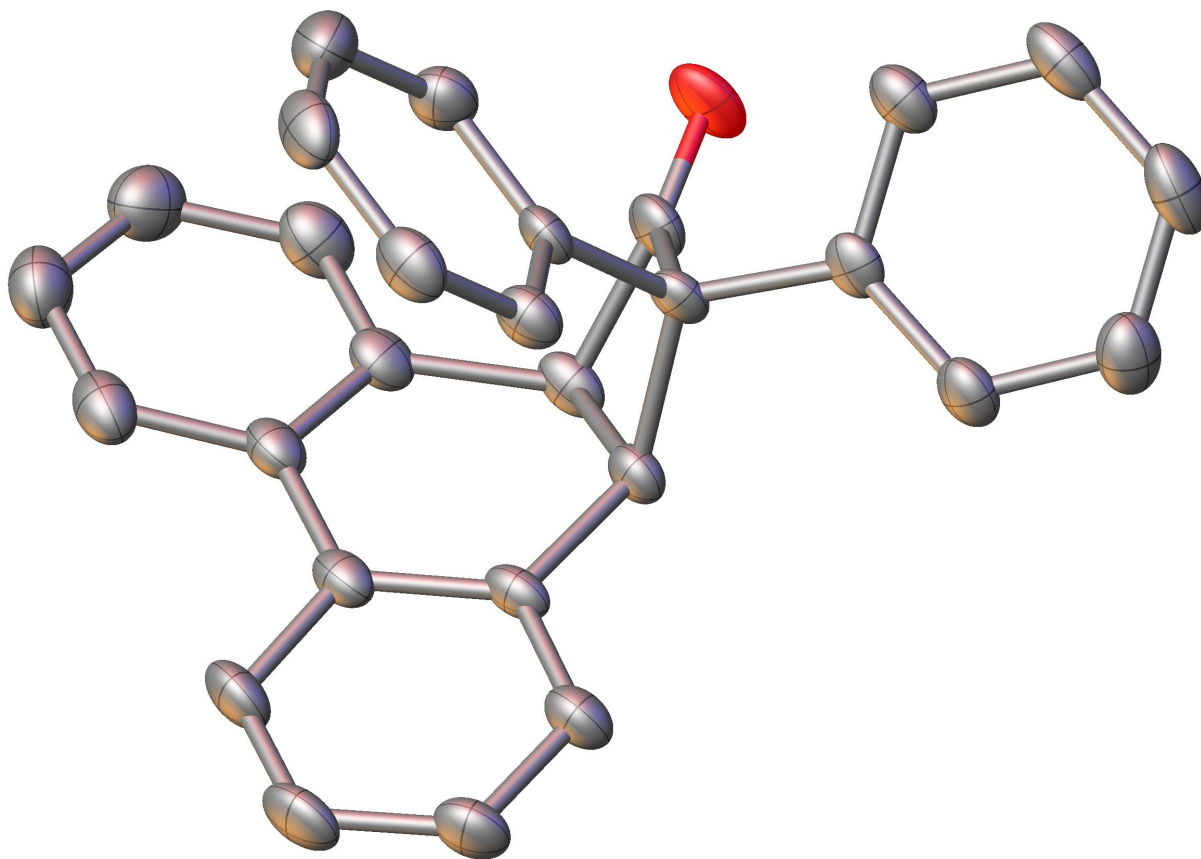


Figure 11.2: Crystal structure for the diphenyl ketene precursor **22**

Crystal Structure Report for THdpkprec

A clear colourless needle-like specimen of $C_{20}H_{28}O$, approximate dimensions 0.020 mm x 0.080 mm x 0.350 mm, was used for the X-ray crystallographic analysis. The X-ray intensity data were measured.

The total exposure time was 10.47 hours. The frames were integrated with the Bruker SAINT software package using a narrow-frame algorithm. The integration of the data using a triclinic unit cell yielded a total of 8575 reflections to a maximum θ angle of 26.40° (0.80 Å resolution), of which 3839 were independent (average redundancy 2.234, completeness = 97.8%, $R_{\text{int}} = 5.88\%$, $R_{\text{sig}} = 10.19\%$) and 2253 (58.69%) were greater than $2\sigma(F^2)$. The final cell constants of $a = 10.1248(8)$ Å, $b = 10.1619(8)$ Å, $c = 10.5305(8)$ Å, $\alpha = 88.410(6)^\circ$, $\beta = 64.598(5)^\circ$, $\gamma = 78.503(6)^\circ$, volume = $957.02(14)$ Å³, are based upon the refinement of the XYZ-centroids of 2122 reflections above $20\sigma(I)$ with $5.457^\circ < 2\theta < 52.27^\circ$. Data were corrected for absorption effects using the Multi-Scan method (SADABS). The ratio of minimum to maximum apparent transmission was 0.833. The calculated minimum and maximum transmission coefficients (based on crystal size) are 0.6210 and 0.7454.

The structure was solved and refined using the Bruker SHELXTL Software Package, using the space group P -1, with $Z = 2$ for the formula unit, $C_{20}H_{28}O$. The final anisotropic full-matrix least-squares refinement on F^2 with 262 variables converged at $R1 = 6.64\%$, for the observed data and $wR2 = 14.95\%$ for all data. The goodness-of-fit was 1.028. The largest peak in the final difference electron density synthesis was 0.206 e⁻/Å³ and the largest hole was -0.243 e⁻/Å³ with an RMS deviation of 0.052 e⁻/Å³. On the basis of the final model, the calculated density was 1.292 g/cm³ and $F(000)$, 392 e⁻.

Table 1. Sample and crystal data for THdpkprec.

Identification code	THdpkprec	
Chemical formula	$C_{20}H_{28}O$	
Formula weight	284.44 g/mol	
Wavelength	0.71073 Å	
Crystal size	0.020 x 0.080 x 0.350 mm	
Crystal habit	clear colourless needle	
Crystal system	triclinic	
Space group	P -1	
Unit cell dimensions	$a = 10.1248(8)$ Å	$\alpha = 88.410(6)^\circ$
	$b = 10.1619(8)$ Å	$\beta = 64.598(5)^\circ$
	$c = 10.5305(8)$ Å	$\gamma = 78.503(6)^\circ$
Volume	$957.02(14)$ Å ³	
Z	2	

Density (calculated)	1.292 g/cm ³
Absorption coefficient	0.077 mm ⁻¹
F(000)	392

Table 2. Data collection and structure refinement for THdpkprec.

Theta range for data collection	2.73 to 26.40°	
Index ranges	-12<=h<=11, -12<=k<=12, -13<=l<=12	
Reflections collected	8575	
Independent reflections	3839 [R(int) = 0.0588]	
Coverage of independent reflections	97.8%	
Absorption correction	Multi-Scan	
Max. and min. transmission	0.7454 and 0.6210	
Structure solution technique	direct methods	
Structure solution program	XT (Sheldrick, 2015)	
Refinement method	Full-matrix least-squares on F ²	
Refinement program	XL (Sheldrick, 2008)	
Function minimized	$\Sigma w(F_o^2 - F_c^2)^2$	
Data / restraints / parameters	3839 / 0 / 262	
Goodness-of-fit on F ²	1.028	
Final R indices	2253 data; I>2σ(I)	R1 = 0.0664, wR2 = 0.1246
	all data	R1 = 0.1343, wR2 = 0.1495
Weighting scheme	w=1/[σ ² (F _o ²)+(0.0531P) ² +0.3037P] where P=(F _o ² +2F _c ²)/3	
Largest diff. peak and hole	0.206 and -0.243 eÅ ⁻³	
R.M.S. deviation from mean	0.052 eÅ ⁻³	

Table 3. Atomic coordinates and equivalent isotropic atomic displacement parameters (\AA^2) for THdpkprec.

U(eq) is defined as one third of the trace of the orthogonalized U_{ij} tensor.

	x/a	y/b	z/c	U(eq)
O001	0.5182(2)	0.1916(2)	0.54588(18)	0.0375(5)
C002	0.2908(3)	0.3513(3)	0.4044(2)	0.0230(6)
C003	0.2227(3)	0.1556(3)	0.5510(2)	0.0232(6)
C004	0.4428(3)	0.1116(3)	0.2877(2)	0.0235(6)
C005	0.3460(3)	0.2058(3)	0.4290(2)	0.0223(6)
C006	0.4274(3)	0.1495(3)	0.1551(2)	0.0234(6)
C007	0.4927(3)	0.1834(3)	0.4453(3)	0.0266(7)
C008	0.1698(3)	0.2203(3)	0.6840(3)	0.0291(7)
C009	0.1627(3)	0.0491(3)	0.5376(3)	0.0299(7)
C00A	0.1802(3)	0.3785(3)	0.3567(2)	0.0275(7)
C00B	0.6201(3)	0.2902(3)	0.0992(2)	0.0270(7)
C00C	0.5888(3)	0.1280(3)	0.2936(2)	0.0257(6)
C00D	0.6604(3)	0.2366(3)	0.2048(3)	0.0267(6)
C00E	0.3441(3)	0.4576(3)	0.4302(3)	0.0315(7)
C00F	0.5132(3)	0.2357(3)	0.0654(2)	0.0252(6)
C00G	0.3301(3)	0.0971(3)	0.1198(3)	0.0300(7)
C00H	0.0609(3)	0.1767(3)	0.8009(3)	0.0352(7)
C00I	0.1267(3)	0.5082(3)	0.3341(3)	0.0331(7)
C00J	0.0528(3)	0.0068(3)	0.6552(3)	0.0365(7)
C00K	0.4975(3)	0.2650(3)	0.9411(3)	0.0330(7)
C00L	0.3139(3)	0.1299(3)	0.9982(3)	0.0326(7)
C00M	0.6828(3)	0.3972(3)	0.0305(3)	0.0343(7)
C00N	0.7633(3)	0.2866(3)	0.2336(3)	0.0365(7)
C00O	0.1815(3)	0.6133(3)	0.3591(3)	0.0352(7)
C00P	0.2894(4)	0.5887(3)	0.4074(3)	0.0394(8)
C00Q	0.3987(3)	0.2136(3)	0.9088(3)	0.0362(7)
C00R	0.0025(3)	0.0699(3)	0.7862(3)	0.0386(8)
C00S	0.7830(3)	0.4478(3)	0.0613(3)	0.0397(8)

	x/a	y/b	z/c	U(eq)
C00T	0.8244(3)	0.3916(3)	0.1629(3)	0.0406(8)

Table 4. Bond lengths (Å) for THdpkprec.

O001-C007	1.202(3)	C002-C005	1.529(4)
C002-C00A	1.391(3)	C002-C00E	1.380(3)
C003-C005	1.521(3)	C003-C008	1.395(3)
C003-C009	1.380(4)	C004-H004	0.98
C004-C005	1.596(3)	C004-C006	1.502(3)
C004-C00C	1.547(4)	C005-C007	1.539(4)
C006-C00F	1.403(3)	C006-C00G	1.387(4)
C007-C00C	1.521(3)	C008-H008	0.93
C008-C00H	1.388(3)	C009-H009	0.93
C009-C00J	1.392(3)	C00A-H00A	0.93
C00A-C00I	1.377(4)	C00B-C00D	1.402(4)
C00B-C00F	1.477(4)	C00B-C00M	1.395(4)
C00C-H00C	0.98	C00C-C00D	1.516(3)
C00D-C00N	1.388(4)	C00E-H00E	0.93
C00E-C00P	1.393(4)	C00F-C00K	1.402(3)
C00G-H00G	0.93	C00G-C00L	1.383(3)
C00H-H00H	0.93	C00H-C00R	1.377(4)
C00I-H00I	0.93	C00I-C00O	1.377(4)
C00J-H00J	0.93	C00J-C00R	1.375(4)
C00K-H00K	0.93	C00K-C00Q	1.378(4)
C00L-H00L	0.93	C00L-C00Q	1.378(4)
C00M-H00M	0.93	C00M-C00S	1.379(4)
C00N-H00N	0.93	C00N-C00T	1.378(4)
C00O-H00O	0.93	C00O-C00P	1.370(4)
C00P-H00P	0.93	C00Q-H00Q	0.93
C00R-H00R	0.93	C00S-H00S	0.93
C00S-C00T	1.379(4)	C00T-H00T	0.93

Table 5. Bond angles (°) for THdpkprec.

C00A-C002-C005	118.8(2)	C00E-C002-C005	122.8(2)
C00E-C002-C00A	118.4(3)	C008-C003-C005	117.6(2)
C009-C003-C005	123.7(2)	C009-C003-C008	118.7(2)
C005-C004-H004	109.5	C006-C004-H004	109.5
C006-C004-C005	119.9(2)	C006-C004-C00C	116.6(2)
C00C-C004-H004	109.5	C00C-C004-C005	90.45(18)
C002-C005-C004	113.92(19)	C002-C005-C007	113.7(2)
C003-C005-C002	110.5(2)	C003-C005-C004	119.2(2)
C003-C005-C007	112.5(2)	C007-C005-C004	84.90(19)
C00F-C006-C004	120.1(2)	C00G-C006-C004	120.0(2)
C00G-C006-C00F	119.9(2)	O001-C007-C005	132.4(2)
O001-C007-C00C	133.4(3)	C00C-C007-C005	93.64(19)
C003-C008-H008	119.7	C00H-C008-C003	120.6(3)
C00H-C008-H008	119.7	C003-C009-H009	119.9
C003-C009-C00J	120.3(3)	C00J-C009-H009	119.9
C002-C00A-H00A	119.7	C00I-C00A-C002	120.7(3)
C00I-C00A-H00A	119.7	C00D-C00B-C00F	120.5(2)
C00M-C00B-C00D	117.3(3)	C00M-C00B-C00F	122.1(2)
C004-C00C-H00C	114.1	C007-C00C-C004	87.19(18)

C007-C00C-H00C	114.1	C00D-C00C-C004	114.4(2)
C00D-C00C-C007	110.0(2)	C00D-C00C-H00C	114.1
C00B-C00D-C00C	121.3(2)	C00N-C00D-C00B	120.1(2)
C00N-C00D-C00C	118.6(2)	C002-C00E-H00E	119.6
C002-C00E-C00P	120.7(3)	C00P-C00E-H00E	119.6
C006-C00F-C00B	120.9(2)	C00K-C00F-C006	117.9(3)
C00K-C00F-C00B	121.3(2)	C006-C00G-H00G	119.4
C00L-C00G-C006	121.3(3)	C00L-C00G-H00G	119.4
C008-C00H-H00H	120.0	C00R-C00H-C008	120.1(3)
C00R-C00H-H00H	120.0	C00A-C00I-H00I	119.8
C00O-C00I-C00A	120.5(3)	C00O-C00I-H00I	119.8
C009-C00J-H00J	119.7	C00R-C00J-C009	120.7(3)
C00R-C00J-H00J	119.7	C00F-C00K-H00K	119.3
C00Q-C00K-C00F	121.4(3)	C00Q-C00K-H00K	119.3
C00G-C00L-H00L	120.4	C00Q-C00L-C00G	119.3(3)
C00Q-C00L-H00L	120.4	C00B-C00M-H00M	118.9
C00S-C00M-C00B	122.2(3)	C00S-C00M-H00M	118.9
C00D-C00N-H00N	119.4	C00T-C00N-C00D	121.2(3)
C00T-C00N-H00N	119.4	C00I-C00O-H00O	120.1
C00P-C00O-C00I	119.7(3)	C00P-C00O-H00O	120.1
C00E-C00P-H00P	120.0	C00O-C00P-C00E	120.0(3)

C00O-C00P- H00P	120.0	C00K-C00Q- C00L	120.3(3)
C00K-C00Q- H00Q	119.9	C00L-C00Q- H00Q	119.9
C00H-C00R- H00R	120.2	C00J-C00R- C00H	119.6(3)
C00J-C00R- H00R	120.2	C00M-C00S- H00S	120.2
C00T-C00S- C00M	119.7(3)	C00T-C00S- H00S	120.2
C00N-C00T- C00S	119.4(3)	C00N-C00T- H00T	120.3
C00S-C00T- H00T	120.3		

Table 6. Anisotropic atomic displacement parameters (\AA^2) for THdpkprec.

The anisotropic atomic displacement factor exponent takes the form: $-2\pi^2[h^2 a^{*2} U_{11} + \dots + 2 h k a^* b^* U_{12}]$

	U_{11}	U_{22}	U_{33}	U_{23}	U_{13}	U_{12}
O001	0.0382(13)	0.0591(14)	0.0227(10)	0.0091(9)	-0.0207(9)	- 0.0096(10)
C002	0.0257(15)	0.0288(16)	0.0131(12)	0.0047(10)	- 0.0080(11)	- 0.0037(12)
C003	0.0221(15)	0.0301(16)	0.0217(13)	0.0082(11)	- 0.0150(11)	- 0.0028(12)
C004	0.0264(16)	0.0264(15)	0.0174(12)	0.0046(10)	- 0.0107(11)	- 0.0026(12)
C005	0.0243(15)	0.0300(16)	0.0157(12)	0.0030(11)	- 0.0119(11)	- 0.0047(12)
C006	0.0267(16)	0.0261(15)	0.0163(12)	0.0001(11)	- 0.0119(11)	- 0.0032(12)
C007	0.0325(17)	0.0310(16)	0.0193(13)	0.0093(11)	- 0.0146(12)	- 0.0064(13)
C008	0.0275(16)	0.0379(17)	0.0220(13)	0.0053(12)	- 0.0132(12)	- 0.0019(13)
C009	0.0328(17)	0.0380(18)	0.0229(14)	0.0090(12)	- 0.0160(12)	- 0.0081(14)
C00A	0.0290(16)	0.0315(16)	0.0229(13)	0.0032(12)	- 0.0144(12)	- 0.0010(13)

	U₁₁	U₂₂	U₃₃	U₂₃	U₁₃	U₁₂
C00B	0.0296(16)	0.0274(16)	0.0179(13)	0.0007(11)	0.0067(12)	0.0006(13)
C00C	0.0232(15)	0.0327(16)	0.0194(13)	0.0037(11)	0.0117(11)	0.0036(12)
C00D	0.0217(15)	0.0318(16)	0.0200(13)	0.0008(11)	0.0051(11)	0.0003(12)
C00E	0.0355(18)	0.0367(18)	0.0283(15)	0.0038(12)	0.0188(13)	0.0092(14)
C00F	0.0296(16)	0.0232(15)	0.0179(13)	0.0004(11)	0.0088(12)	0.0021(12)
C00G	0.0322(17)	0.0363(17)	0.0199(13)	0.0022(12)	0.0119(12)	0.0024(14)
C00H	0.0306(17)	0.050(2)	0.0198(13)	0.0066(13)	0.0103(12)	0.0018(15)
C00I	0.0332(17)	0.0372(18)	0.0274(14)	0.0071(13)	0.0161(13)	0.0017(14)
C00J	0.0344(18)	0.0447(19)	0.0378(17)	0.0140(14)	0.0198(14)	0.0159(15)
C00K	0.0396(19)	0.0383(18)	0.0174(13)	0.0064(12)	0.0113(13)	0.0031(15)
C00L	0.0378(18)	0.0399(18)	0.0251(14)	0.0005(12)	0.0201(13)	0.0032(14)
C00M	0.0372(18)	0.0307(17)	0.0262(14)	0.0048(12)	0.0083(13)	0.0009(14)
C00N	0.0301(18)	0.048(2)	0.0311(15)	0.0048(14)	0.0143(13)	0.0053(15)
C00O	0.0425(19)	0.0250(16)	0.0307(15)	0.0092(12)	0.0123(14)	0.0000(14)
C00P	0.051(2)	0.0330(18)	0.0349(16)	0.0040(13)	0.0158(15)	0.0163(16)
C00Q	0.046(2)	0.0425(19)	0.0204(14)	0.0038(13)	0.0194(14)	0.0006(15)
C00R	0.0285(17)	0.058(2)	0.0277(15)	0.0182(15)	0.0106(13)	0.0115(16)
C00S	0.0394(19)	0.0388(19)	0.0355(16)	0.0085(14)	0.0101(15)	0.0116(15)
C00T	0.0347(19)	0.045(2)	0.0405(17)	0.0003(15)	0.0137(14)	0.0114(15)

Table 7. Hydrogen atomic coordinates and isotropic atomic displacement parameters (\AA^2) for THdpkprec.

	x/a	y/b	z/c	U(eq)
H004	0.4294	0.0190	0.3063	0.028
H008	0.2079	0.2933	0.6944	0.035
H009	0.1959	0.0055	0.4496	0.036
H00A	0.1421	0.3083	0.3398	0.033
H00C	0.6590	0.0429	0.2835	0.031
H00E	0.4173	0.4415	0.4631	0.038
H00G	0.2748	0.0389	0.1790	0.036
H00H	0.0274	0.2198	0.8893	0.042
H00I	0.0531	0.5248	0.3017	0.04
H00J	0.0129	-0.0650	0.6451	0.044
H00K	0.5550	0.3202	-0.1209	0.04
H00L	0.2465	0.0959	-0.0231	0.039
H00M	0.6560	0.4357	-0.0385	0.041
H00N	0.7916	0.2485	0.3018	0.044
H00O	0.1453	0.7007	0.3432	0.042
H00P	0.3261	0.6596	0.4251	0.047
H00Q	0.3892	0.2356	-0.1736	0.043
H00R	-0.0705	0.0407	0.8644	0.046
H00S	0.8226	0.5194	0.0138	0.048
H00T	0.8929	0.4244	0.1836	0.049